FROM LIGHT TO LIFE: THE ENERGY CONVERSION AND STORAGE IN PLANTS AND ALGAE

by

YUAN ZHANG

A dissertation submitted to the

School of Graduate Studies

Rutgers, The State University of New Jersey

In partial fulfillment of the requirements

For the degree of

Doctor of Philosophy

Graduate Program in Microbial Biology

Written under the direction of

G. Charles Dismukes

And approved by

_____

_____

_____

_____

New Brunswick, New Jersey

October 2018

ABSTRACT OF THE DISSERTATION

From light to life: the energy conversion and storage in plants and algae

by YUAN ZHANG

Dissertation Director:

Dr. G. Charles Dismukes

Photosynthesis, the physico-chemical process converting sunlight into chemical energy, is the basis to feed the world and fuel the planet. To satisfy the growing demand for food and fuel, the efficiency of the natural photosynthesis needs to be optimized for maximum crop yield, while the photosynthetically assimilated carbon needs to be more sophisticatedly recruited for generating energy-dense renewable products. There are two objectives of this dissertation, the first is to explore the feasibility to boost biomass yield of crop plants by genetically engineering their photosystem II (PSII), and the second is to create robust microalgal transgenic strains with enhanced lipid content and CO_2 utilization efficiency, which will contribute to microalgal biofuel production as well as CO_2 mitigation.

In Chapter 2, we explore whether the prokaryotic design principal of PSII D1 subunit is applicable in a higher plant model *Nicotiana tabacum*. By introducing single point mutations into tobacco *psbA* gene (coding for the reaction center D1 subunit of Photosystem II) to mimic the cyanobacterial high-light and low-light D1 isoforms, the

tobacco mutants exhibit the biophysical traits of the prokaryotic PSII. The tobacco mutant expressing the engineered high light isoform exhibits higher photosynthetic efficiency, higher tolerance to photoinhibition and increased biomass production under the tested light conditions. The only benefit of incorporating the cyanobacterial low light mutation into tobacco D1 protein is restricted to improving the Water Oxidizing Complex catalytic efficiency at low light intensity, while the biomass yield was impaired at all the tested light conditions.

In Chapter 3, *Nannochloropsis oceanica* CCMP1779 (*N.o1779*), the emerging oleaginous model alga, is chosen for application of the "push and pull" strategy to enhance its lipid productivity by metabolic engineering. The regulatory importance of citrate synthase (CIS) in directing carbon flux towards protein synthesis pathway, and the functional role of glycerol 3-phosphate dehydrogenase (G3PDH) in diverting carbon precursors from glycolysis to TAG assembly are fully examined in the transgenic strains of *N.o1779*. Downregulation of a putative endogenous gene encoding CIS via RNA interference technology and expression of a yeast gene encoding the cytosolic G3PDH lead to higher accumulation of the storage lipid triacylglycerols (TAGs) and increased abundance of the lipid building block free fatty acids, advancing our understanding of the genetic and molecular basis of algal TAG metabolism.

In Chapter 4, the goal was to create a robust industrial strain that can be cultivated in the open culture using flue gas as carbon source. By applying insertional mutagenesis combined with high-throughput screening strategy to the oleaginous microalga *N.o1779*, a winning mutant was successfully identified for its advantages in photoautotrophic growth and intrinsic photosynthetic efficiency under both normal growth condition and

acidic environment. The genome sequencing project of this mutant currently in progress will potentially unlock the regulatory mechanism responsible for its beneficial phenotypes.

In summary, my dissertation advances the understanding of the PSII design principal and the central carbon metabolism in the oxygenic photosynthetic organisms. Novel genetic engineering strategies have also been developed throughout this dissertation to improve biomass productivity in a higher plant and enhance lipid productivity and carbon utilization in a eukaryotic microalga.

Acknowledgements

First and foremost, I want to express my deepest gratitude to my Ph.D. advisor, Dr. G. Charles Dismukes. The moment Chuck decided to accept me as a rotation student into the lab changed my whole education path and led me to the amazing fields of photosynthesis and bioenergy. Though setting very high scientific standards in the lab, Chuck has been providing me with the most professional mentorship and the strongest support, and patiently waiting me to grow up and become an independent researcher until the end of my Ph.D journey. Besides his professionalism and passion in science, Chuck's great sense of social responsibility as a true scientist will continue inspiring me in the next stages of my life and career. I would also like to thank my co-advisor, Dr. Pal Maliga, who trained me from scratch to do experiments in plant molecular biology and supervised me to lay a solid foundation of my primary Ph.D project. I also would like to thank the rest of my committee members: Dr. Debashish Bhattacharya and Dr. Jeff Boyd for their encouragement, warm help, and insightful suggestions to complete my thesis work.

Without the collaborations, supports, encouragements and friendship from my colleagues in several labs, much of the work in this thesis is impossible to be completed. I would like to thank all my lab mates past and present in Dismukes lab, Dr. Gennady Ananyev, Dr. Xiao Qian, Dr. Yunbing Ma, Dr. Colin Gates, Hoa Vu, Jonah Williams, Apostolos Zournas, Dr. David Vinyard, Dr. Anagha Krishnan, Dr. Kumaraswamy G. Kenchappa and Dr. Tiago Guerra in the bioenergy subgroup, and all the members in the chemistry subgroup. I also would like thank the two visiting undergraduate students, Endong Zhang and Haoran Shi from Jilin University for their assistance. I would like to

thank all my collegues in the Maliga lab, Dr. Zora Svab, Qiguo Yu, Dr. Tarinee Tungsuchat-Huang, Dr. Massimo Bosacchi and Dr. Csanad Gurdon. Outside of Rutgers, I would like to thank Dr. Christoph Benning and all the co-workers in his lab who were extremely friendly and helpful to me during my two months visiting in Michigan State University, especially Dr. Eric Poliner, Dr. Zhiyan Du and Tomomi Takeuchi for their further contribution to my thesis work. And I also would like to thank Dr. Jun Cheng and his student Dr. Hongxiang Lu from Zhejiang University in China for their efforts to push forward the application of microalgae in industry for biofuel production.

For the higher plant photosynthesis engineering project described in Chapter 2, I would like to thank Dr. Gennady Ananyev for his advices and technical support in the biophysical measurements, and the Waksman Greenhouse manager Marc Probasco for the set-up of plant growth experiments. The derived manuscript has been submitted to Nature Plants and suggested for revision.

For the two microalgal bioenergy projects described in Chapter 3 and Chapter 4, I would like to thank all my collaborators, Dr. Yunbing Ma, Dr. Gennady Ananyev, Hoa Vu and Jonah William from Dismukes lab and Dr. Eric Poliner, Dr. Zhiyan Du and Tomomi Takeuchi from Benning lab. Two derived manuscripts are *in prep*, and will be submitted soon.

I cannot be more grateful to anyone than my dearest parents, Fengzhen Qi and Qipeng Zhang, for their unconditional love, trust and support. They are the best parents in the world and the truly role models for me. They rarely care about personal gains and losses, while always being dedicated to making as much contribution as they can to the culture and education in China. There spirits will support me in all the future stages of

my life. I also want to give special thanks to my boyfriend, Dr. Jianli Cheng, who has accompanied me throughout this tough journey of Ph.D., tolerating all my bad tempers, but loving me as always.

Lastly, my doctoral work was supported by the Teaching Assistantship from the Chemistry Department in Rutgers, GCEP, and the Charles and Joanna Busch Predoctoral Fellowship from the Waksman Institute of Microbiology.

Dedication

To my amazing parents, Fengzhen and Qipeng, and my loving boyfriend, Jianli.

Table of Contents

List of Tables

List of Figures

Chapter 1. Introduction and background

1.1 Photosystem II and photochemical adaptation of the green lineage

1.1.1 Photosystem II

Photosystem II (PSII) is the main protein-pigment complex that converts sunlight to chemical energy in the oxygenic photoautotrophs, comprising all known species of cyanobacteria, algae, and higher plants (Vinyard et al., 2013a). The key components of the PSII complex include a peripheral antenna system, a reaction center (RC) core, the water oxidation complex (WOC) and a binding pocket for the reduction of plastoquinone (Govindjee, 2010). Following the light absorption by chlorophyll and other pigment molecules in the antenna complexes, the excitation energy in a photon was funneled to the PSII RC, powering the primary charge-separation reaction. The PSII RC photochemistry drives two chemical reactions: the oxidation of water into oxygen molecules and protons, which is catalyzed by WOC with an inorganic Mn_4CaO_5 cluster (equation 1a), and the reduction of plastoquinone (PQ) to plastoquinols (H_2PQ) (equation 1b) (Colin Gates, 2017; Govindjee, 2010; McConnell et al., 2010; Nishiyama & Murata, 2014; Nixon et al., 2010) .

$$2H_2O + 4h\nu \rightarrow 4e^- + O_2 + 4H^+_{lumen} \quad (1a)$$

$$2PQ + 4e^- + 4H^+_{stroma} \rightarrow 2PQH_2 \quad (1b)$$

The supercomplex of PSII is a dimer with a molecular mass of more than 600 kDa and comprises of distinct protein subunits (17 membrane proteins and 3 extrinsic

proteins), pigments (35 chlorophyll molecules, 2 pheophytin molecules and 12 carotenoid molecules), and cofactors (2 hemes, 1 non-heme iron, 2 (+1) quinones, 4 Mn ions, 1 Ca^{2+} ion and at least 1 Cl^- ion, and at least 25 lipids) (Colin Gates, 2017; Ferreira et al., 2004; Guskov et al., 2009; Loll et al., 2005; Sugiura et al., 2010b). While the extrinsic subunits of PSII may vary among phylogenetically and ecologically diverse photoautotrophs, the PSII RC including D1, D2, CP43, CP47 and cyt b_{559} is remarkably conserved, providing a single blueprint for solar energy conversion (Vinyard et al., 2013a). The D1/D2 (PsbA/PsbD) heterodimer make up the photochemical reaction center, ligating most of the redox active components of PSII, including the manganese cluster (Mn_4CaO_5) of WOC; CP43 (PsbC) and CP47 (PsbB) are the chlorophyll-binding antenna proteins that transfer excitation energy from the PSII peripheral antenna towards the photochemical reaction center; Cyt b559 (PsbE and PsbF) coordinates a heme group known to be redox-active over slow time scales, however its role remains vague in the PSII RC (A. Cramer & Kallas, 2016; Kaminskaya & Shuvalov, 2016; Thompson & Brudvig, 1988).

1.1.2 Natural D1 variants in cyanobacteria and eukaryotic phototrophs

Among the PSII core proteins, the only significant variation is observed in the cyanobacterial D1 subunit (Vinyard et al., 2013a). All eukaryotic oxygenic phototrophs contain a single D1 isoform, encoded in the chloroplast genome by two identical copies of the *psbA* gene in many green algae, and by a single *psbA* gene in higher plants (Mulo et al., 2009; Vinyard et al., 2013c). However, cyanobacteria typically have a small *psbA* gene family with one to six members that are differentially expressed according to the environmental cues (Mulo et al., 2009). In all cyanobacteria studied to date, four classes

of D1 isoforms ($D1_m$, D1:1, D1:2 and D1') have been identified, depending on their expressional pattern under acclimated growth conditions and upon stress (Mulo et al., 2012; Mulo et al., 2009). Most cyanobacterial species usually have one dominating D1 isoform under their normal growth environment, while the expression of other isoforms will be induced upon shifting to adverse or stressed conditions (Mulo et al., 2012). In an intensively studied cyanobacterial model organism *Synechococcus elongates* PCC 7942, the D1:1 isoform encoded by *psbAI* gene is expressed under low or moderate light conditions, while the stress-induced D1:2 protein encoded by *psbAII* and *psbAIII* is upregulated and preferentially incorporated into PSII when shifting to high light conditions (Campbell et al., 1996; Clarke et al., 1993a; Clarke et al., 1993b; Sane et al., 2002; Schaefer & Golden, 1989; Tichy et al., 2003). In another well-studied cyanobacterial model strain *Synechocystis* sp. PCC 6803, $D1_m$ encoded by the *psbA2* and *psbA3* genes is expressed under standard growth conditions, while D1' encoded by *psbA1* gene is upregulated under low O_2 or microaerobic conditions (Sicora et al., 2009; Summerfield et al., 2008). Further investigation of D1 protein in other cyanobacterial species including *Thermosynechococcus elongates* (Kos et al., 2008; Sander et al., 2010; Sugiura et al., 2010a; Sugiura et al., 2010b), *Gloeobacter violaceus*, (Sicora et al., 2008), *Anabaena 7120 and Synechococcus WH 780* (Garczarek et al., 2008) have revealed the presence of functionally distinct D1 proteins encoded by multiple *psbA* genes.

Cyanobacteria has evolved two strategies to cope with fluctuating light conditions in their natural habitat based on the regulation of *psbA* gene expression: 1) express a different D1 isoform under high light stress to replace the isoform present in the normal growth conditions; 2) increase the turn-over of the same D1 isoform upon light stress by

upregulating its expression (Mulo et al., 2012). However, the first strategy has been discarded by all known eukaryotic oxygenic phototrophs as they contain a single D1 isoform which is structurally and functionally most similar to the cyanobacterial D1:2 high light isoform (Mulo et al., 2009; Vinyard et al., 2013a; Vinyard et al., 2013c). To cope with potential damage caused by excess solar energy, plants evolved multiple mechanisms of photoprotection, which is discussed in the next section (Erickson et al., 2015; Murchie & Niyogi, 2011).

1.1.3 Photoprotection mechanisms in higher plants

The natural habitats of higher plants are highly variable in light conditions, from very high intensities in full sunlight (approximately 2000 μmol photons m^{-2} s^{-1}) to very dim light in heavily shaded conditions. These conditions can fluctuate rapidly on a time scale of seconds, days, seasons and the position of leaf within canopy (Erickson et al., 2015; Murchie & Niyogi, 2011). Absorption of excess solar energy can lead to generation of high level of reactive oxygen species (ROS) that can induce photo-oxidative damage to the photosynthetic apparatus, causing decreased efficiency and rate of photosynthesis (photoinhibition) (Erickson et al., 2015). To cope with potential damage caused by excess energy, higher plants have evolved multiple mechanisms of photoprotection, including avoiding excess light absorption, dissipating excess excitation energy, photochemical sinks for excess electrons, and efficient antioxidant systems to remove ROS (Murchie & Niyogi, 2011).

Many plants can position their leaves and optimize chloroplast movement in leaves to benefit light harvesting in low light and photoprotection in high light (Murchie

& Niyogi, 2011). Nonphotochemical quenching (NPQ) is a major mechanism of photoprotection via dissipating excess excitation energy harmlessly as heat. There are 3 types of NPQ in plants: energy-dependent feedback de-excitation quenching (qE) (Muller et al., 2001), zeaxanthin-dependent quenching (qZ) (Nilkens et al., 2010), and photoinhibitory quenching (qI) (Krause, 1988). In higher plants, qE depends on the formation of a proton gradient (ΔpH) across the thylakoid membrane, and is regulated by two well-characterized molecules: PsbS and zeaxanthin (Murchie & Niyogi, 2011). While the PSII protein PsbS functions as a sensor of lumen PH for activating quenching (Li et al., 2004), the role of zeaxanthin is still under discussion, either a direct quencher or an allosteric effector (Murchie & Niyogi, 2011). Besides its function in qE, zeaxanthin is also involved in qZ, the ΔpH-independent type of NPQ. Excess light activates violaxanthin de-epoxidase (VDE), which converts violaxanthin to zeaxanthin (Hieber et al., 2000). qI quenching is related to photoinhibition of PSII, which occurs when the rate of D1 photodamage outpaces the rate of its replacement and PSII repair. PSII photoinhibition-repair cycle protects the photosynthetic machinery by controlling electron flow to PSI, the photodamage of which is permanent if exceeding the capacity of its electron acceptors (Tikkanen et al., 2014).

There are also multiple electron transport pathways providing efficient sink for excess electrons produced by water splitting in PSII and reducing the risk of photodamage, including photorespiration, PSI cyclic electron transport and the Mehler reaction (water-water cycle) (Murchie & Niyogi, 2011). PSI cyclic electron flow (CEF) has two roles: adjusting the ATP/ NADPH ratio to meet the demands of carbon fixation by producing ATP only; increasing qE by elevating ΔpH. The predominant pathway of

CEF in flowering plants is the PGR5-dependent route (Shikanai, 2007). The water-water cycle is two molecules of water being produced from one molecule of O_2 at the reducing side of PSI using electrons striped from two molecules of water in PSII. This reaction not only helps avoiding ROS damage by removing superoxide and hydrogen peroxide, but also helps dissipating excess excitation energy in PSII and excess electrons in PSI (Murchie & Niyogi, 2011).

The photoprotective processes described above is essential to maintain survival, reproduction and fitness of plants. Elimination of photoprotection mechanism will make the plants less tolerant to high light stress and more easily to be photodamaged by excess solar energy. Arabidopsis mutants lacking essential protein or enzyme involved in the photoprotection mechanisms showed higher sensitivity to photoinhibition and lower fitness under fluctuating light conditions, e.g. mutant *npq4-1* lacking PsbS (Li et al., 2002), mutant *npq1* unable to convert violaxanthin to zeaxanthin (Niyogi et al., 1998), and the low-NPQ mutant *pgr5* (Munekage et al., 2002). Whereas the Arabidopsis mutants overexpressing the relevant protein may have improved photoprotection in adverse environments, e.g. PsbS-overexpressing mutant (Li et al., 2002).

Environmental stress like low CO_2, N deficiency and elevated O_2 pressure may influence the photoprotection. Kramer and co-workers found that, under conditions of low CO_2 (LC, 50 ppm CO_2 and 21% O_2) and limited electron acceptors (LEA, 50 ppm CO_2 and 1% O2), the sensitivity of qE can be increased by ~2-fold and ~6-fold, respectively, compared to that in the ambient conditions, indicating an increasing NPQ (Avenson et al., 2004). qE sensitivity is defined as the response of qE to linear electron flow (LEF) (Avenson et al., 2004). N deficiency in plant may lead to lower capacity of

carbon assimilation partially due to the limitations of synthesis of Rubisco enzyme (Terashima & Evans, 1988), which has similar effect on plant with low CO_2. Verhoeven and co-workers found that the N-deficient spinach exhibited increased thermal energy dissipation involving the xanthophyll cycle, measured as nonphotochemical fluorescence quenching (NPQ) (Verhoeven et al., 1997). Elevated O_2 pressure may result in inhibition of photosynthetic biomass accumulation due to illumination, because the accumulation of reactive oxygen species (ROS) inhibit the recovery of photodamaged PSII by suppressing the *de novo* synthesis of D1 and other photosynthetic proteins (Kolling et al., 2009; Kreslavski et al., 2007).

1.2 Microalgae for biofuels

1.2.1 Potential of microalgal biodiesel

Climate change and depletion of the finite fossil fuel resources are not only threatening the global energy security but also significantly contribute to the anthropogenic greenhouse gas (GHG) emissions, causing the most pressing environmental problem, climate change (Ahmad et al., 2011; Ottmar et al., 2011). Eco-friendly renewable energy offers the opportunity to secure energy supply, mitigate global warming, and reduce the negative effect of GHG on environment and human health (Ottmar et al., 2011). Among the various sustainable sources, photosynthetic organisms, the sunlight-driven cell factories that convert CO_2 into biomass and storage compounds, appear to be an important feedstock of biodiesel. Biodiesel is a mixture of fatty acid methyl esters primarily produced from vegetable oils obtained from agricultural crops (Du & Benning, 2016; Liang & Jiang, 2013). Replacing only 50% of the transport fuel with biodiesel in the United States will required at least 24% of arable land being recruited for the cultivation of oil crop (Chisti, 2007a). The “food vs. fuel” paradigm for the land-based-biofuel feedstocks can be possibly solved by including biofuels derived from aquatic microbial oxygenic photoautotrophs (AMOPs) into the bioenergy portfolio (Dismukes et al., 2008b).

AMOPs including cyanobacteria, algae, and diatoms are more efficient than land crops in converting sunlight to chemical energy. While the theoretical maximum conversion efficiency is about 4.6% for C3 plants and 6% for C4 plants, AMOPs can convert up to 9% of the received solar energy to chemical energy in the ideal conditions

(Chisti, 2013a; Chisti, 2013b; Dismukes et al., 2008b; Reich et al., 2018; Zhu et al., 2008), and double their biomass within 24 hours (Chisti, 2007a). More importantly, it is very common for many microalgal species to accumulate 20–50% of their dry biomass as triacylglycerols (TAG), an ideal precursor for making biodiesel by transesterification (Ma et al., 2017a; Zienkiewicz et al., 2017b). Under certain conditions like nitrogen deprivation, the lipid content of some oleaginous algal species can even reach 90% of their dry weight (Jr Metting, 1996; Liang & Jiang, 2013; Spolaore et al., 2006).

1.2.2 Strain improvement by metabolic engineering

While the world production of palm oil is nearly 40 million tons, with a market value of $0.52/L (Chisti, 2007a; Sun et al., 2011; Wijffels & Barbosa, 2010), the microalgal manufacturing infrastructure only enable ~5000 tons dry biomass production, yet with the estimated cost between $2.88/L-$3.52/L. Therefore, despite its potential as a promising alternate renewable source, some key improvements on microalgae must occur to minimize the cost before its successful commercialization for biofuel production, especially strain improvement for enhanced lipid content (Zhu et al., 2014a). Substantial accumulation of triacylglycerols (TAGs), the major precursor for biodiesel production, usually occurs when microalgae are exposed to environmental stresses, such as nutrient starvation, and high light illumination (Wijffels & Barbosa, 2010; Zienkiewicz et al., 2016a). However, the adverse environment will also reduce their proliferation and biomass productivity, leading to a decrease in the overall yield of lipid (Tan & Lee, 2016a).

Our current understanding on the genetic and molecular basis of algal TAG metabolism heavily relies on the knowledge obtained from higher plants (Zienkiewicz et al., 2016a). Therefore, advancing our knowledge of algal lipid accumulation mechanism by whole genome sequencing and genetic manipulation may open new opportunity of developing efficient strategies to induce lipid accumulation instead of imposing physiological stress (Wijffels & Barbosa, 2010). Among the 300 microalgal species identified by the US "Aquatic Species Program" as promising biofuel producers, full genome sequence is only available to a few species, such as *Thalassiosira pseudonan*a (Armbrust et al., 2004), *Phaeodactylum tricornutu*m (Bowler et al., 2008), *Nannochloropsis gaditana* (Radakovits et al., 2012), *Nannochloropsis oceanica* (Vieler et al., 2012), and *Chlorella vulgaris* (Guarnieri et al., 2018). Efficient transformation method and advanced molecular toolkit for genetic engineering are even more limited to algal species, probably due to the broad evolutionary diversity of microalgae (Walker et al., 2005). Removing such limitations in the future is crucial for rational strain development in oleaginous microalgae (Hlavova et al., 2015; Wei et al., 2017c).

Based on the general understanding of the central carbon metabolism and lipid metabolism in microalgae as shown in Figure 1.1, three different strategies of metabolic engineering have been developed so far to enhance the neutral lipid accumulation in microalgae with mixed results being achieved: 1) overexpressing enzymes involved in the fatty acid (FA) biosynthesis pathway; 2) overexpressing rate-limiting enzymes for TAG assembly; 3) partially blocking competing pathways (Liang & Jiang, 2013).

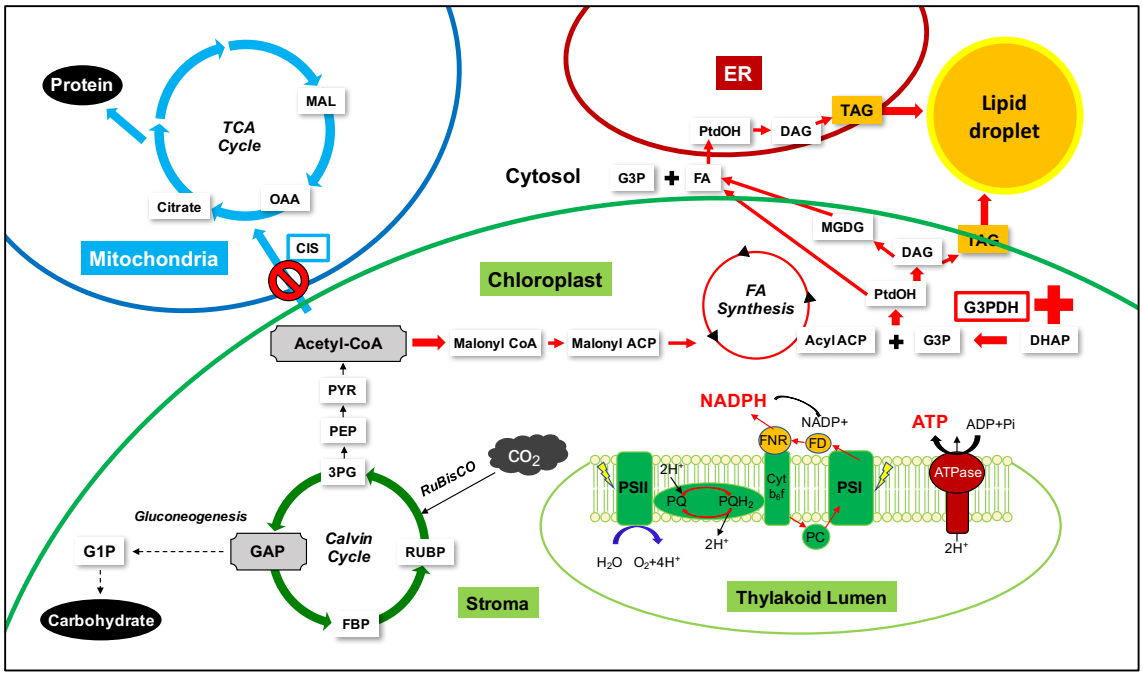

Figure 1.1 Simplified scheme of central carbon metabolism in microalgae.

The first strategy of metabolic engineering targeting the FA biosynthesis genes has shown to be inefficient to enhanced FA or TAG production. The first committed step of FA biosynthesis is catalyzed by acetyl-CoA carboxylase (ACCase), which diverts photosynthetic fixed carbon from the central carbon metabolism towards FA by catalyzing the formation of malonyl-CoA from acetyl-CoA. However, overexpression of ACCase in two transgenic diatoms, *Cyclotella cryptica* and *Navicula saprophila*, only led to increase in the enzymatic activity, but no improvement in FA production (Dunahay et al., 1996; Dunahay et al., 1995; Roessler et al., 1994; Roessler & Ohlrogge, 1993). Besides ACCase, another five genes involved in the FA biosynthesis have been investigated in *Haematococcus pluvialis*, a green microalga as a potential biodiesel feedstock. While the content of total FA has no significant change with the overexpression of any of these genes, the expressional level of acyl carrier protein (ACP), 3-ketoacyl-ACP-synthase (KAS), and acyl-ACP thioesterase (FATA) only led to marginal, if any increase in monounsaturated FA (MUFA) and polyunsaturated FA (PUFA) (Lei et al., 2012).

Compared to the targets in the FA biosynthesis pathway, genes involved in the downstream TAG assembly pathway have triggered more interest in general. Among the four enzymes involved in the TAG synthesis, including glycerol-3-phosphate dehydrogenase (G3PDH), lysophosphatidic acyltransferase (LPAAT), diacylglycerol acyltransferase (DGAT), and glycerol-3-phosphate acyltransferase (GPAT) (Griffiths & Harrison, 2009), the most successful attempt has been achieved by the amplification of diacylglycerol acyltransferase (DGAT), the crucial enzyme catalyzing the final and committed step of TAG synthesis. Though the overexpression of three DGAT

homologues genes in the model organism of green algae, *Chlamydomonas reinhardtii*, failed to enhance TAG accumulation (La Russa et al., 2012), it has been proved as a successful strategy in several oleaginous algal species. Genes encoding both type-1 and type-2 DGAT have been manipulated in *Nannochloropsis oceanica* strains. Wei et al reported that overexpression of type 1 DGAT in *Nannochloropsis oceanica* IMET1 promoted TAG accumulation in the transgenic strain by ~2.4 fold under nitrogen replete condition and by ~39% under nitrogen deplete condition (Wei et al., 2017b). In another *N. oceanica* strain CCMP1779 with 12 type-2 DGAT genes, Zienkiewicz et al reported that NoDGTT5 is the most promising target for engineering TAG synthesis among the 12 genes, and its overexpression in the transgenic line led to an 164% increase in the TAG content (Zienkiewicz et al., 2016a). In the same strain, overexpression of a different type-2 DGAT gene increased the cellular TAG content by 62.1% in the transgenic line (Li et al., 2016a). Another promising gene target is G3PDH, which supplies the fundamental glycerol backbone glycerol 3-phospate (G3P) for TAG assembly. By catalyzing the formation of G3P from dihydroxyacetone phosphate (DHAP), G3PDH is believed to channel the photosynthetic assimilates from the upper glycolysis pathway towards lipid biosynthesis in microalgae (Tan & Lee, 2016b). The overexpression of G3PDH in a diatom species *Phaeodactylum tricornutum* led to a 60% increase in neutral lipid content during stationary phase (Yao et al., 2014). Besides DGAT and G3PDH, the heterologous expression of the *Brassica napus* LPAAT driven by a promoter which is inducible by heat shock also resulted in an 44.5% increase in the total FA in the transgenic *Chlamydomonas reinhardtii* with treatment heat shock (Wang et al., 2018).

Based on the substrate competition hypothesis proposed by Sugimoto et al (Sugimoto et al., 1989), knocking down competing pathways, such as protein biosynthesis and starch biosynthesis, may also divert more metabolic fluxes to TAG biosynthesis (Liang & Jiang, 2013). It has been repeatedly observed in different microalgal species that the improved productivity of lipid induced either by genetic manipulation or stress conditions is always accompanied by decreased level of protein when data is available. Downregulation of two gene targets relevant to protein synthesis in microalgae have been proved as efficient strategies to benefit *De novo* FA synthesis by supplying abundant acetyl-CoA. The first gene target encodes Citrate synthase (CIS), which catalyzes the first step in the TCA cycle by condensing acetyl-CoA with oxaloacetate to generate citrate. Attempt to knockdown CIS has been made in the model green alga *Chlamydomonas reinhardtii* by Deng et al, resulting in a 169.5% increase in TAG content of the transgenic line (Deng et al., 2013b). The second target is phosphoenolpyruvate carboxylase (PEPC), which converts phosphoenolpyruvate (PEP) into oxaloacetate. However, PEP can also be converted into pyruvate, which can then be transformed by pyruvate dehydrogenase into acetyl-CoA for the anabolism of FA. The repression of PEPC has been found to increase the lipid content by 46.9% in a cyanobacterial species, *Anabaena* sp. (Hou et al., 2008).

Starch is another major sink for photosynthetic assimilated carbon. Attempts to block the starch biosynthesis pathway has been made in *Chlamydomonas reinhardtii* by downregulating ADP-glucose pyrophosphorylase (AGPase), which catalyzes the conversion from glucose 1-phoshate and ATP to ADP-glucose and Pi, the first committed step in this pathway (Li et al., 2010). A 10-fold increase of TAG in the transgenic strain

indicates the potential of this strategy to manipulate the lipid biosynthesis pathway (Li et al., 2010; Liang & Jiang, 2013).

To sum up, though numerous attempts have been made to manipulate individual key genes in several species of either conventional model algae or emerging oleaginous algae, only a few successes have been achieved to enhance their lipid productivity. It was recognized only recently that the key characteristics of oleaginous microalgae are inherently correlated and interact with each other, sometimes making the independent manipulation of single trait futile (Wang et al., 2012). The apparent conflicts between algal growth rate and lipid content is one of the examples.

In the future, applying genomic, transcriptomic and metabolomics analysis to more oleaginous algal species is important to advance our understanding on the complicated metabolic network and regulatory mechanisms underlying the microalgal lipid production. With more advanced molecular toolkits developed, the inter-trait crosstalk in microalgae can also be further investigated by simultaneous manipulation of multiple genes involved in different pathways (Wang et al., 2012).

1.2.3 Strain selection by random mutagenesis

In addition to the algae themselves, CO_2 is another major input for large-scale cultivation of microalgae for biofuel production (Wijffels & Barbosa, 2010). Production of 1 ton algal biomass requires 1.8 tons of CO_2, representing up to 60% of the costs along with nutrients, utilization (Kliphuis et al., 2010; Wijffels & Barbosa, 2010). Exhaust gases from power plants contribute to ca. 40% of the U.S. annual CO_2 emission in 2010 (Liu et al., 2013). Therefore, utilizing the flue gas from industrial plants to feed the microalgae in the raceway open pond could serve as an effective strategy not only to reduce costs but also to mitigate the release of greenhouse gas (Zhu et al., 2014a). Flue gases released from the power plants is composed mainly of 10-15% (v/v) CO_2, after the traces of harmful acid gases such as sulfur oxides and nitrogen oxides being removed by the post-combustion gas capture processes (Martelli et al., 2011; Wall, 2007; Zeiler et al., 1995). Compared to the limited CO_2 level in the natural habitat of the aquatic photosynthetic organisms, flue gas with substantially enriched CO_2 usually exert deleterious effects on growth and photosynthesis (Cheng et al., 2016a; Koberg et al., 2011; Solovchenko & Khozin-Goldberg, 2013). All cyanobacteria and most eukaryotic algae rely inorganic carbon concentrating mechanisms (CCMs) to elevate the CO_2 concentration near the Rubisco enzyme for fixation (Jungnick et al., 2014; Raven, 2010). It is believed that CCM was evolved by the aquatic phototrophs to adapt to the declined atmospheric CO_2 level on earth over the past 30 million years (Jungnick et al., 2014; Raven et al., 2011). Therefore, the majority of microalgae will be saturated with 2-5% CO_2 (Solovchenko & Khozin-Goldberg, 2013). While more efforts have been dedicated to investigate the mechanism and function of CCM in diverse microalgal species under

low CO_2 environment, the underlying mechanism responsible for tolerance to elevated CO_2 levels are still poorly understood (Solovchenko & Khozin-Goldberg, 2013). It is believed that maintaining the cellular pH homeostasis is critical for the microalgae's tolerance to the flue gas supplied environment, which is not only enriched with dissolved inorganic carbon (DIC), but also substantially acidified (Solovchenko & Khozin-Goldberg, 2013). To prevent acidification of the cytoplasm and chloroplast stromal compartment under such conditions, microalgae may developed several mechanisms including: photosynthetic apparatus state transitions that increase ATP generation; upregulation of H+-ATPases pumping protons out of the cell; rapid shutdown of CCM, and adjustment of membranes' FA composition (Solovchenko & Khozin-Goldberg, 2013).

Due to the limited knowledge on physiological effects and mechanisms of high-CO_2 tolerance in microalgae, it's very difficult to modify the wild strain for flue gas cultivation by reverse mutagenesis with sophisticatedly chosen gene targets. Therefore, attempts on forward mutagenesis of oleaginous microalgae and mutant screening have been inspired to isolate promising strain exhibiting tolerance to elevated CO_2 level, which is suitable for industrial application. Some successful attempts have been made in several microalgal species to isolate random mutants showing enhanced flue gas tolerance as well as advantages in growth and lipid productivity. By applying the random mutagenesis strategy of γ irradiation from ^{60}Co or ^{137}Se on several microalgal species including *Chlorella pyrenoidosa*, *Chlorella* sp., and *Spirulina* sp., Cheng and his colleagues have generated random mutant library for each species and been able to isolate winning strains

that can not only outcompete the wild strains under air bubbling conditions, but also tolerate up to 15% CO_2 (Cheng et al., 2013; Cheng et al., 2017; Cheng et al., 2016b).

Random mutagenesis has been proved to be an efficient approach to rapidly developing new strains with novel phenotypes. However, the radiation mutagenesis as mentioned above and another widely used strategy chemical mutagenesis usually induces multiple point mutations, making the identification of the mutated gene(s) responsible for the observed phenotype complicated and laborious (Perin et al., 2015b). From this perspective, the insertional mutagenesis approach using a drug resistance cassette offers many advantages in terms of greater control of the number of genes mutated, the density of mutations (alleles) and ease of identification of the locus of insertion. Recently, a robust strategy for high-throughput genotyping of the random mutant library has been developed for *Chlamydomonas reinhardtii* (Zhang et al., 2014). The *Mme*1-based insertion site sequencing (MmeSeq) can massively identify the mutation site of thousands random mutants by the 20-21 bp sequences immediately flanking the insertional cassettes (Li et al., 2016b; Zhang et al., 2014). This mapping strategy developed for *C. reinhardtii* can be adapted for more industrial relevant strains with available transformation protocol and holds great promise to unlock the regulatory mechanism responsible for the high CO_2 tolerating phenotype in the screened mutants.

Chapter 2. PSII engineering inspired by cyanobacterial design enhances photosynthesis in higher plants

Summary

The D1 polypeptide of the photosystem II (PSII) reaction center complex encodes domains that regulate the yield of primary photochemistry. All eukaryotic oxygenic phototrophs (algae and higher plants) encode a single isoform of D1 that functions at all light intensities, while many prokaryotic oxygenic phototrophs contain two or more D1 isoforms that are differentially expressed in response to changes in solar intensity. D1:1 and D1:2 confer functional advantages for growth at low or high light intensities, respectively. Here we report that the *Synechococcus* high light mutation (HL, A152S) in the tobacco D1 protein increased PSII primary charge separation yield, resulting in 11% increase in fresh weight and 9.9% increase in dry weight. The low light mutation (LL, E130Q) improved the efficiency of water oxidation, but this photonic improvement did not yield more biomass at low light. Replacement of the plastid *psbA* gene with the engineered form was achieved by selection for the spectinomycin resistance conferred by the *aadA* gene. This marker gene was subsequently removed to eliminate potential metabolic burden imposed by *aadA* expression. Our findings indicate that at all light intensities increasing charge separation yield and photochemical conversion produces more biomass in a higher plant, and that photosynthetic designs from prokaryotic phototrophs can be employed to improve the productivity of crop plants.

2.1 Introduction

The improvement of primary productivity of terrestrial crops used for agriculture and energy (biomass) has a long history of advances based on plant breeding and, more recently, genetic engineering. This strategy has recently been applied to improving the primary light energy capture in the antenna complex of a higher plant model (Kromdijk et al., 2016), but has not yet been demonstrated for conversion of captured light energy into chemical energy (charge separation) in reaction centers.

Photosystem II (PSII) is the main protein-pigment complex that converts sunlight to chemical energy in all oxygenic phototrophs by splitting water in the Mn_4CaO_5 water-oxidizing complex (WOC) and reducing plastoquinone (PQ) to plastoquinols (H_2PQ) (Nishiyama & Murata, 2014; Nixon et al., 2010). The D1 protein is one of six core polypeptides that make up the PSII reaction center performing the primary photochemistry of light-driven charge separation and water oxidation (Mulo et al., 2009). While the photosynthetic apparatus of prokaryotic oxygenic phototrophs evolved multiple D1 isoforms to optimize photosynthetic efficiency under different light conditions, this mechanism was discarded by all eukaryotic oxygenic phototrophs as they contain a single D1 isoform. Photoprotection at high light intensities in algae and higher plants relies upon other mechanisms to function efficiently (Erickson et al., 2015; Murchie & Niyogi, 2011). In the model organism *Synechococcus elongatus* PCC 7942, D1:1 encoded by *psbAI* gene is expressed under low or moderate light conditions, while D1:2 encoded by *psbAII* and *psbAIII* is upregulated and preferentially incorporated into PSII when shifting to high light conditions (Schaefer & Golden, 1989). The plastid genome of green algae and higher plants carries a single *psbA* gene encoding the high

light D1 isoform, which is structurally and functionally most similar to the D1:2 isoform in cyanobacteria.

Evolutionary conservation of the PSII D1 subunit enabled experimental replacement of the native D1 protein in *Chlamydomonas reinhardtii* with the *Synechococcus elongatus* 7942 D1 isoforms (Vinyard et al., 2013c; Vinyard et al., 2014). The *Synechococcus* D1:1 isoform in *Chlamydomonas* showed a functional advantage when cells were grown in low light, whereas the D1:2 isoform had higher photosynthetic efficiency and biomass yield when cultures were grown at high light. The D1:1 isoform, encoded by *psbAI* gene, and the D1:2 isoform, encoded by *psbAII* and *psbAIII* genes, differ by 25 out of 360 amino acids (Golden et al., 1986; Holtman et al., 2005) (GenBank Accession No. NC_007604.1). To determine which amino acid residues contribute to the functional properties of the two isoforms, (Vinyard et al., 2014) analyzed seven *Chlamydomonas* strains carrying one, two or three amino acid substitutions in the high-light D1:2 protein which are unique to the D1:1 low-light isoform. The E130Q point mutation converted the high-light isoform into a low-light functional isoform. Glutamate (E) occupies site D1-130 in high-light D1:2 isoforms in all cyanobacteria as well as in green algae and higher plants, whereas glutamine (Q) is highly conserved at site D1-130 in the D1:1 low-light isoform of cyanobacteria. The D1-130 residue hydrogen bonds to Pheophytin (Phe), an electron transport co-factor in the PSII reaction center, and the presence of E or Q significantly affects the midpoint potential of Phe (Mulo et al., 2009). In contrast, the A152S mutation in the D1:2 protein confered substantially greater photoprotection at high light intensity (Vinyard et al., 2014). Thus, primary charge separation and charge recombination rates are traded-off between the D1:1 and D1:2

isoforms in the PSII reaction center, and are most sensitively correlated with the amino acid residues at positions 130 and 152.

To test if the functional role of E130Q and A152S amino acids is conserved in higher plants, we introduced these point mutations at a cognate position in the tobacco D1 sequence. We isolated homoplastomic transgenic tobacco plants and tested for primary light energy conversion in whole leaves (PSII charge separation and water oxidation), whole plant growth rate and biomass yield. Our findings indicate that increased photosynthetic charge separation rate results in more biomass, and that the photosynthetic designs of prokaryotic phototrophs, the evolutionary precursors to higher plants, can be employed to improve the productivity of crop plants.

2.2 Material and Methods

2.2.1 Construction of transformation vectors

The pYZ14 and its two derivatives pYZ15 and pYZ16 were constructed as plastid transformation vectors. Plasmid pYZ14 derives from pYZ4, the synthetic tobacco ptDNA fragment containing *psbA*, *trnH*, *rpl2* and *rpl23*, cloned in the BlueHeron pUC minus vector. Plasmid pYZ14 is a pYZ4 derivative into which the excisable *aadA* gene flanked by 215 bp *attP* and 54 bp *attB* has been introduced into the *Stu*I site. pYZ15 carries a point mutation replacing glutamate with glutamine at position 130 of D1 protein (E130Q), while in pYZ16, alanine is replaced by serine at position 152 (A152S).

The c-myc tagged *aadA* marker gene is expressed in a cassette with the PrrnLatpB+DB promoter and His/Thre attenuator. The *aadA* expression cassette is flanked by directly oriented non-identical bacterial *attB* (54 bp) and phage *attP* (125 bp) attachment sites (Kittiwongwattana et al., 2007). Since AAD content is found to vary considerably with leaf age, leaf material for soluble protein isolation was taken from the first fully expanded true leaf of 30-days plantlets. On the Coomassie brilliant blue R250 stained SDS-PAGE gel, two extra bands near 32 kDa were present in Nt+*aadA,* Nt^{HL}+*aadA* and Nt^{LL}+*aadA* lines, while being absent in the soluble protein of Nt-WT tobacco leaves (**Fig. 2.2 A**). The dense higher band and the faint lower band are every close to each other, and together account for ~7% of the total soluble cellular protein. It is confirmed by the immunoblot analysis probing with c-Myc antibody that both bands are AAD protein (**Fig. 2.2 B**).

The transformation vectors carry a 3588 bp synthetic DNA fragment as plastid targeting sequence including a 1741 bp synthetic segment encoding *psbA* variant gene as

the left targeting region (LTR) and a 1847 bp synthetic segment encoding *trnH*, *rpl2* and *rpl23* as the right targeting region (RTR). A selectable spectinomycin resistant marker gene (*aadA*) is flanked by the LTR at the 5' end and the RTR at the 3' end. Besides the single amino acid substitution in the variant *psbA* gene, silent mutations were also made on the *psbA* gene and the *rpl2* gene of the transformation vector to provide restriction markers differentiating the synthetic vector DNA from the wild-type plastid DNA, as well as improve DNA handling convenience. 6 restriction sites in the *psbA* gene and 6 restriction sites in the coding region of *rpl2* gene were removed by silent mutations.

In the transplastomic clones with *aadA* insertion, the *psbA* point mutation carried in the transformation vector may or may not be incorporated into the plastid genome, depending on the sites of homologous recombination (**Fig. 2.1 A**). Transgenic lines carrying the point mutation were first screened by diagnostic digestion of *psbA* amplicons and then confirmed by sequencing. Transgenic lines expressing different D1 variants were successfully obtained: control line Nt+*aadA* expressing native tobacco D1 protein; Nt^{LL}+*aadA* expressing the mutated low-light (LL) D1 isoform encoded by a synthetic *psbA* gene with E130Q point mutation; and Nt^{HL}+*aadA* expressing the engineered high-light (HL) D1 isoform encoded by a synthetic *psbA* gene with A152S point mutation (**Fig. 2.1**).

Altogether 20 transplastomic events were obtained. The presence of restriction markers flanking the point mutation in the synthetic *psbA* gene predicted the incorporation of point mutation in the plastid genome, which was subsequently confirmed by sequencing PCR-amplified ptDNA. By DNA sequencing, it was found that the E130Q point mutation was present in one of four transplastomic events, and the A152S point

mutation was present in four of eight independent events, where recombination took place at the LTR site distal to *aadA* gene. Interestingly, none of the clones derived from the 20 transplastomic events carried the synthetic RTR.

Uniform transformation of the plastid genome was confirmed by DNA gel blot analysis, probing with the *psbA* probe (**Fig. 2.1 B**). In *Acc*I digested total leaf DNA of Nt-WT, a 1.6 kb and a 0.5 kb fragment were detected. In transplastomic clones with *aadA* insertion, the *psbA* probe can detect either one fragment of 3.7 kb or two fragments which are 3.2 kb and 0.5 kb respectively, depending on where the homologous recombination took place. The homoplastomic marker gene control, low-light (LL) and high-light (HL) tobacco mutants were successfully achieved.

2.2.2 Plastid transformation

Plastid transformation was carried out by the biolistic protocol, as previously described (Lutz et al., 2006; Svab & Maliga, 1993). Briefly, sterile *Nicotiana tabacum* leaves were bombarded with gold microprojectiles coated with pYZ14, pZY15 and pYZ16 vector DNA respectively by the PDS-1000 biolistic gun (Bio-Rad, Hercules, CA, USA). Transplastomic clones were selected by spectinomycin resistance manifested as formation of green shoots on the selective RMOP plant regeneration medium containing 500 mg/l spectinomycin dihydrochloride. Leaf pieces from the primary shoots were applied for the first round of purification by regenerating secondary shoots on the selective RMOP medium containing 500 mg/l spectinomycin dihydrochloride. Leaf sections of the secondary shoots were transferred to for the second round of purification by shoot regeneration on the spectinomycin selective medium. Uniform transformation of

the plastid genome in the resulting shoots from the second purification was confirmed by DNA gel blot analysis of total leaf DNA. The homoplastomic plants were rooted on RM plant maintenance medium in sterile culture and transferred to greenhouse later.

2.2.3 DNA gel blot analysis of ptDNA

DNA gel blot analysis was carried out as described (Svab & Maliga, 1993). Total cellular DNA extracted from tobacco leaf was digested with the restriction endonuclease *Acc*I. The DNA fragments were separated by electrophoresis in 1% agarose gel and transferred to Hybond-N membranes (GE Healthcare, Piscataway, NJ) by capillary transfer. A double-strand DNA probe was prepared by random-primed ^{32}P-labeling. The template for probing is a 3584 bp *Kpn*I-*Sac*I fragment prepared from the targeting region. Hybridization with the probe was carried out in Church buffer at 65 ^{o}C for overnight.

2.2.4 Agrobacterium-mediated transformation of the plant nucleus with the *int* gene

A binary plasmid pKO117 carrying an engineered integrase gene (*int*) that can be expressed in the plant nucleus is available in the Agrobacterium strain EHA101 (Kittiwongwattana et al., 2007; Lutz et al., 2004). Leaf pieces of the Nt+*aadA,* Nt^{LL}+*aadA* and Nt^{HL}+*aadA* transplastomic plants were co-cultivated with Agrobacterium carrying binary plasmid pKO117 for two days, then transferred onto RMOP medium containing 100 mg/l gentamycin and 500 mg/l carbenicillin (Kittiwongwattana et al., 2007). The shoots can only regenerated on the selective medium if transformed with the gentamycin resistant plant marker gene (*aacC*I) linked to the *int* gene carried in the

pKO117 plasmid (Kittiwongwattana et al., 2007). Carbenicillin was supplied for killing the Agrobacterium.

2.2.5 Antibiotic resistance in seed progeny

Seeds were sterilized with 20% bleach in a 1.5ml Eppendorf tube for 5 minutes. Bleach was discarded and seeds were rinsed 3 times with deionized water. Surface-sterilized seeds were plated onto RM solid medium containing 500 mg/l spectinomycin and incubated in the culture room.

2.2.6 SDS-PAGE and immunoblotting

SDS-PAGE and immunoblotting were carried out to detect the expression level of the *psbA* gene and the c-Myc tagged spectinomycin resistance marker gene (*aadA*). Leaves for protein extraction were taken from greenhouse plants 30 days post germination. About 200 mg leaf was used for total soluble protein and membrane-bound protein extraction as described (Kittiwongwattana et al., 2007). Briefly, leaf was homogenized in 0.1 ml Extraction Buffer containing 50 mM Hepes/KOH (pH 7.5), 10 mM potassium acetate, 5 mM magnesium acetate, 1 mM EDTA, 10 mM DTT and 2 mM PMSF. After centrifugation, total soluble protein went into the supernatant, while insoluble membrane-bound protein precipitated into the pellet. Insoluble protein was solubilized from the pellet by adding 0.1 ml Solubilization Buffer containing 50 mM Hepes/KOH (pH 7.5), 2% sodium dodecyl sulfate (SDS) and heating for 10 min at 95 ^{o}C. The insoluble cell debris was then removed by centrifugation. Soluble protein concentrations were quantified with the Bradford Protein Assay Reagent kit (Bio-Rad,

Hercules, CA); membrane-bound protein were determined by the bicinchonic acid (BCA) method (Pierce, Rockford, IL).

Protein were separated by SDS-PAGE (15% acrylamide gel) and stained in Comassie brilliant blue R-250 solution. Immunoblot analysis of D1 protein and aminoglycoside 3''-adenylyltransferase (AAD) was carried out as described using commercial D1 C-Term antibody (1:11,000) purchased from Agrisera Antibodies (Sweden) and c-Myc antibody (1:1,100) purchased from Santa Cruz Biotechnology, Inc. (Santa Cruz, CA).

2.2.7 RNA gel blot analysis

RNA gel blot was carried out as described (Silhavy & Maliga, 1998; Sinagawa-Garcia et al., 2009). Briefly, total cellular RNA was extracted from leaves (Stiekema et al., 1988) and 5 mg RNA was electrophoresed on 1% agarose/formaldehyde gels, and then transferred to Hybond-N membranes (GE Healthcare, Piscataway, NJ) by capillary transfer. Hybridization to random-primed labeled fragment was carried out in a modified Church hybridization buffer (0.5 M phosphate buffer, pH 7.2, 10 mM EDTA, 7% SDS) at 65 ^{o}C for overnight. Radioactive probes were prepared by random primed ^{32}P-labeling of PCR amplified DNA fragments of *psbA* gene and *aadA* gene.

2.2.8 Fast Repetition Rate (FRR) Fluorometry

FRR fluorometry measurements were performed on a home-built instrument as described previously (Ananyev & Dismukes, 2005). Tobacco plants were grown in the greenhouse, where the natural sunlight was supplemented with sodium lights for 16 hours

(about 0 to 700 μE m^{-2} s^{-1}). 6 mm leaf disc sampled from 60 days old tobacco were dark-adapted for 2 min and then subjected to 50 single turnover flashes (STFs) applied at 0.5-100 Hz. The Chl-a variable fluorescence yield, Fv/Fm, was measured on each STF using 60 μs pulses at 656 nm. Fv/Fm was calculated from the dark-adapted value (Fo) and the light-saturated value (Fm) from each flash in the train of flashes, with Fv = Fm – Fo.

2.2.9 Isolation of thylakoid

Thylakoid membranes were isolated from tobacco using a modified method by Robinson *et al* (Robinson & Yocum, 1980) and Ünnep et al (Ünnep et al., 2014). Tobacco plants were grown in the greenhouse under natural sunlight conditions for 45 days. 20 g of tobacco leaves were ground using a blender in 200 ml chilled Homogenization Buffer containing 20 mM Tricine (pH 7.6), 5 mM $MgCl_2$, 5 mM KCl, and 0.4 M sorbitol. The homogenate was filtered through 2 layers of miracloth. After removing the remaining debris by centrifugation at 200 xg for 2 min, the supernatant was centrifuged at 4000 xg for 10 min. The chloroplast pellet was resuspended using a soft paintbrush in 10 ml chilled osmotic shock medium containing 20 mM Tricine (pH 7.6), 5 mM $MgCl_2$, and 5 mM KCl. The suspension was then centrifuged at 4000 xg for 10 min to spin down the thylakoids. The resulting pellet was washed twice with 4 ml chilled Homogenization buffer (4500 xg, 10 min) and then resuspended in Storage Buffer containing 20 mM Tricine (pH 7.6), 5 mM $MgCl_2$, 5 mM KCl, and 10% (v/v) glycerol. The thylakoid suspension was flash-frozen in liquid nitrogen at ~2 mg/ml of Chl/ml by dilution with the Storage Buffer. Thylakoid samples were kept at -80 °C prior to assay. All steps were carried out at 4 °C under dim green light.

2.2.10 O_2 evolution rates

Steady-state O_2 evolution rates from thylakoid membrane were measured using a commercial Clark-type electrode (Hansatech) at 25 ^oC as previously described (Vinyard et al., 2013c). Isolated membrane was diluted to 400 μg of Chl/ml. Freshly prepared 2 mM $K_3Fe(CN)_6$ and 0.25 mM DMBQ were added immediately before each experiment began. Continuous saturating illumination was provided by a red LED (600 μE m^{-2} s^{-1}, λ_{max} = 627 nm). O_2 evolution rates were measured as μmol of O_2 (mg of Chl)$^{-1}$ h^{-1}.

2.2.11 Photoinhibition

Sensitivity to photoinhibition was determined by temporal tracking of Fv/Fm losses during exposure to 700μE m^{-2} s^{-1} light intensity over a period of 60 hours in the presence of 1 g/L lincomycin. the chloroplast protein synthesis inhibitor as described by Tyystjarvi et al (Tyystjarvi & Aro, 1996). Seeds from Nt-WT and transgenic lines were germinated in soil and grown for 50 days in the greenhouse. The leaves were harvested at the end of the dark period and incubated in darkness for 6 hours in lincomycin solution. In some case, water was used instead of lincomycin as indicated. After the dark incubation, tobacco leaves were illuminated by a 2000 μE m^{-2} s^{-1} light source in a 22 ^oC chamber. The tobacco leaves were in the lincomycin solution during the whole illumination period. The actual light intensity received by the tobacco leaves was 700 μE m^{-2} s^{-1} and the temperature of the illuminated leaves was around 27 ^oC. During the illumination, 6 mm disc were taken from the leaves for fluorescence measurements. The leaf discs were dark adapted for 1 hour, after which Fv/Fm was measured by a

commercial PAM fluorometer (Photon Systems Instruments, Brno, Czech Republic). This process was repeated over a 60-hour period. The decreasing values of Fv/Fm over time were fit to a one-component exponential function.

2.2.12 Biomass accumulation measurement

For the greenhouse full sunlight growth assay, tobacco seed were sown in the green house. Seed germination was synchronized by storing wet seed for three days at +4 ^{0}C prior to planting. The seed was spread on soil and allowed to germinate in 2” deep plastic trays (12’x12’). 20 days post-planting (dpp) seedlings were transferred to cells (54 per 1’ x 2’ plastic trays) and grown under normal greenhouse conditions, when the natural light was supplements with sodium lights for 16 hrs (about 700 μE m-2 s-1). After 30 dpp, seedlings were transferred to 5’x5’x5’ plastic pots and grown until harvesting for fresh and dry weight measurement. After 60 dpp, dry weight of 15 plants of Nt-WT and each transgenic line were measured.

For the low light growth assay, tobacco seed were germinated on soil in a growth chamber under 40 μE light intensity at 22C. After 30 dpp, seedlings were harvested for fresh and dry weight measurement.

2.2.13 Statistics

Data are presented as mean ± s.e.m. The significance between data sets was measured using two-tailed unpaired Student's t-test. P values were not considered significant when $P > 0.05$ and significant when $P < 0.05$ and $P < 0.01$.

2.3 Results

2.3.1 Incorporation of the point mutations in the *psbA* gene

We constructed dedicated vectors to replace the native *psbA* gene with mutant forms. In the control plasmid pYZ14, the selectable spectinomycin resistance gene (*aadA*) is cloned downstream of the *psbA* gene, so that insertion of *aadA* is targeted *via* the *psbA* coding region (left targeting region, LTR) and the plastid DNA fragment encoding the *trnH*, *rpl2* and part of the *rpl23* genes (right targeting region, RTR) (**Fig. 2.1 A**). Vector pYZ15 carries the E130Q amino acid exchange that confers low light adapted photochemistry, while vector pYZ16 carries the A152S point mutation conferring high light beneficial photochemistry. The plastid transformation vectors were introduced into tobacco leaves by the biolistic process and transplastomic clones were selected by spectinomycin resistance. Spectinomycin resistance was obtained as the result of incorporation of the *aadA* gene downstream of *psbA* via the targeting LTR and RTR regions. The transplastomic *Nicotiana tabacum* (Nt) plants were designated by the plasmid name and a serial number, such as Nt-pYZ14-3.

Integration of *aadA* may occur at any place via the LTR and RTR regions. Recombination via the L1 site distal to *aadA* results in the incorporation of point mutations in the *psbA* gene, while recombination proximal to *aadA* (L2 site) introduces the *aadA* marker gene, but not the point mutations (**Fig. 2.1 A**). Identification of plants carrying the A152S mutation (pYZ16 vector) was simple, because the amino acid exchange creates a novel *Pvu*II site that could be readily identified by digesting PCR-amplified ptDNA. The E130Q amino acid exchange (pYZ15) does not create a novel

restriction site. To facilitate tracking of incorporated DNA, we introduced 12 silent mutations in the LTR and RTR of the vectors. Transplastomic plants potentially carrying the E130Q mutation were identified by the presence of adjacent *Alw*NI- (site removed in vector) and *Ssp*I+ (site created in vector) restriction sites in vector pYZ15. Incorporation of the E130Q mutation in the *psbA* gene was confirmed by sequencing PCR-amplified DNA.

Uniform transformation of plastid genomes was confirmed by DNA gel blot analyses (**Fig. 2.1 B**) and uniform spectinomycin resistance of the seed progeny (not shown). We then grew plants to assess changes conferred by mutations in the engineered D1 proteins by measuring biomass and characterizing photochemical properties. Lines with wild-type *psbA* are referred to as Nt+*aadA* (for control), and those carrying the LL (E132Q) or HL (A152S) mutations as Nt^{LL}+*aadA* and Nt^{HL}+*aadA* lines. This designation applies when the *aadA* marker gene is present. When *aadA* has been removed, +/-*aadA* is used as an extension instead, such as Nt+/-*aadA*.

Figure 2.1 Construction of tobacco plants with *psbA* mutations. A) Map of the targeted region of the plastid genome (Nt-ptDNA) included in the plastid transformation vectors, and the targeting regions of plastid transformation vectors. Note the *psbA, trnH, rpl2, and rpl23* plastid genes; the *aadA* spectinomycin resistance gene and *attB*/*attP* sites (black boxes) for the excision of *aadA* gene. The pYZ14, pYZ15 and pYZ16 vectors carry a wild type *psbA* gene, and its low light E130Q and high light A152S variants, respectively. L1 and L2 are alternative sites for homologous recombination in the left targeting region (LTR); R denotes one of the potential recombination sites in the right targeting region (RTR). Recombination via L1 and R results in the incorporation of the *psbA* point mutations. Recombination via L2 and R incorporates only the *aadA* gene but not the point mutations in *psbA*. On top are shown the restriction sites by which the vector DNA can be distinguished from native ptDNA. **B)** DNA gel blots to confirm uniform transformation of plastid genomes. Total cellular DNA was digested with the *Acc*I restriction endonuclease and probed with the *psbA* coding region and part of the *psbA*-*trnH* intergenic region marked in Figure 2.1 A.

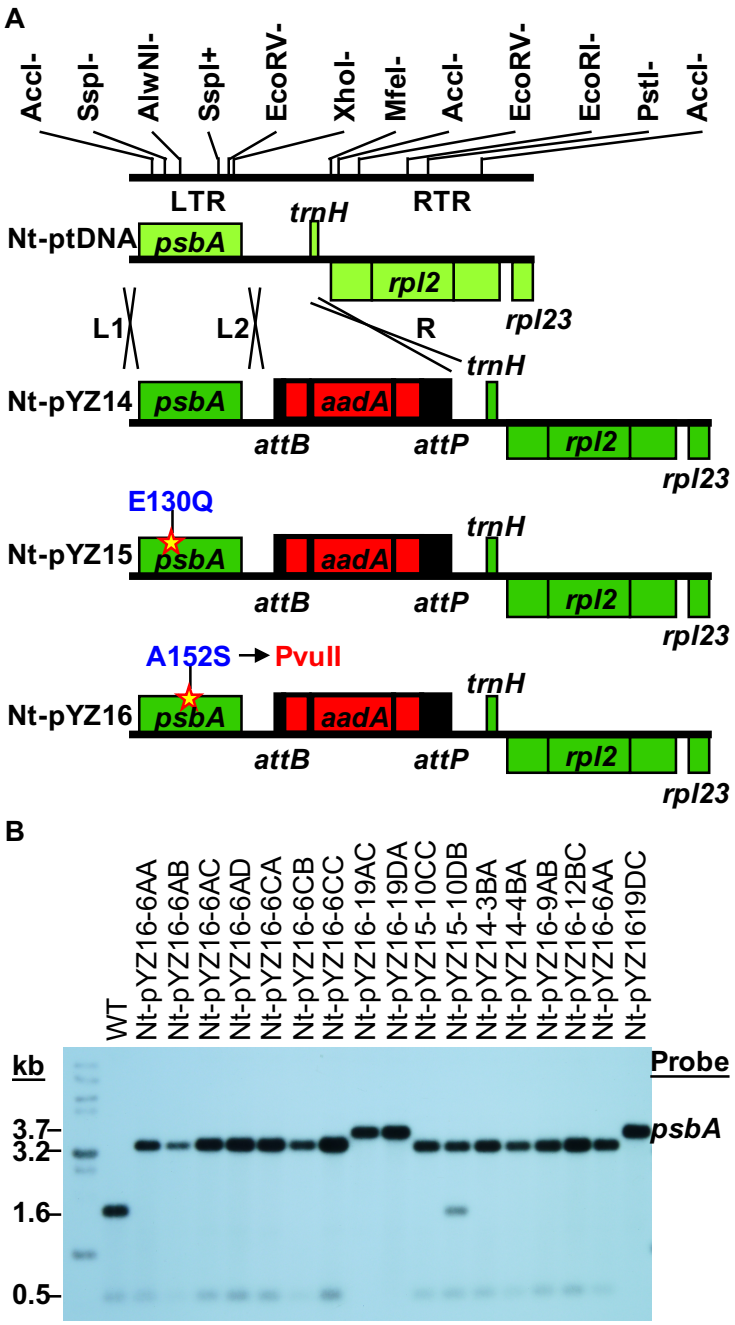
A
AccI-
SspI-
AlwNI-
SspI+
EcoRV-
XhoI-
MfeI-
AccI-
EcoRV-
EcoRI-
PstI-
AccI-
LTR
RTR
trnH
Nt-ptDNA
psbA
rpl2
rpl23
L1
L2
R
trnH
Nt-pYZ14
psbA
aadA
attB
attP
rpl2
rpl23
E130Q
trnH
Nt-pYZ15
psbA
aadA
attB
attP
rpl2
rpl23
A152S → PvuII
trnH
Nt-pYZ16
psbA
aadA
attB
attP
rpl2
rpl23
B
WT
Nt-pYZ16-6AA
Nt-pYZ16-6AB
Nt-pYZ16-6AC
Nt-pYZ16-6AD
Nt-pYZ16-6CA
Nt-pYZ16-6CB
Nt-pYZ16-6CC
Nt-pYZ16-19AC
Nt-pYZ16-19DA
Nt-pYZ15-10CC
Nt-pYZ15-10DB
Nt-pYZ14-3BA
Nt-pYZ14-4BA
Nt-pYZ16-9AB
Nt-pYZ16-12BC
Nt-pYZ16-6AA
Nt-pYZ1619DC
kb
Probe
3.7
3.2
1.6
0.5
psbA

2.3.2 Transplastomic plants are impaired in growth and development

We evaluated the impact of D1 mutations by growing wild type (Nt-WT), and transplastomic tobacco carrying *aadA* genes in the greenhouse. The plants were grown under three light conditions: normal greenhouse conditions, when the natural sunlight was supplemented with sodium lights for 16 hours (about 60 to 700 $\mu E\ m^{-2}\ s^{-1}$) and under shading nets with 50% and 90% cutoff. Delay in plant growth and flowering were observed in all transgenic lines compared to Nt-WT. Among the three transplastomic lines, the Nt^{HL}+*aadA* high-light plants yielded he highest biomass, followed by the Nt+*aadA* control and Nt^{LL}+*aadA* low-light plants. Under normal greenhouse conditions, Nt-WT flowered in 68 days. The transplastomic plants developed slower: the control plants and the high-light plants flowered in 72 days, while the low-light plants flowered in 76 days.

We hypothesized that impaired growth and development of transplastomic plants were caused by the metabolic burden imposed by the expression of the *aadA* marker gene. Therefore, we tested *aadA* expression in the transplastomic plants. Protein gel stained with Coomassie Brilliant Blue confirmed AAD accumulation at a high (~7%) level (**Fig. 2.2 A**). The identity of the 32-kDa band as AAD was confirmed by western blot analysis, using antibody recognizing the AAD c-Myc tag (**Fig. 2.2 B**). Interestingly, D1 protein accumulation in the transplastomic plants was not affected by *aadA* expression, as shown by probing protein gel blots with D1 antibody (**Fig. 2.2 C**). This observation indicates that AAD does not interfere with PSII assembly or stability, but may impose a metabolic burden on growth.

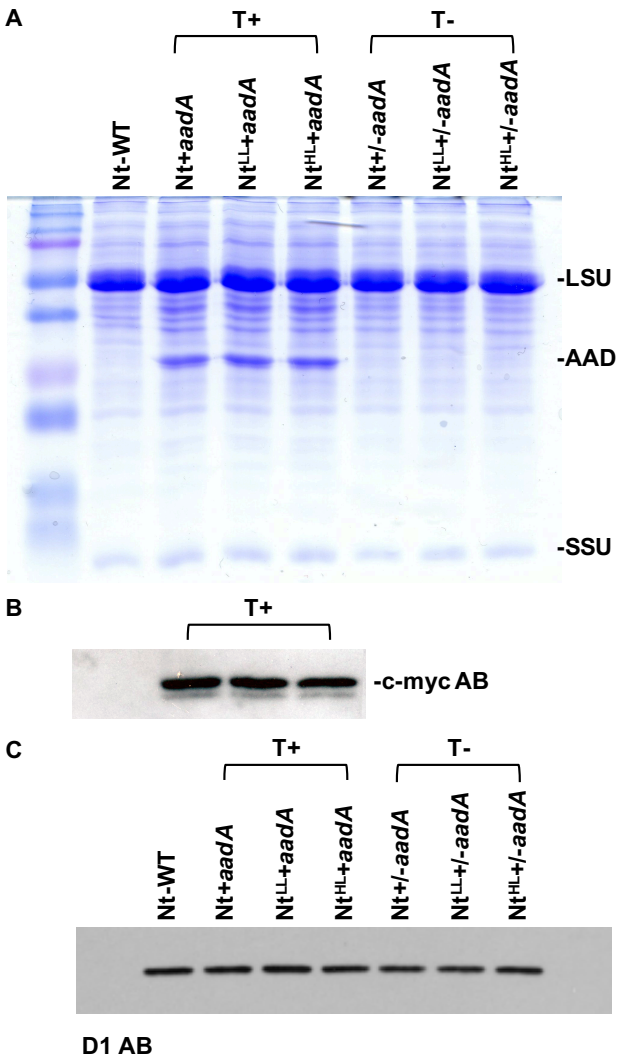

Figure 2.2 Expression of the AAD and the D1 proteins in transplastomic plants. A) Separation of total cellular protein in SDS-PAGE gels stained with Coomassie Brilliant Blue R250. The positions of Rubisco large (LSU) and small (SSU) subunits and AAD, the *aadA* gene product are marked. Data are shown for the Nt+*aadA*, Nt^{HL}+*aadA*, Nt^{LL}+*aadA* transplastomic lines carrying the *aadA* gene (T+), and the *aadA* deletion derivatives Nt+/-*aadA,* Nt^{HL}+/-*aadA* and Nt^{LL}+/-*aadA* plants (T-). Note absence of AAD after the excision of the *aadA* gene. **B)** Immunoblot analyses confirm the identity of AAD using c-myc antibody. **C)** D1 antibody detects the *psbA* gene product on Western blots.

2.3.3 Excision of marker gene restores growth of control plants and reveals increased biomass potential of Nt-HL plants

Anticipating potential interference of AAD with plant growth, we incorporated recombinase target sites for marker gene excision. In the vectors, the *aadA* gene is flanked by the PhiC31 phage integrase (Int) attB/attP sites, which were incorporated in the plastid genome along with the *aadA* gene. The plastid genome has been stable in the absence of the Int site-specific recombinase (Kittiwongwattana et al., 2007). To assess the impact of *aadA* expression on growth, we excised the *aadA* marker gene. Marker gene excision was achieved by transforming the transplastomic plants with an Agrobacterium vector carrying a plastid-targeted Int gene in binary plasmid pKO117 (Lutz et al., 2004). The presence of the *aadA* gene in the parental transplastomic lines was confirmed by DNA gel blot analyses after digesting total cellular DNA with the *Acc*I restriction enzyme (**Fig. 2.3 A, B**). The *psbA* probe detects a 1.6-kb fragment in the wild-type plastid genome and 3.2-kb fragment in the Nt+*aadA* and Nt^{LL}+*aadA* plants due to inclusion of the *aadA* gene. The *psbA* fragment in Nt^{HL}+*aadA* plants is 3.7 kb because the *Acc*I^{-} mutation from vector pYZ16 is present in the plastid genome. Excision of *aadA* reduced the hybridizing fragment size to 1.8 kb in the Nt+/-*aadA* and Nt^{LL}+/-*aadA* lines, and to 2.3 kb in the Nt^{HL}+/-*aadA* line. Marker gene excision has also been confirmed on RNA gel blots using the *aadA* and *psbA* probes (**Fig. 2.3 C**).

We evaluated the impact of marker gene excision and the consequences of D1 mutations by growing 20 plants of each line in the greenhouse under full sunlight (0 to 700 $\mu E\ m^{-2}\ s^{-1}$) and 24 plants of each line in a growth chamber under low light (40 μE, 16 hrs). Plant height, fresh weight and dry weight were evaluated after 60 days growing in

the greenhouse. Fresh weight and dry weight measurements indicated that normal growth and development is restored in the control plants Nt+/-*aadA* after the excision of the *aadA* gene, confirming that the *aadA* gene impairs plant growth and development (**Fig. 2.4**). The marker-free Nt^{HL}+/-*aadA* high-light plants grown in the greenhouse exceeded the Nt-WT plants in both fresh weight by 11% and dry weight by 9.9 %. The marker-free Nt^{LL}+/-*aadA* low-light plants were handicapped under both greenhouse and low light (40 μE) conditions as compared to Nt-WT. In both greenhouse environment and the low light conditions, the higher fresh weight and dry weight values for the high-light plants w/o the maker gene were not statistically significant. Other light conditions were not examined.

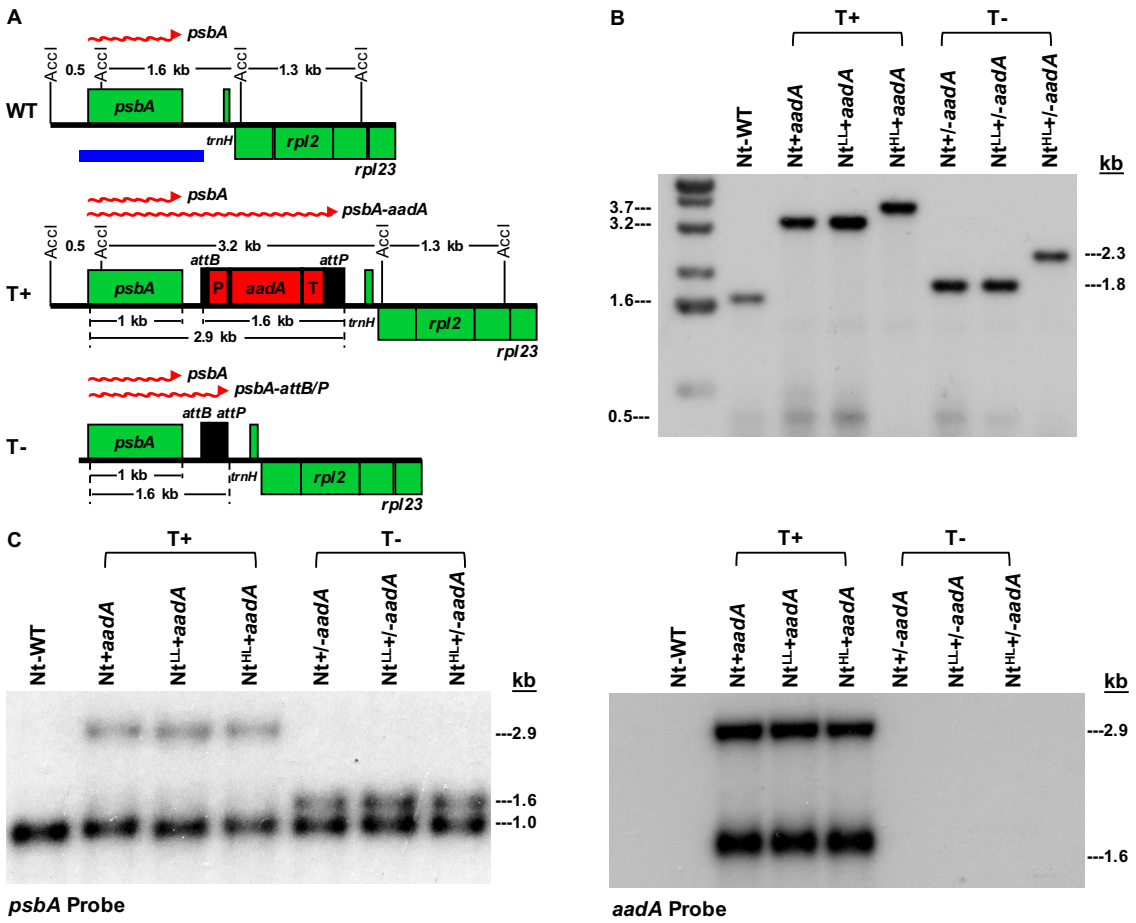

Figure 2.3 Excision of the *aadA* gene from the plastid genome. A) Schematic maps of the targeted region of plastid genome (WT), the targeted region with the *aadA* gene (T+), and after *aadA* excision with the *attB/attP* junction (T-). **B)** DNA gel blot confirms *aadA* excision using the *psbA* probe. Predicted fragment sizes are given in Figure 2.3 A. **C)** RNA gel blot confirms *aadA* excision using the *psbA* and *aadA* probes.

Figure 2.4 The impact of D1 mutations on plant growth and biomass. A) Tobacco plants grown in greenhouse for 60 days illuminated with full sunlight. Note increased height after excision of the *aadA* marker gene. **B)** Fresh weight and dry weight of greenhouse-grown plants. Error bars show s.e.m. centered at mean (n = 15 biological replicates). Asterisks indicate significant differences (α=0.05) between the control plant Nt+*aadA* and the low significant differences (α=0.05) between Nt-WT and the marker free low light plant Nt^{LL}+/-*aadA* on the right panel. **C)** Fresh weight and dry weight of plants after 30 days grown in growth chamber under low light (40 μE). Error bars show s.e.m. centered at mean (n = 24 biological replicates). Asterisks indicate significant differences (α=0.05) between Nt-WT and the marker free low light plant Nt^{LL}+/-*aadA*.

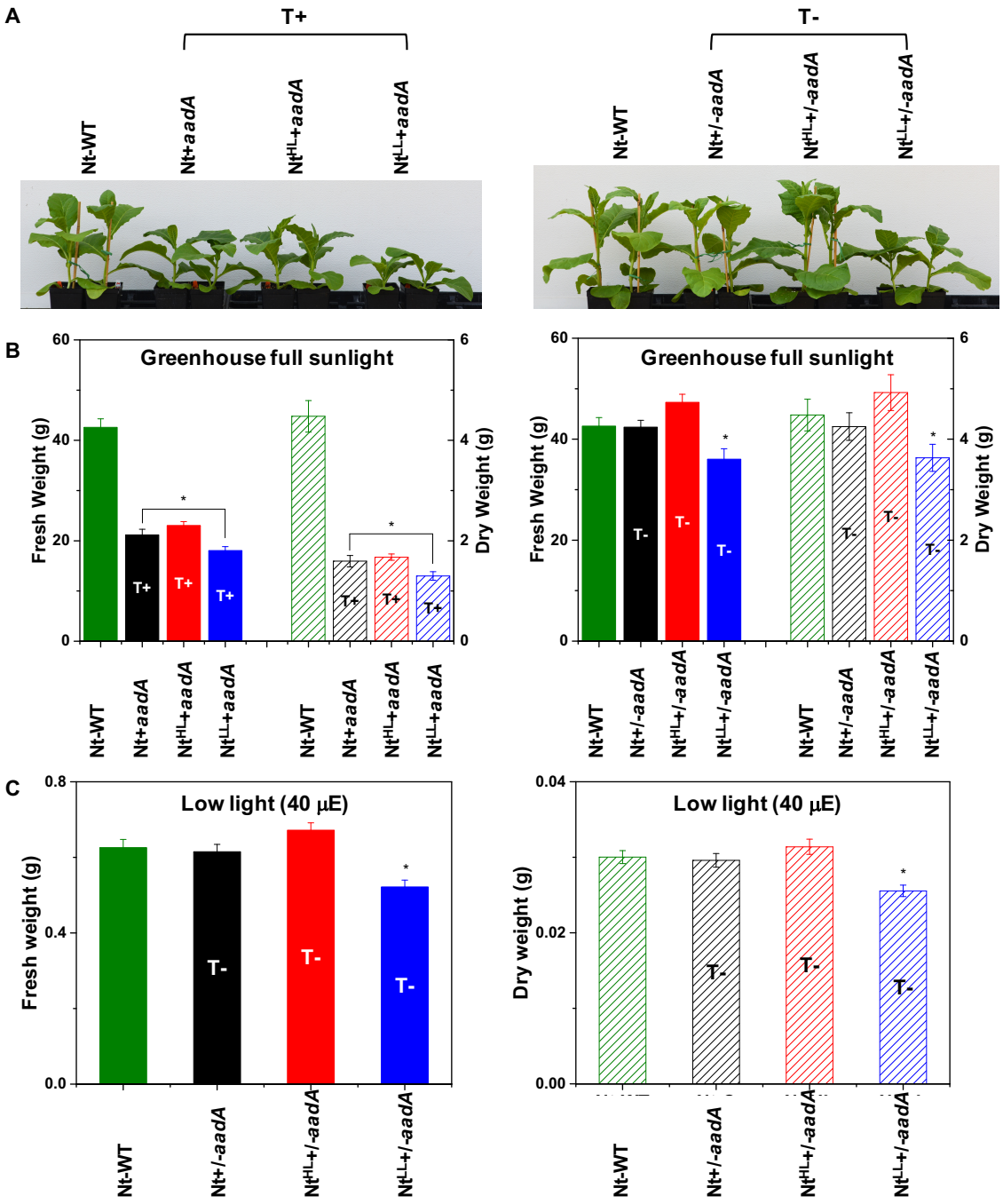
A
T+
T-
Nt-WT
Nt+aadA
Nt^HL+aadA
Nt^LL+aadA
Nt+/-aadA
Nt^HL+/-aadA
Nt^LL+/-aadA
B
Greenhouse full sunlight
Fresh Weight (g)
Dry Weight (g)
C
Low light (40 µE)
Fresh weight (g)
Dry weight (g)

2.3.4 Photochemical changes conferred by the D1 point mutations

The efficiency of the primary photoreaction and subsequent chemical conversion by water oxidation (net production of O_2 and reduced PQH_2) were measured to determine if the cyanobacterial phenotypes were introduced in the tobacco mutants. To do so, we measured *in vivo* chlorophyll-a fluorescence yield, light-saturated oxygen evolution rate and photoinhibition rate (D1 photoinactivation) of the marker free tobacco plants under various light conditions (Ananyev & Dismukes, 2005; Vinyard et al., 2013b). The Chl-a variable fluorescence yield, Fv/Fm, measures the fraction of light emitted by chlorophyll that competes with photochemical conversion (Fv), divided by the maximum emission yield (Fm). The steady-state yield of Fv/Fm is proportional to the quantum yield of PSII charge separation ($0 < Fv/Fm < 1$), while its transient period-4 oscillations, produced using single turnover pulses, are proportional to those charge separations that go on to accomplish O_2 evolution (Ananyev & Dismukes, 2005). Data in Figure 2.5 A taken at 1 Hz flash rate, indicates that the A152S mutation (Nt^{HL}+/-*aadA*) results in higher efficiency of PSII charge separation, while the E130Q mutation (Nt^{LL}+/-*aadA*) is significantly less efficient as compared to both the control (Nt+/-*aadA*) and the wild type (Nt-WT) plants. By contrast, the amplitude of the period-4 oscillations of Fv/Fm, differ in precisely the opposite way, with lower amplitude in the high-light plant (less photochemical conversion) than in both the control plant and Nt-WT, and significantly more amplitude in the low-light plant (**Fig. 2.5 D**). The same phenotype is observed at 10 and 100 Hz flash rates, with charge separation in the high-light plant outperforming both the control and Nt-WT plants, and the low-light plant performing even less efficiently at progressively higher light fluxes (**Fig. 2.5 B**). The opposite remains true of the amplitude

of period-4 Fv/Fm oscillations at these higher light fluxes, with the high-light plant invariably lower and the low-light plant invariably higher than both the control plant and Nt-WT (**Fig. 2.5 D**). These differences in Fv/Fm follow precisely the two cyanobacterial D1:1 and D1:2 phenotypes.

Greater PSII charge separation also results in more efficient oxygen evolution catalyzed by the water oxidation complex. We observe that when supplemented with artificial electron acceptors, isolated thylakoid membrane of the high-light plant generated oxygen at 15.5% faster rate than Nt-WT under saturating light conditions, indicating more efficient photosynthesis (**Fig. 2.6**). Under the same conditions, oxygen evolution by the low-light mutant is 21.9% slower rate than Nt-WT.

Photoinhibition results from photodamage to the D1 subunit (Nishiyama & Murata, 2014), and was measured by recording steady-state Fv/Fm after a fixed but extended illumination time at high light intensity in the presence of a protein synthesis inhibitor (Vinyard et al., 2014). Figure 2.6 shows that the high-light plant has a longer half-life of photoinhibition ($t_{1/2}$ = 33.5 hours) than Nt-WT and the control plant ($t_{1/2}$ = 30 hours), indicating greater photoprotection. The low-light plant showed an increased sensitivity to photoinhibition, with a half-life of only 25 hours.

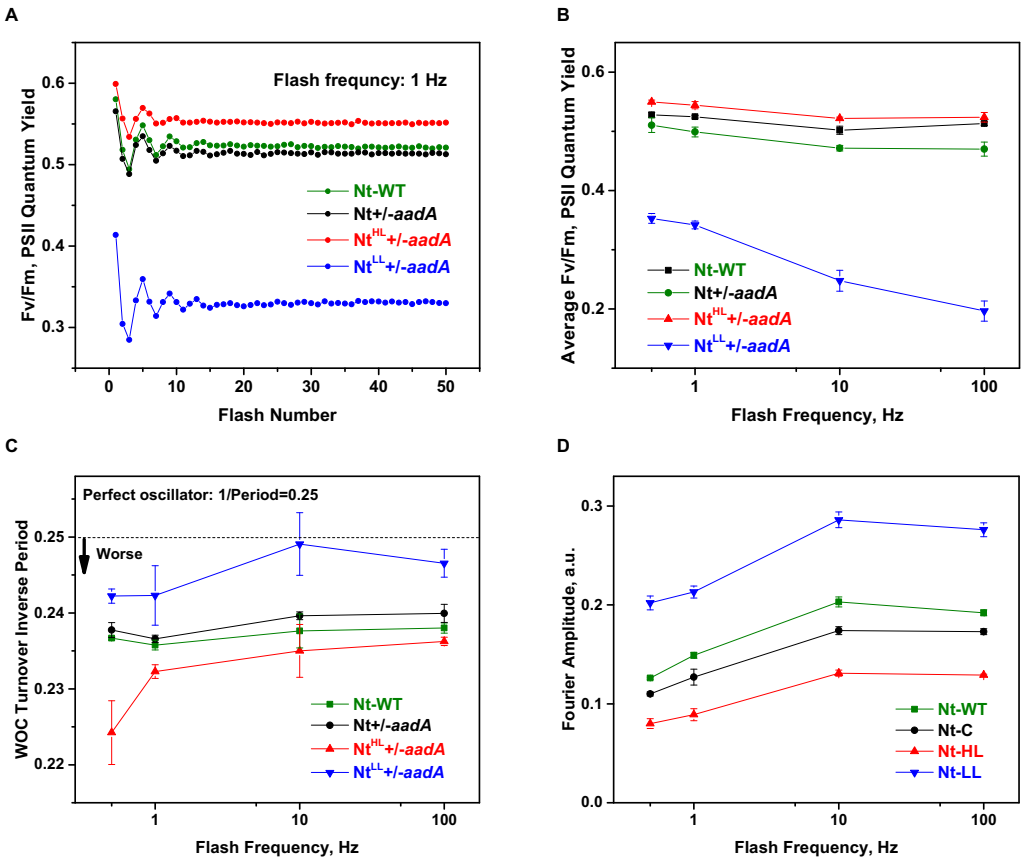

Figure 2.5 Photochemical characteristics of the tobacco D1 mutants. A) Representative oscillation trace at 1 Hz flash frequency. **B)** Steady state variable Chl-a fluorescence yield (Fv/Fm) over 30 flashes. **C)** Period^{-1} (inverse peak period) of oscillations of Fv/Fm in tobacco leaf disc as determined by the peak of the Fourier transformation. **D)** Peak amplitude of the period-4 oscillations taken from the Fourier transform. Error bars show s.e.m. centered at mean (n=3 biological replicates) in B, C and D.

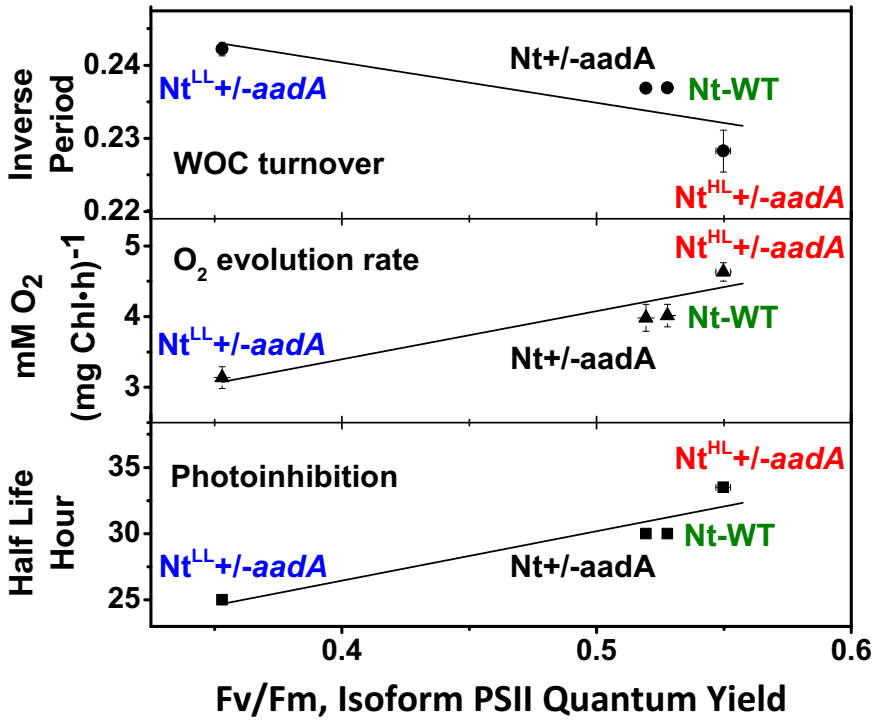

Figure 2.6 The PSII photochemical quantum yield (Fv/Fm) of D1 variants is inversely proportional to A) WOC turnover inverse period at a low flash rate (0.5 Hz; top), while proportional to **B)** light-saturated O_2 evolution rate (middle) and **C)** the half-life of photoinhibition (bottom). Data were fit to linear trend lines with the following equations: A, $y = -0.031x + 0.253$, $R^2 = 0.71$; B, $y = 6.686x + 0.727$, $R^2 = 0.81$; and C, $y = 36.172x + 11.992$, $R^2 = 0.82$. Error bars show s.e.m. centered at mean (n = 3 independent replicates).

2.4 Discussion

2.4.1 PSII trade-off between photosynthetic efficiency and photoprotection

A previous study in *Chlamydomonas*, investigating cyanobacterial D1 isoforms including two natural variants (D1:1 (LL) and D1:2 (HL)), plus 7 point mutants intermediate between these two D1 isoforms, revealed a continuous trade-off between several photochemical performance metrics beneficial at low light versus high light intensities (Vinyard et al., 2014). In Figure 2.7 A, two such metrics are plotted for all 9 strains as a function of the PSII Quantum Yield (Fv/Fm), the probability of WOC turnover (O_2 evolution) at light limiting intensity and the light saturated O_2 evolution rate. Here, we find the same relative trade-off is observed in Nt-WT (and Nt+/-*aadA*) with native D1, and the two genetically modified D1 variants, Nt^{HL}+/-*aadA* (the marker free high-light plant) and Nt^{LL}+/-*aadA* (the marker free low-light plant), with single amino acid point mutations. As shown in Figure 2.7 B, relative to Nt-WT, the high-light plant exhibits a higher yield of light-saturated O_2 evolution and has less efficient photochemical turnover at light-limiting intensity, measured either as the lower period-4 oscillation amplitude or a longer WOC cycle period. The high-light plant also exhibits better photo-protection against photoinhibition under light-saturating intensity. Conversely, the low-light plant with its lower PSII charge separation quantum yield has a higher WOC cycling efficiency under light-limiting intensity, while at high light intensity it has lower O_2 evolution rate and poor tolerance to photoinhibition. In conclusion, PSII charge separation serves two purposes that cannot be independently optimized, either better photochemical yield (O_2 and PQH_2) or protection against PSII photoinhibition

(Vinyard et al., 2014). The design of the PSII reaction center is a trade-off between these two consequences of photon conversion lifestyles at high and low solar intensities.

More specifically, this trade-off can be understood as competition between forward electron/hole transfer between PSII cofactors terminating in capture by the PQ-pool and WOC, respectively, versus charge recombination that serves in photoprotection at high light intensity. PSII reaction centers can be designed to operate better at high light intensity by having faster charge recombination as it affords better photoprotection, or for optimal operation at low light intensity by having slower charge recombination which results in more efficient capture of holes by the WOC and ultimately water oxidation.

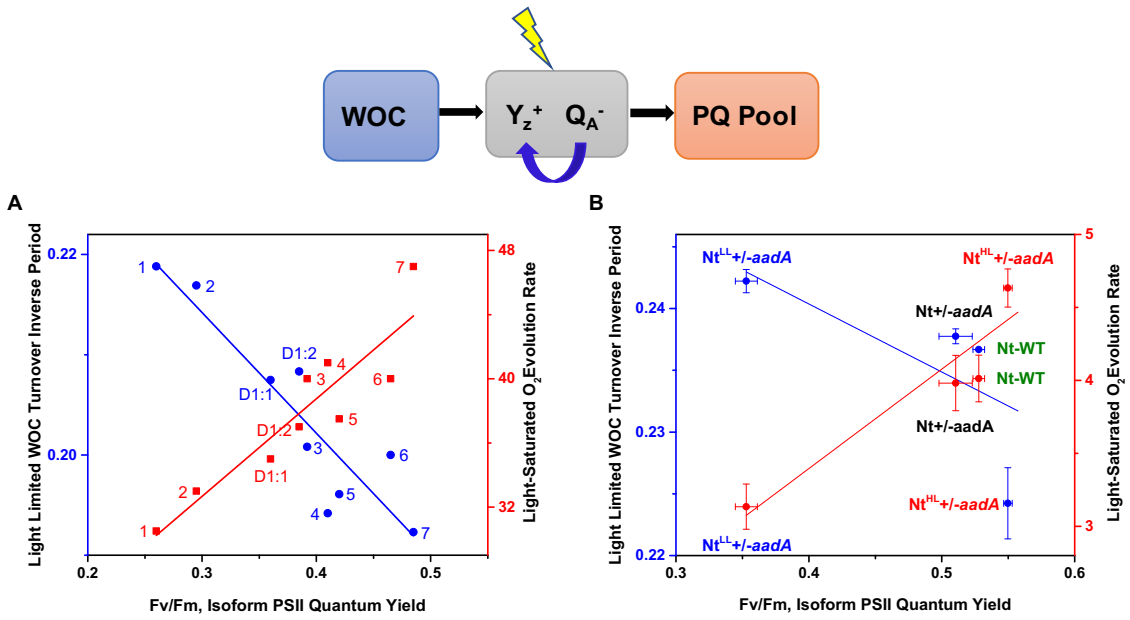

Figure 2.7 PSII trade-off between photosynthetic efficiency and photoprotection in **A)** the nine *Synechococcus* D1 variants investigated by (Vinyard et al., 2014), and in **B)** the tobacco D1 variants. It is shown in both cases that the PSII photochemical quantum yield (Fv/Fm) is inversely proportional to the WOC turnover efficiency measured at low flash rate where charge recombination contributes, while directly proportional to the light-saturated O_2 evolution rate. Error bars show s.e.m. centered at mean (n = 3 independent replicates).

2.4.2 Structure-function analyses of D1 isoforms and evolutionary implications

In the *Chlamydomonas* D1 variants expression model, it was hypothesized that modulation of the PSII reaction center primary photochemistry in the two cyanobacterial natural D1 isoforms and seven D1 point mutants results from a shifted free energy level of the primary electron acceptor Phe, and possibly also the secondary electron acceptor Q_A (Vinyard et al., 2014). Consistent with this interpretation, we see the same phenotype for the two tobacco D1 mutants with point mutation E130Q and A152S, which are specifically localized to interactions around Phe and Q_A.

The amino acid residue at D1-130 has caught much attention. It has been confirmed by EPR (Dorlet et al., 2001) and FTIR (Shibuya et al., 2010) studies that the side-chain of the D1-130 residue acts as the hydrogen bond donor to the 13^1 keto group of Phe. The side chain of residue Glu-130 (E) provides a stronger H-bond compared to Gln-130 (Q) to the 13^1 keto group of Phe (Merry et al., 1998). Consequently, E130Q results in a more negative midpoint potential (Em) of Phe. By contrast, the A152S point mutation on the *Synechococcus* 7942 D1:2 isoform expressed in *Chlamydomonas* produces the opposite effect on the efficiency of PSII, and postulated complementary influence in altering the Em of Phe (Vinyard et al., 2014). The methyl side chain of Ala-152 (A) on D1 and the phenyl group of Phe-435 on CP43 support a hydrophobic interaction between the two PSII subunits. It is hypothesized that when Ala is substituted with Ser on D1-152, the D1-CP43 interface becomes less hydrophobic, causing movement of the D1 α helix. Due to the presence of Pro-150 trans to Ser-152, the Phe binding pocket would be altered and the Em of Phe becomes less negative (Vinyard et al., 2014).

We postulate a more negative Em (Phe/Phe$^-$) in the low-light plant expressing D1-E130Q, which decreases the charge separation efficiency due to a smaller free energy gap between P_{680}^* and Phe. Given the increased charge separation quantum yield observed in the high-light plant, it is reasonable to expect a more positive Em (Phe/Phe$^-$), and a larger energy gap between the primary radical pair. In addition to its impact on charge separation rate, Em (Phe/Phe$^-$) has also been found to regulate the rate of the $^1[P_{680}^+Phe^-]$ → P_{680} direct charge recombination. The increase of Em (Phe/Phe$^-$) and larger radical pair energy gap in the high-light plant expressing D1-A152S should increase the rate of the radiative pathway of charge recombination, thereby protecting PSII against photodamage. Conversely, the low-light plant expressing D1-E130Q has the opposite effect with slower recombination arising from a smaller radical pair energy gap and resulting in higher sensitivity to photoinhibition.

From the previous research on natural D1 isoforms in *Thermosynechococcus*, Em (Q_A/Q_A^-) was found to be more positive in D1:2 (Ogami et al., 2012) than in D1:1 (Shibamoto et al., 2009). A more positive Em (Q_A/Q_A^-) in the high-light plant would increase the energy gap (Phe-Q_A), suppressing the efficiency of the thermally-activated backward step: $P_{680}^+Q_A^-$ to $P_{680}^+Phe^-$, thereby suppressing the formation of $^3[P_{680}^+Phe^-]$ and $^3P_{680}$-mediated singlet oxygen ($^1O_2$) that accompany D1 photodamage. Meanwhile, because of the smaller energy gap between $P_{680}^+Q_A^-$ in the high-light plant, the direct recombination pathway from $P_{680}^+Q_A^-$ to $P_{680}Q_A$ gains higher efficiency which provides better photoprotection (Vass & Cser, 2009). Taken together, the high-light plant with more positive reduction potentials of Phe and Q_A achieve higher charge separation

quantum yield and faster overall charge recombination rate, while the low-light plant has the opposite energetic and photochemical phenotypes.

2.4.3 The intrinsic PSII photochemical advantage in tobacco D1 high light mutant benefit biomass accumulation in the high solar intensities.

Besides the higher PSII charge separation efficiency and the faster charge recombination rate that benefit the photosynthetic efficiency under high light condition, the high-light plant also shows a higher intrinsic efficiency of PSII by normalizing the light-saturated O_2 evolution rate to D1 concentration. These various photochemical advantages of the high-light plant in high light conditions resulted in a modestly higher biomass accumulation rate. Compared to Nt-WT and the control plant, the high-light plant exhibits a 9.9% increase in average dry weight after 60 days post planting in the greenhouse conditions.

In a previous study, the *Chlamydomonas* strain expressing the *Synechococcus* 7942 D1:1 (LL) isoform not only showed more efficient WOC cycling, but also achieved higher biomass accumulation at low light intensities, compared to the control strain and the D1:2-PSII strain (Vinyard et al., 2013c). By mutating the tobacco native high light D1 isoform into the low light isoform in Nt^{LL}+/-*aadA* by single point mutation E130Q, although a higher WOC cycling efficiency at low light intensity is successfully achieved, unexpectedly it was handicapped in growth. Compared to Nt-WT and the control plant, the low-light plant shows a 19% decrease in biomass under greenhouse conditions. The physiological result indicates that although the presence of Glu or Gln at position 130 plays a crucial role in regulating the redox potential of Phe and Q_A, amino acid residues

at other positions likely also contribute to the overall beneficial properties at low light intensity of the cyanobacterial low light isoform D1:1.

2.4.4 Removal of the antibiotic marker gene is necessary for reliable evaluation of physiological performance

The high-level expression of the spectinomycin and streptomycin resistant marker gene *aadA* not only delayed the growth rate and developmental phase of the transgenic lines, but also partially masked the impact of the D1 point mutation on the plant growth. After *aadA* excision, the slight growth advantage of the high light plant Nt^{HL}+/-*aadA* over the control plant Nt+/-*aadA* increased from 5.1% to 9.9% more dry biomass. The physiological benefit still doesn't show up in the low-light plant Nt^{LL}+/-*aadA* after *aadA* removal. Since the maker gene becomes dispensable after obtaining the homotransplastomic plant, removal of it will better reveals the intrinsic influence of genetic modifications on the transgenic plants and enable more reliable evaluation of the physiological performance of the mutant plants.

2.5 Conclusion

We have shown the prokaryotic design principal of PSII D1 subunit is applicable in higher plants. Slight change of the redox potential of Phe and Q_A caused by D1 point mutation could have a great impact on the primary PSII photochemistry of charge separation and charge recombination. By introducing the single point mutation into tobacco *psbA* gene at A152S mimicking the cyanobacterial HL D1:2 strain, we created a high light mutant exhibiting higher photosynthetic efficiency, higher tolerance to photoinhibition and modestly increased biomass potential under high light conditions. By contrast, the only benefit of incorporating the E130Q point mutation mimicking the LL isoform is restricted to improving WOC cycling efficiency at low light intensity, while the biomass yield was impaired at low light intensity. The intrinsically lower light utilization efficiency of this point mutation (Fv/Fm) appears to generate insufficient primary energy (PQH_2 and pH gradient) to allow adequate growth at the low light tested (40 $\mu E\ m^{-2}s^{-1}$). Either lower growth light intensity may be needed or the entire *Synechococcus* 7942 D1:1 sequence may need to replace the tobacco D1 to achieve the biomass advantage at low light intensity. This hypothesis could be further tested by substituting the native tobacco isoform with the whole sequence of *Synechococcus* 7942 D1:1. Excision of the antibiotic marker gene *aadA* is necessary for reliable evaluation of the biophysical and physiological performance on the transgenic plants and likely reflects removal of the metabolic burden of marker gene expression/translation. The most advantageous strategy for photochemical fitness in light shifting environments remains the differential expression of D1 isoforms.

Chapter 3. Metabolic engineering of central carbon metabolism for enhanced TAG accumulation

Summary

Little attention has been paid to investigate the influence of photosynthetically assimilated carbon intermediates on the downstream steps of fatty acid biosynthesis and accumulation of triacylglycerides (TAGs). In the present study, the importance of citrate synthase (CIS) in partitioning the photosynthetic assimilates through the TCA cycle and the functional role of glycerol 3-phosphate dehydrogenase (G3PDH) in diverting carbon precursors from glycolysis to TAG assembly are fully examined in transgenic strains of *Nannochloropsis oceanica* CCMP 1779 (hereafter *N.o1779*). By targeting these key enzymes of two carbon metabolism pathways, four robust lipid production strains were generated. Inhibiting protein synthesis by downregulating Citrate Synthase, and improving TAG assembly by heterologous expression of the yeast gene encoding the cytosolic G3PDH are proved to be effective strategies for enhancing microalgal lipid production. However, biomass yield and the photosynthetic carbon fixation rate were slightly sacrificed in all the oil mutants. Therefore, improving the photosynthetic efficiency and the carbon assimilation rate to supply abundant photosynthetically assimilated carbon precursor is critical to optimize the impact of metabolic engineering.

3.1 Introduction

Eco-friendly fuels (Rajagopal et al., 2009; Stephens et al., 2010; Tan & Lee, 2016b), like biodiesel, derived from phototrophic microalgae, is considered a promising renewable fuel that has generated significant R&D in the energy markets (Ahmad et al., 2011; Lv et al., 2013; Rajagopal et al., 2009). The challenges to commercialization are economics and sustainability, with a main shortcoming being the low solar to biodiesel precursor conversion efficiency intrinsic to natural microalgae (Dismukes et al., 2008a). Natural strains of microalgae are capable of accumulating as much as 20–50% of their dry biomass as triacylglycerols (TAG), an ideal precursor for making biodiesel by transesterification (Ma et al., 2017; Zienkiewicz et al., 2017b). Despite this potential, the lipid productivity from the naturally occurring algal strains fall well short of this upper limit, owing to the slower growth rate of TAG accumulating microalgae. This trade-off has triggered substantial efforts to improve TAG productivity by metabolic engineering of heterologous pathways and genetic manipulation of native pathways, based on the current understanding of the mechanisms of lipid metabolism (Wei et al., 2017a).

Prior studies of several model organisms have focused on regulation of the presumed rate-limiting enzymes involved in *de novo* fatty acid (FA) synthesis and TAG biosynthesis, with mixed results being achieved. One of the most widely investigated enzymes is acetyl-CoA carboxylase (ACCase), which catalyzes the first step in FA biosynthesis pathway: forming malonyl-CoA via carboxylation of acetyl-CoA using a molecule of bicarbonate and requiring ATP. However, manipulation of this gene led to only minor, if any, increased lipid content in a higher plant and a diatom (Tan & Lee, 2016b). Other genes involved in the downstream TAG assembly pathway have been

given more attention, with the most successful attempt achieved by the amplification of diacylglycerol acyltransferase (DGAT), the crucial enzyme catalyzing the final and committed step of TAG synthesis.

De novo FA synthesis can only be maintained at a high rate with continuous supply of acetyl-CoA, the carbon precursor also competed by protein synthesis (Rawsthorne, 2002; Sugimoto et al., 1989; Tan & Lee, 2016b). Therefore, one way to overcome this competition could be to selectively downregulate the activity of citrate synthase (CIS), which catalyzes the first step in the TCA cycle by condensing acetyl-CoA with oxaloacetate to generate citrate. It has been repeatedly observed in different microalgal species that the improvement in neutral lipids production, induced either by genetic manipulation or environmental stress, is always accompanied by a decreased level of protein accumulation, where data are available. However, there is only a single report on the influence of CIS downregulation on lipid accumulation by Deng et al. in *Chlamydomonas reinhardtii* (Deng et al., 2013a).

Another obvious target is glycerol 3-phosphate dehydrogenase (G3PDH), which converts dihydroxyacetone phosphate (DHAP) into glycerol 3-phospate (G3P), the glycerol backbone needed for TAG formation. The proposed functional importance of G3PDH has been supported by a transcriptome analysis of *Chlamydomonas reinhardtii*, which revealed the upregulation of *g3pdh* gene expression when neutral lipids were highly accumulated, as well as the previous successful attempts to enhance lipid production by overexpression of endogenous *g3pdh* in the green alga *Chlamydomonas reinhardtii* (Wang et al., 2018), and the diatom *Phaeodactylum tricornutum* (Yao et al.,

2014), or heterologous expression of *g3pdh* in the higher plant *Brassica napus* (Vigeolas & Geigenberger, 2004).

The highly diverse evolution across the algal realm leads to different regulation of lipid metabolism between oleaginous and non-oleaginous microalgae (Liu & Benning, 2013; Zienkiewicz et al., 2016b; Zienkiewicz et al., 2017a). Therefore, though functional analysis of *cis* and *g3pdh* genes have been carried out in the model organism *Chlamydomonas reinhardtii*, a poor lipid-producing green alga, the functional roles of these gene on lipid synthesis need to be further investigated in the oleaginous microalgal species. With a fully sequenced and assembled genome, an efficient transformation protocol, and advanced genetic tools, *Nannochloropsis oceanica* CCMP1779 (hereafter *N.o1779*), a highly oleaginous heterokont, serves as an ideal platform for applying strategies of metabolic engineering to enhance TAG accumulation (Tan & Lee, 2016b). Here we investigate the effect of decreased CIS abundance by RNAi-mediated silencing and elevated G3PDH dosage by expressing an exogenous yeast *G3PDH* on the lipid metabolism in *N.o1779* (Vieler et al., 2012). Furthermore, with the advanced genetic engineering toolkit recently developed by Poliner and his colleagues, the endogenous *cis* gene and the yeast *g3pdh* gene can be co-regulated under the control of an endogenous bidirectional promoter on a stacking vector (pNOC-stacked vector), allowing the application of the "push and pull" strategy in *N.o1779* (Poliner et al., 2018; Tai & Stephanopoulos, 2013). This report demonstrates the promising role of CIS and G3PDH in regulating the substrate supply for lipid biosynthesis and provides insights into metabolic engineering of photosynthetically driven cell factories for trait improvement and biofuel production.

3.2 Material and methods

3.2.1 Algal strain and cultivation conditions

Nannochloropsis oceanica CCMP1779 (*N.o* 1779) was obtained from the Bigelow National Center for Marine Algae and Microbiota (NCMA, https://ncma.bigelow.org/). All strains described in this manuscript were derived from this parental background.

Cells were cultivated in a 45ml working volume in a 250ml culture flasks at 22 °C under the cool-white fluorescent lights (85 μmol/m^2/s) with 16-h light, 8-h dark diel period. Air (0.04% CO_2) was directly supplied to the culture. Cultures were inoculated at an OD_{750nm} of 0.1 measured by the Neo2 microplate reader with 200 μl culture.

3.2.2 Vector construction

To construct the S.cG3PDH expression vector, the full sequence of yeast *g3pdh* was amplified with the primers containing *Mlu*I and *Hpa*I restriction sites. An intermediate S.cG3PDH overexpression construct pNOC-ox-g3pdh was generated by cloning the gel-purified and the *Mlu*I/*Hpa*I digested PCR product into the *Asc*I-*Hpa*I site of the pNOC-OX-NanoLuc vector by T4 DNA ligase. To achieve the pNOC-stacked-GOX-AS vector, the DNA fragment containing the coding sequence of S.cG3PDH linked to the HA-tagged Nano-Luciferase reporter gene by the glycine-serine-glycine encoded linker was amplified by primers containing *Mlu*I and *EcoR*V restriction sites and sub-cloned into the pNOC-stacked vector between the *Asc*I and *Stu*I site where the green fluorescence protein (eGFP) was removed. To achieve the pNOC-stacked-GOX-PA

vector, the same fragment was amplified by primers containing the *PspOM*I and *EcoR*V sites and sub-cloned into the pNOC-stacked vector downstream of the BleR-P2A(60) sequence.

To construct the CIS RNAi vector, the 3' end of *cis* exon 2 was chosen to be the target of the RNAi inverted repeat. Based on the *CIS* sequences retrieved from Benning Lab GBrowse v. 2.00, a 227 bp sense fragment and a 382 bp hairpin plus antisense fragment were amplified by PCR using the primers with overlapping sequences for Gibson assembly. The two fragments share 227 bp sequence as inverted repeats. The hairpin junction is from the intergenic region between *cis* and nanno_1035: 65895..66842. The pNOC-411 vector containing Zeocin resistant cassette was PCR amplified using primers providing the overlapping sequence to orient the short and long fragments to form an inverted repeat in the appropriate direction and generate the intermediate construct pNOC-411-CISi. To achieve the pNOC-stacked-CISi-AS vector, the *cis* RNAi inverted repeat fragment was digested from pNOC-411-CISi by *Mlu*I/*Afe*I and sub-cloned into the *Asc*I-*Stu*I site of the pNOC-stacked vector.

Finally, to construct the push and pull stacking vector pNOC-stacked-GOX+CISi-AS (GOX+CISi-AS hereafter), the *cis* RNAi inverted repeat was obtained from digestion of pNOC-411-CISi with *Xho*I/*Afe*I and cloned into the *Xho*I-*Afe*I site of the pNOC-stacked-GOX-AS vector downstream of the BleR-P2A(60) sequence.

3.2.3 Nuclear transformation by electroporation

The transformation of *N.o1779* was performed as described previously in Vieler et al. (2012) (Vieler et al., 2012). *N.o1779* cells were harvested at a density of 1–2 x 10^7

cells/mL, washed with ice cold 375 mM sorbitol three times and resuspended in a final volume of 0.2 mL to a concentration of 5 x 10^8 cells/mL. 2–10 μg *Sca*I linearized Plasmid DNA mixed with a 10-fold excess of salmon sperm DNA (Invitrogen, http://www.invitrogen.com) was supplied into the 2 mm electroporation cuvette. Electroporation was performed using a Bio-Rad (http://www.bio-rad.com) GenePulser II set to 600 resistance at a field strength of 11 kV/cm leading to time constants of 20 to 25 ms. After the pulse the cells were resuspended in 5 mL f/2 media and allowed to recover for 48 h in continuous light with shaking before they were spread on selection agar containing 5 μg/mL Zeocin using warm top agar (f/2 media, 0.05% Phytoblend (Caisson Laboratories, http://www.caissonlabs.com) in 1:1 dilution (vol:vol). Resistant colonies were observed as early as 10–14 days after electroporation; colonies were usually transferred after about 4 weeks.

3.2.4 Luminescence assay

The luminescence assay was performed as described previously in Poliner et al. (2018) (Poliner et al., 2018). *N.o1779* culture was mixed with f/2 supplemented with NanoLuciferase substrate (Promega), at a final volume of 200 μL, with 10,000 x dilution of NanoLuciferase substrate. Luminescence of 1 million cells from each line was measured with a Centro XS3 LB960 luminometer (Berthold Technologies) over a 0.3-s exposure.

3.2.5 Fluorometric measurements with Nile Red

The Nile Red staining method reported by Cirulis et al. (2012) (Cirulis et al., 2012) was optimized for *N.o1770* to ensure its accuracy and reproducibility. Nile red (9-diethylamino-5-benzo [α] phenoxazinone, Sigma-Aldrich) stock solution was prepared in 200 μg/mL in absolute acetone, and store in the dark at 4 °C. The stock solution was replenished every month. To start the measurement, the working solution of Nile Red at the concentration of 8 μg/mL was made from diluting the stock solution with deionized water, and then equilibrated in the dark for 30 minutes. Algal culture or growth medium and the Nile Red working solution were mixed at 1:1 ratio by vortex and incubated in dark for 30 minutes at room temperature. Fluorescence signals were read and recorded with Synergy Neo2 Hybrid Multi-Mode Reader (Biotek) with a wavelength of 530 nm for excitation and a 575 nm for emission. After removing the background fluorescence from the growth medium, the cellular lipid content of each line was calculated and expressed as Nile Red fluorescence intensity normalized to OD750.

3.2.6 Lipid extraction and gravimetric quantification

To compare the correlation between the Nile Red fluorescence intensity and the accurate neutral lipid content, cultures measured for Nile Red fluorescence were also harvested for extraction and gravimetric quantification of the neutral lipids. The Bligh-Dyer type methanol:chloroform phase extraction method was modified in house for lipid extraction (Bligh & Dyer, 1959; Lee et al., 2010; Mitra et al., 2016; Surendhiran & Vijay, 2014; Thawechai et al., 2016; Zhu et al., 2014b). 150 ml air bubbled *N.o1779* WT or randomly selected transgenic cultures were pelleted down by centrifugation (4000 x g, 10

min). After discarding the supernatant, pellet was resuspended in remaining supernatant and dried in the oven (65 ^{o}C) for overnight. The dry pellet was ground thoroughly into power by mortar and pestle, and around 0.1 g of powdered biomass was weighed out for lipid extraction. The biomass powder was suspended in 6 mL lipid extraction solvent (methanol:chloroform:formic acid, 2:1:0.1). After vortexing, the mixture was incubated in oven (65 ^{o}C) for 30 min with occasional shaking. Then the mixture was supplied with 2 ml ionic phase buffer (1 M KCl, 0.2 M H_3PO_4) and vigorously vortexed. Cell debris was removed by centrifugation for 3 min at 13,780 x g. The lower organic phase containing crude lipid extracts were dried under argon gas and then weighed by scale. The ratio of dry lipid mass to dry culture mass was defined as the lipid content.

3.2.7 Western blot analysis

The expression of S.cG3PDH in the selected target mutants was examined by protein extraction and western blot analysis as described previously in Poliner et al. (2018) (Poliner et al., 2018). Briefly speaking, 5 mL culture was pelleted down by centrifugation and then ball-milled by a TissueLyser II (Qiagen) after frozen. Total protein was extracted with buffer containing 100 mM Tris (pH 8.0), 2 mM PMSF, 2% β-mercaptoethanol and 4% SDS, and then quantified by the RCDC assay (Bio-Rad). Equal quantity of protein from each line was loaded for SDS-PAGE and then transferred to PVDF membranes (Bio-Rad) overnight at 4 °C. Blots were blocked in TBST with 5% milk for 1 h at room temperature and washed six times with TBST. The α-HA-HRP antibody solution (Roche 3F10) at 1:1000 in TBST with 5% milk was used for HA detection. Signals were detected using clarity chemiluminescence reagent (Bio-Rad).

Intensity of the detected protein bands was quantified using Image Lab software (Bio-Rad).

3.2.8 RNA extraction and transcriptional analysis by qRT-PCR

For each biological replicate, 30 mL culture from the exponential phase were harvested for RNA extraction using Trizol reagent following the guidelines provided (Invitrogen). Contaminating DNA was removed by DNase treatment (Roche Applied Science) and was further cleaned up using an RNeasy kit (Qiagen). Total RNA was used for cDNA synthesis following the manufacturer's instructions (Roche Applied Science) using poly(dT) primers. Synthesized cDNA was then subjected to quantitative RT-PCR analysis using SYBR Green Premix (Takara) using an ABI 7000 Real Time PCR System (Applied Biosystem) to determine the transcript level of S.cG3PDH. The housekeeping gene encoding Actin was used as internal reference.

3.2.9 Fluorescence and confocal microscopy analyses

For microscopy analysis, cell pellet was suspended in phosphate-buffered saline (PBS) and fixed with 4% formaldehyde at 4 ^{o}C for overnight. The fixed cells were washed with PBS three time and then stained with Nile Red at a final concentration of 4 μg/mL (from a stock of 200 μg/mL in acetone) for 30 minutes in dark. The Nile Red stained cells were pellet down, washed with PBS buffer, and resuspended in residual PBS buffer. The 5-10 μl cell resuspension was mixed with a drop of the ProLong™ Diamond Antifade Mountant with DAPI, and cure for 24 hours at room temperature in the dark before observing under the microscope.

For fluorescence microscopy analysis, the fluorescence of Nile Red staining neutral lipids and of DAPI staining nuclear DNA were detected using a UV light source. By counting the number of Nile Red positive cells and of DAPI positive cells using Image J software, the percentage of cells with lipid droplets over the total population was calculated.

For confocal microscopy analysis, a Leica TCS SP8 microscope was used. Nile Red and DAPI treated cells were viewed with a 100 x oil immersion lens objective. Post-acquisition image handling was done with LAS X and Image J software.

3.2.10 Dry weight determination

To quantify the dry biomass, algal cells from each line were collected by filtering the culture through pre-weighed and pre-dried Whatman GF/F filter paper. Then, the filter paper harboring the algal cells was dried in a 65 °C oven for overnight. The biomass of the culture was determined gravimetrically.

3.2.11 Quantification of carbohydrates

The content of carbohydrates in *N.o1779* WT and transgenic lines was determined by an acid-hydrolysis method (Passonneau & Lauderdale, 1974) combined with glucose quantification using the commercial Amplex Red glucose assay kit (Invitrogen, Cat# A22189). To hydrolyze carbohydrates into monosaccharides, cell pellet harvested from 1 mL culture was resuspended with 1 mL 4 M HCl in a 2 mL Eppendorf tube. The tube was sealed tightly with locking lid and boiled on the heat block for 1 hour. To achieve complete hydrolysis, the tube was vigorously vortexed every 10 min during the whole

process. After cooling to room temperature, the hydrolysis sample was neutralized with ~1 mL 4 M NaOH and its concentration can be quantified by the Amplex Red glucose assay kit according to the manufacturer's instructions. Briefly, to generate the glucose standard curve, standards with concentrations of 0-180 μM were prepared by appropriate dilutions of the 10g/L glucose stock solution. A volume of 50 μl of each standard and experimental sample was pipetted into the 96-well plate. Fifty-microliter of Amplex Red working solution was then added to each well and mixed with the glucose standards and experimental samples. After a dark incubation of the plate for 30 min, absorbance at 560 nm was measured by a microplate reader and used for calculating the glucose concentration according to the standard curve.

3.2.12 Statistical analysis

All experiments were determined in biological triplicate to ensure the reproducibility. Experimental results were presented as the mean ± standard error. The significance of differences between mean values were determined with student t-test. Differences at $P<0.05$ were considered significant.

3.3 Results

3.3.1 Generation of *N.o1779* transgenic lines expressing S.cG3PDH and/or downregulating N.oCIS

The gene stacking system developed by Poliner et al provides an excellent platform for co-regulation of multiple gene targets (Poliner et al., 2018). The pNOC-stacked vector contains an endogenous bidirectional promoter (Ribi) driving the expression of a reporter gene encoding the green fluorescent protein (eGFP) on one side and the coding sequence linking the bleomycin selection marker and P2A (BleR-P2A(60)) on the other side. It was used for construction of all the expression vectors (**Fig. 3.1**).

Two transformation vectors were constructed for solely expressing S.cG3PDH in *N.o1779*: pNOC-GOX-AS (GOX-AS hereafter) is generated by replacing eGFP with the coding sequence of S.cG3PDH and the HA-tagged NanoLuciferase (Nlux), while pNOC-GOX-PA is created by placing the coding sequence of S.cG3PDH-Nlux-HA downstream of BleR-P2A(60). In order to knockdown N.oCIS via the RNAi mediated gene silencing approach, the transformation vector pNOC-CISi-AS (CISi-AS hereafter) was created by replacing eGFP with an inverted repeat targeting the 3' end of the N.oCIS exon 2. Furthermore, the push and pull stacking vector pNOC-GOX+CISi-AS (GOX+CISi-AS hereafter) was generated by cloning the N.oCIS RNAi sequence into GOX-AS and placing it downstream of BleR-P2A(60).

Transformation of *N.o1779* with vectors GOX-AS, GOX-PA, CISi-AS and GOX+CISi-AS was carried out via electroporation, yielding 150, 12, 339 and 273 Zeocin resistant clones, respectively.

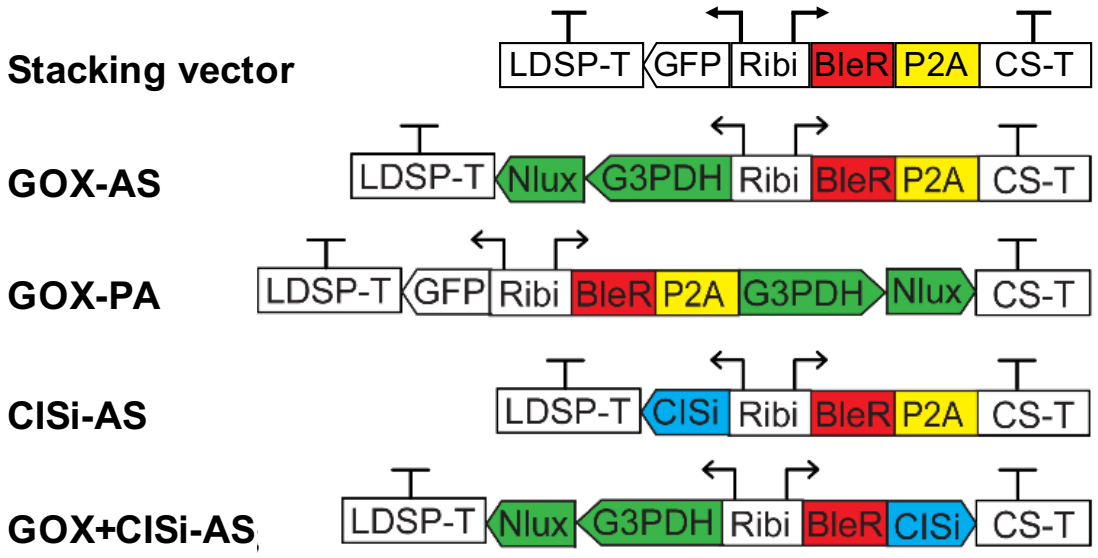

Figure 3.1 Schematic diagram of transformation vectors for expression of the *Saccharomyces cerevisiae* G3PDH (S.cG3PDH) or/and downregulation of the *N.o1779* CIS (N.oCIS).

3.3.2 High-throughput screening for winning industrial strains

The randomly selected resistant clones from GOX-AS, GOX-PA and GOX+CISi-AS were first analyzed for their expressional level of S.cG3PDH by the assay detecting luminescence from the NanoLuciferase reporter, the epitope tag that was translationally fused to the N terminus of S.cG3PDH. The top 10-20 candidates with the highest luminescence intensity together with the randomly selected CISi-AS mutants were inoculated into 24-well plates and subsequently analyzed by PCR using three sets of primers that respectively amplify the full length coding sequence of S.cG3PDH, the forward repeat and the reverse repeat of the N.oCIS RNAi sequence. The transgenic lines yielded from each construct showing successful integration of the transformation vectors were selected for further analysis of their lipid content.

In order to efficiently identify transgenic lines with robust phenotype in lipid production, the Nile Red staining method was optimized for screening all the genetically validated mutants based on the fluorescence intensity. To evaluate the accuracy of this method for estimating lipid content in *N.o1779*, we established the correlation between the dry biomass normalized lipid content determined by lipid extraction and gravimetric quantification and the OD_{750nm} normalized Nile Red fluorescence intensity measured by the microplate reader. Six wild type culture and five randomly picked mutant culture were chosen to ensure the coverage and reflect the *in situ* staining situation. The resulting regression curve with an R square of 0.90 indicated the existence of a positive correlation between the Nile Red fluorescence intensity and the actual oil content of *N.o1779*.

All the PCR validated transgenic lines together with the empty vector control were inoculated into culture flasks and bubbled with filtered building air to provide

carbon source as well as agitation to maintain the uniform distribution of cells in the growth medium. After 4 days of growth, the OD_{750nm} and the Nile Red fluorescence intensity of each line were measured using a microplate reader. The level of OD_{750nm} normalized Nile Red fluorescence intensity was considered as an indicator of the cellular oil content, and used to select the most promising robust lipid producer from each construct for further analysis.

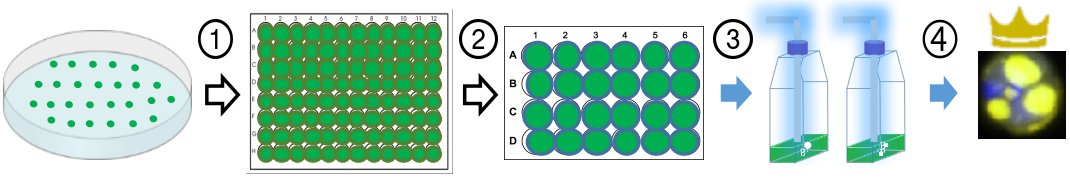

Figure 3.2 Experimental outline of the four-step screening procedure for isolating oil mutants. 1. Random selection of the Zeocin resistant colonies into 96 well plates; 2. Luciferase (Nlux) screening of mutants into 24 well plates; 3. Genetic verification by PCR into culture flask; 4. Nile Red fluorescence screening to identify the robust lipid producers.

3.3.3 Nile Red fluorometric analysis by microplate reader and fluorescence microscope

The winning strain yielded from each construct together with the empty vector control line were inoculated into culture flasks at the initial OD_{750nm} of 0.1 in a total volume of 45 mL. After 4 days of growth, each culture was sampled for measurements of OD_{750nm} and Nile Red fluorescence intensity using a microplate reader. The total Nile Red intensity of all the selected mutant strains are higher than the empty vector control, indicating higher total lipid yield on a per volume basis (**Fig. 3.3 A**). Meanwhile, the level of OD_{750nm} normalized Nile Red fluorescence intensity is also higher in all the mutant strains than the control line, estimating higher cellular lipid content (**Fig. 3.3 B**).

The enhanced lipid content in the selected target mutants was also validated by the abundance of the Nile Red fluorescent cells of the total population observed by the fluorescence microscope as well as the size and number of the lipid body within the individual cell visualized by the confocal microscope. It is clearly showed that the Nile Red positive cell count per total cell count (%) is 60.7 to 235.8% higher in the selected target mutants than the WT and control strain (**Fig. 3.3 C**), and also showed that the transgenic cells have higher number and bigger size of the lipid droplets than the WT and control cells (**Fig. 3.3 D**).

Figure 3.3 Nile Red fluorometric analysis of oil mutants. A) Total Nile Red fluorescence intensity of equal volume algal culture; **B)** Nile red fluorescence intensity normalized to OD750; **C)** Percentage of Nile Red positive cell number per total cell number detected by the fluorescence microscope. The average of three replicates and standard error are shown. Statistical analysis was performed using student t test. Asterisks indicate $P<0.05$. **D)** Representative confocal images of lipid bodies stained with Nile Red (yellow) in the target mutants. Green color shows chlorophyll auto-fluorescence. Scale bar, 5 μm.

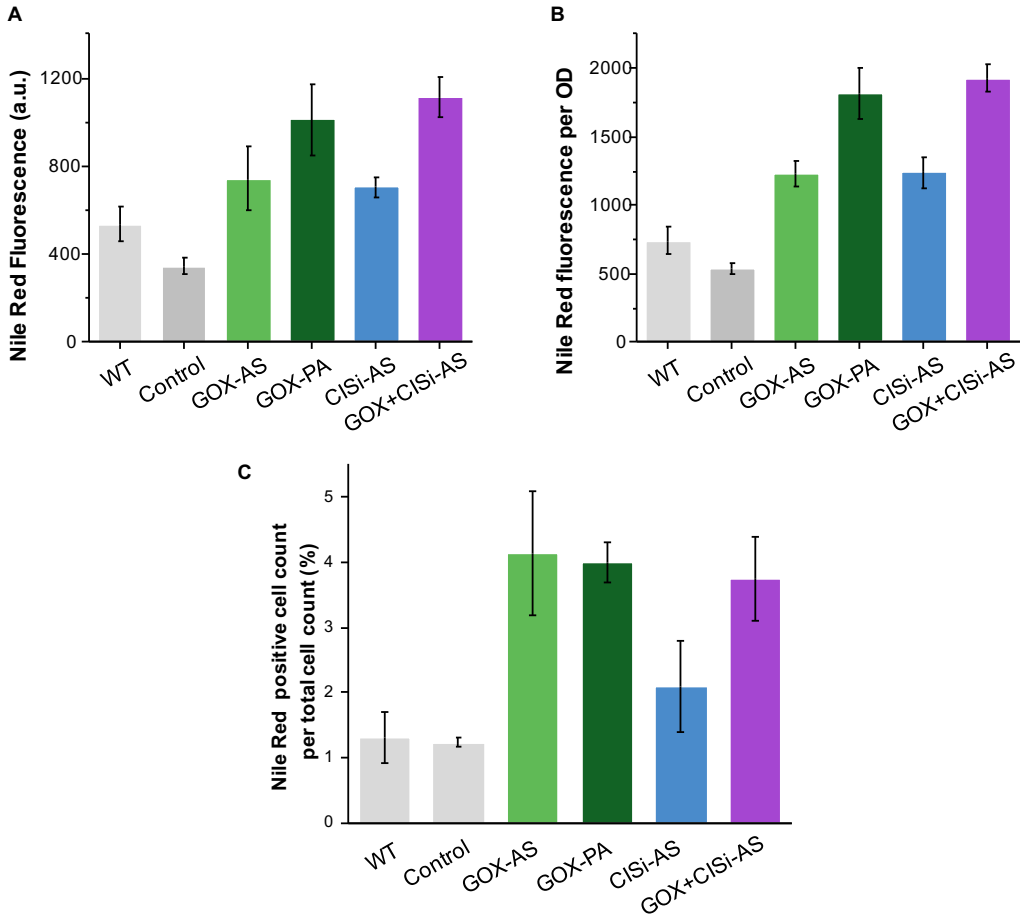
A
Nile Red Fluorescence (a.u.)
0
400
800
1200
WT
Control
GOX-AS
GOX-PA
ClSi-AS
GOX+ClSi-AS
B
Nile Red fluorescence per OD
0
500
1000
1500
2000
WT
Control
GOX-AS
GOX-PA
ClSi-AS
GOX+ClSi-AS
C
Nile Red positive cell count per total cell count (%)
0
1
2
3
4
5
WT
Control
GOX-AS
GOX-PA
ClSi-AS
GOX+ClSi-AS

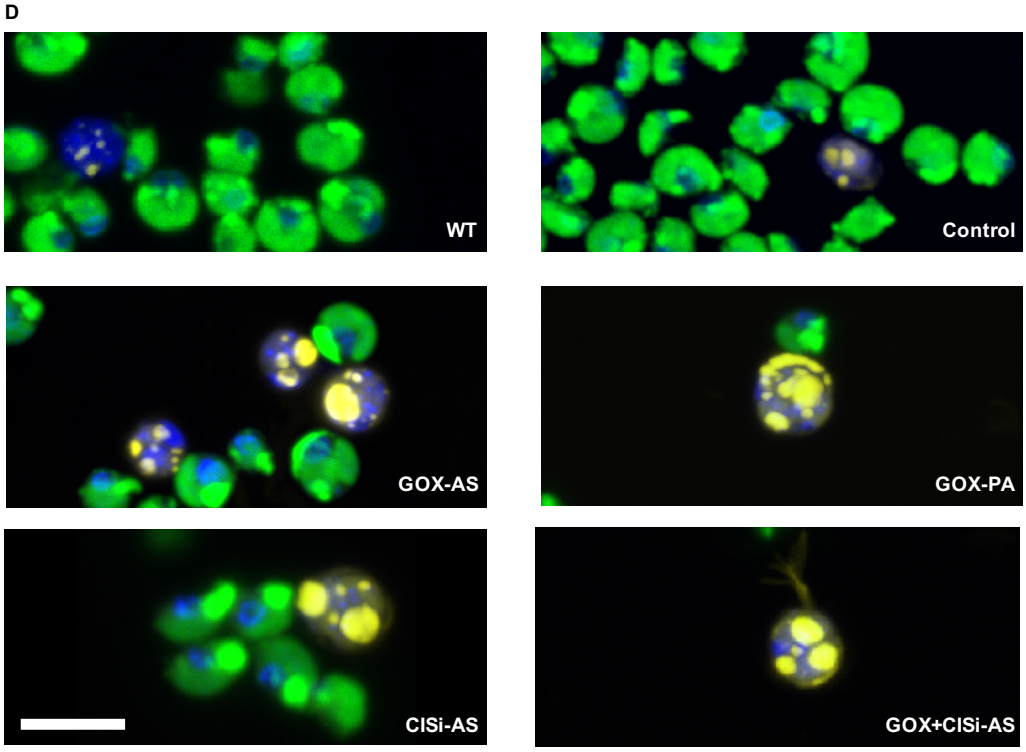
D
WT
Control
GOX-AS
GOX-PA
ClSi-AS
GOX+ClSi-AS

3.3.4 Quantitative lipid analysis by GC-FID

The productivity and composition of the total intracellular lipid in the selected target mutants were further validated by FAME analysis using GC-FID. Total lipids were extracted from each target mutant and the empty vector control harvested at the end of growth period and separated by thin-layer chromatography (TLC). Then the fatty acid methyl esters (FAMEs) were quantified by gas chromatography and flame ionization detection (GC-FID) to quantify TAGs, free fatty acids (FA) and polar lipids on a per cell basis. It was shown that the cellular TAG content in all the target mutants besides G-PA-5A were increased by 94.5 to 187.5%, the cellular free FA in all the mutants achieved 18.6 to 63.4% increase, while the polar lipid content either stay unchanged or only showed marginal increase in the mutants compared to the control strain (**Fig. 3.4 A-D**).

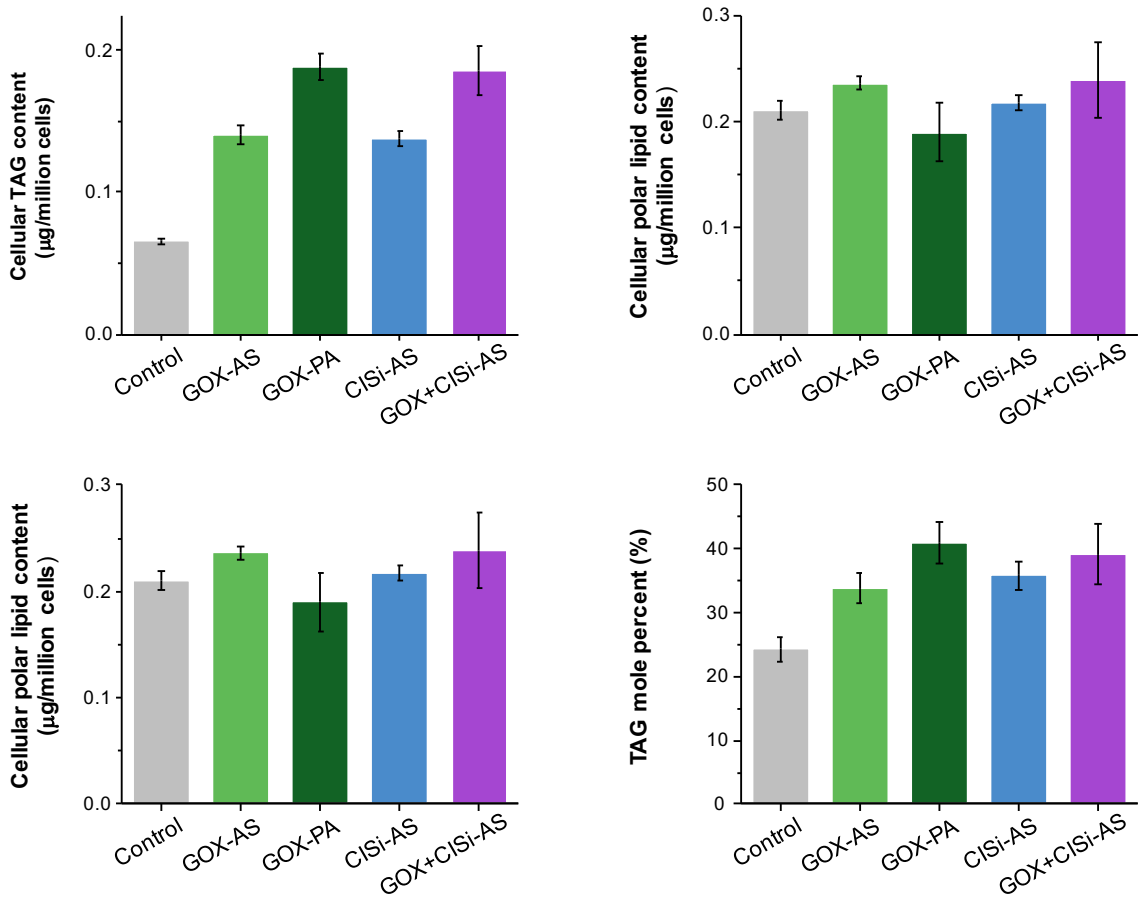

Figure 3.4 Quantitative lipid analysis of *N.o* oil mutants. A) Cellular TAG content; **B)** Cellular free fatty acid content; **C)** Cellular polar lipid content; **D)** TAG mole percentage over total lipids. TAG was isolated from lipid extracts by TLC separation and both TAG and total lipid were subjected to the transesterification reaction and then quantified by GC-FID. Quantification results are normalized based on cell number. The average of three measurements and standard error are shown. Statistical analysis was performed using student t test. *Asterisks* indicate $P<0.05$.

3.3.5 Transcriptional and translational changes in the target mutants

The transcriptional level of S.cG3PDH, N.oG3PDH and N.oCIS in all the selected mutants was quantified by qRT-PCR (**Fig. 3.5**). The calculated relative transcriptional level of S.cG3PDH is highly correlated with the target protein abundance estimated by the Nlux luminescence intensity and quantified by the western blot, with the highest in GOX-PA, followed by GOX+CISi-AS, and the lowest in GOX-AS. The transcriptional level of N.oCIS is only significantly decreased in CISi-AS (~45%), while stay unchanged in the two GOX lines and GOX+CISi-AS. Interestingly, at the presence of S.cG3PDH, the mRNA abundance of the endogenous N.oG3PDH was also slightly increased in the two GOX lines and GOX+CISi-AS.

The expressional level of S.cG3PDH was first estimated by the reporter gene NanoLuciferase (Nlux), which is translationally fused to S.cG3PDH by a glycine-serine-glycine encoded linker. It is shown in Figure 3.5 that all the target mutants harboring S.cG3PDH have higher level of Nlux luminescence than the WT, with the highest in GOX-PA, followed by GOX+CISi-AS, and the lowest in GOX-AS. The estimated protein abundance of S.cG3PDH in the transgenic lines was further confirmed by immunoblotting with antibodies detecting the hemagglutinin (HA) tag at the C terminus of S.cG3PDH. In GOX-PA, in which the Viral-derived P2A(60) peptide is used to tie the BleoR resistant marker (BleoR) to the target protein S.cG3PDH-Nlux, two bands with equal intensity were detected for each line, representing the BleR-2A-S.cG3PDH-Nlux and the S.cG3PDH-Nlux proteins (**Fig. 3.5**). Therefore, the ribosomal skipping efficiency was ~50%, similar to the that reported by Poliner et al (Poliner et al., 2018). A very faint single band representing the S.cG3PDH-Nlux protein was detected in GOX+CISi-AS,

but was absent in GOX-AS, indicating the abundance of the target protein was not high enough to be detected by the western blot in the loaded total protein.

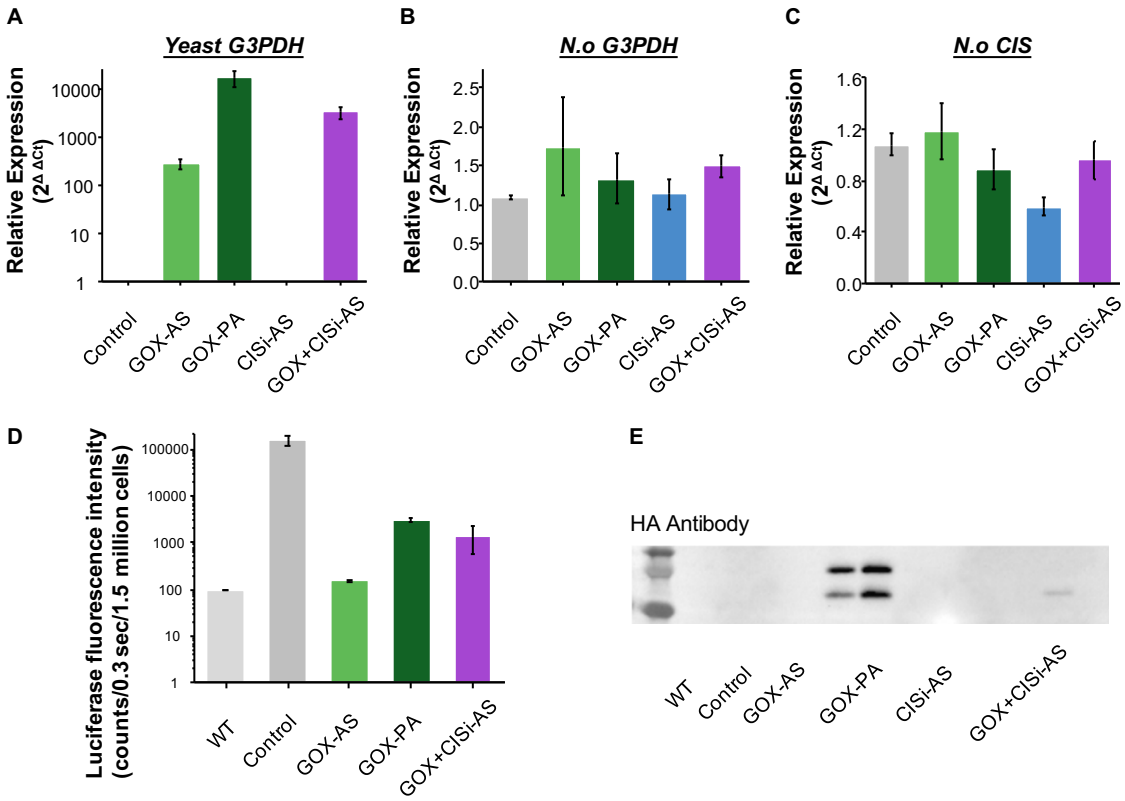

Figure 3.5 Transcriptional and translational analysis of the target mutants. The mRNA abundance of **A)** S.cG3PDH, **B)** N.oG3PDH and **C)** N.oCIS determined by quantitative RT-PCR. D) Luminescence intensity was measured to verify the successful transformation and in-frame transgene expression. E) Expression of the S.cG3PDH detected by western blot with the HA antibody in the selected mutants. The average of at least three replicates and standard error are shown. Statistical analysis was performed using student t test. Significance is indicated as $P<0.05$.

3.3.6 The effect of target mutagenesis on protein and carbohydrate

As the other two major sinks for photosynthetic fixed carbon besides lipid, the abundance of protein and carbohydrates were also quantified in the target mutants. It is shown in Figure 3.6 that while the total protein content decreased in all the transgenic lines, the carbohydrate content was not significantly affected.

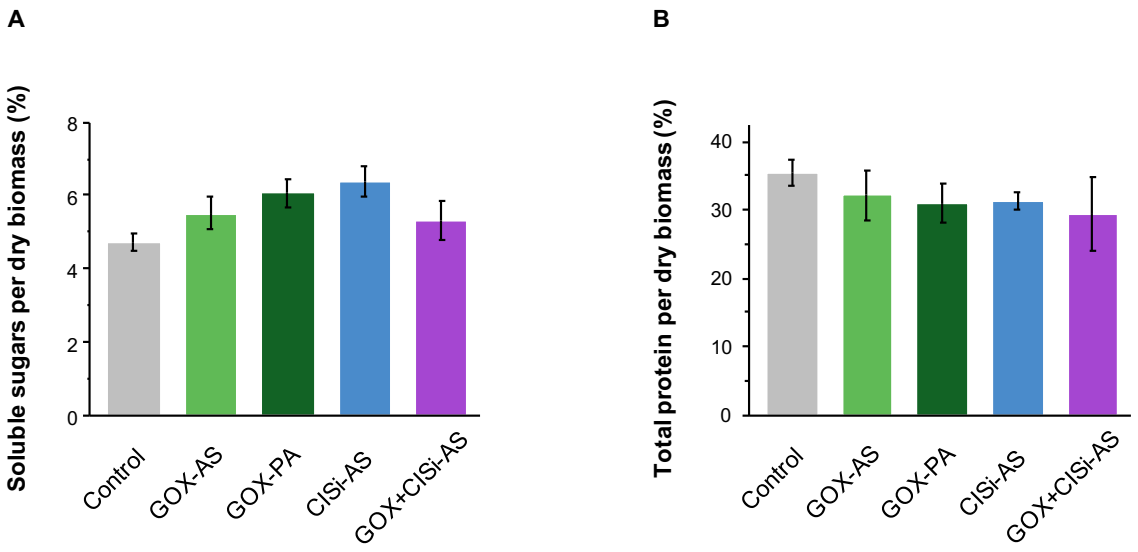

Figure 3.6 Quantification of carbohydrate and protein contents. A) total protein content (% dry biomass), **B)** total soluble sugars hydrolyzed from the storage carbohydrates (% dry biomass) in the target mutants and empty vector control by the end of the growth period. The average of three replicates and standard error are shown. Statistical analysis was performed using student t test. Significance is indicated as $P<0.05$.

3.3.7 Cell growth and photosynthesis

Biomass productivity of the selected target mutants in the exponential phase was determined by the dry weight measurement of the harvested culture. As shown in Figure 3.7, all the selected target mutants have slightly lower biomass accumulated than the control line, though not statistically significant. Therefore, it is of interest to investigate whether the up- and/or down-regulation of the target gene(s) would affect the photosynthetic efficiency in terms of carbon fixation rate in the transgenic lines. A novel CO_2-dependent variable chlorophyll a fluorescence technique was developed for this purpose, allowing the probing of *in vivo* kinetics of the whole electron transport chain from oxygen evolution catalyzed by water oxidizing complex (WOC) in PSII through CO_2 fixation catalyzed by RuBisCO in the Calvin-Benson cycle. Algal culture sampled at the exponential growth phase was dark incubated for 5 min to quench all reaction centers, and then subjected to 220 flash trains consisting of 50 sequential single turnover flashes (11,000 flashes in total) at a fixed frequency of 100 Hz. A typical variable chlorophyll fluorescence response after dark adaptation displays 4 distinct time-resolved features: a sharp decline arising from reduction of the PQ pool, followed by a small broad peak arising from reduction of NADP+, and then a continuous slope arising from CO_2 fixation by the Calvin-Benson cycle, and finally the plateau representing the steady state CO_2 fixation. For the examined *N.o1779* WT and transgenic culture, only 3 features were observed: a sharp decline encompassing the PQ pool turnover, followed by a continuous slope arising from NADP+ reduction and initiation of CO_2 fixation, and lastly the plateau indicating the maximized rate of CO_2 fixation catalyzed by RuBisCO functioning at the steady state. As shown in Figure 3.6, the overall variable chlorophyll fluorescence

kinetics, denoted as Fv/Fm, is higher in WT than all the target mutants in phase 2 and 3. The slower rise of Fv/Fm in phase 2 followed by the lower steady state level in phase 3, indicate the slower CO_2 fixation rate and a less efficiency turnover of Calvin cycle achieved in the selected oil mutants.

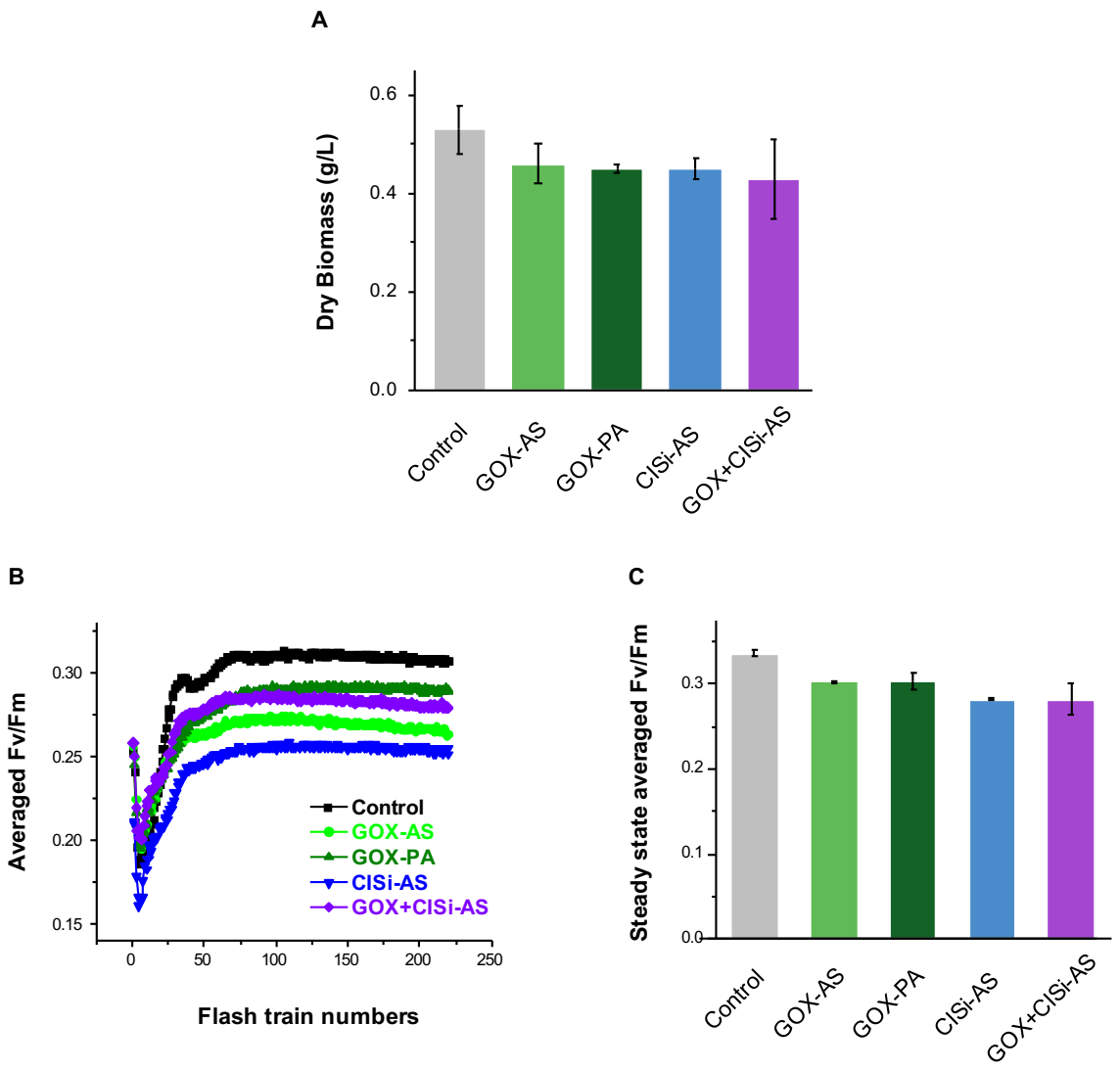

Figure 3.7 Biomass productivity and CO_2 dependent chlorophyll fluorescence kinetics. A) Dry biomass; **B)** Fv/Fm kinetics of the representative target mutants and the control line over 220 flash trains after carbon fixation inhibited baseline normalization; C) Saturating Fv/Fm of the representative target mutants at the steady state after carbon fixation inhibited baseline normalization. Statistical analysis was performed using student t test. Significance is indicated as $P<0.05$.

3.4 Discussion

3.4.1 Effects of N.oCIS knockdown on TAG accumulation

From the increasing reports on the metabolic engineering of microalgae for lipid production, it is worth noting that regardless of the specific target gene, the enhancement of neutral lipid accumulation is always coupled with the restricted protein synthesis. It is suggested that the availability of acetyl-CoA, the essential carbon precursor competed by both pathways, might be a crucial bottleneck for lipid biosynthesis. Acetyl-CoA carboxylase (ACCase) and Citrate Synthase (CIS) are the key enzymes catalyze the first step in the *de novo* fatty acid biosynthesis and TCA cycle, respectively. While a lot of attempts have been made to "push" acetyl-CoA towards free fatty acids (FA) by overexpressing ACCase in diatoms and plants (G. Dunahay et al., 2008; Kindle, 1990; Tan & Lee, 2016b), the role of CIS on lipid accumulation in microalgae remains ambiguous. Deng et al has reported that the silencing of CIS enhanced the lipid production in *Chlamydomonas reinhardtii* (Deng et al., 2013a). Here in our study, by employing the RNAi-mediated gene silencing approach, we created CIS knockdown mutant with elevated fraction of cellular TAG quantified by GC-FID, enhanced Nile Red fluorescence intensity either detected by the microplate reader or visualized by the fluorescence microscope, and increased number and size of the lipid body observed by the confocal microscope. These lipid phenotypes together with the decreased abundance of the CIS transcripts corroborated the functional role of CIS in *N.o1779*. The decreased protein content and the enlarged free fatty acid pool clearly suggested the photosynthetic assimilated carbon was shunt from TCA cycle for protein synthesis to *de novo* fatty acid

biosynthesis. It is also demonstrated that the "push" strategy applied here by artificially blocking TCA cycle, can more efficiently divert the carbon precursors to the FA pool than by overexpressing ACCase, which has achieved little success for enhancing the lipid production (Radakovits et al., 2010).

3.4.2 Effects of S.cG3PDH expression on TAG accumulation

Glycerol-3-phosphate dehydrogenase (G3PDH) catalyzes the formation of glycerol-3-phosphate (G3P) and NAD^+ from the reduction of dihydroxyacetone phosphate (DHAP) and NADH (Herrera-Valencia et al., 2012). While the importance of G3P as the precursor of glycerol has been greatly investigated in the osmoregulation, the functional role of G3P in TAG biosynthesis has been mostly studied in higher plants (Vigeolas & Geigenberger, 2004), but limited in microalgae.

The transcriptome analysis of *Chlamydomonas reinhardtii* reported by Lv et al highlighted the remarkable up-regulation of G3PDH after the start of neutral lipid accumulation (Lv et al., 2013), suggesting its engineering potential in microalgae. Recently, it is also reported by Wang et al that overexpression of the codon optimized yeast G3PDH under the control of an inducible heat shock promoter led to enhanced lipid synthesis in *Chlamydomonas reinhardtii* after intermittent heat shock (Wang et al., 2018). In the present work, by introducing the full length coding sequence of the yeast cytosolic G3PDH (S.cG3PDH) under the control of an *N.o1779* endogenous bidirectional promoter, the TAG content was found to be significantly increased in the transgenic lines by 95% to 188% compared to the control line. The elevated TAG content in the target mutants are in accordance with the higher Nile Red fluorescence intensity detected by the

microplate reader and the fluorescence microscope, as well as the increased number and size of the lipid body observed by the Confocal microscope. These results together with the abundant S.cG3PDH transcripts as revealed by quantitative RT-PCR, demonstrate the functional role of G3PDH in elevating the TAG accumulation in the target mutants of *N.o1779*. In addition to TAG, the increase of free FA was also observed in the target mutants, indicating the contribution from the *de novo* fatty acid biosynthesis instead of the degradation of the membrane polar lipid.

3.4.3 The simultaneous regulation of N.oCIS and S.cG3PDH does not lead to an additive effect

In the stacking mutant with the simultaneous regulation of N.oCIS and S.cG3PDH, though the lipid productivity was also promoted compared to the control line, however not beyond the level of the transgenic lines with the single gene manipulation. The absence of an additive effect might be explained by the inefficient knockdown of N.oCIS as revealed by qRT-PCR. It can be either due to the well-known drawbacks of the RNAi technology itself, in which the specific knockdown effect can be easily masked by its off-target signature, or due to the complicated interplay and crosstalk of the metabolic pathways in microalgae. Microalgae may defend themselves against the attempt to drain the TCA cycle and divert the limited carbon precursors into the lipid biosynthesis pathway. To guarantee enough proteins being synthesized for maintaining healthy cell status, it might upregulate the CIS level to cancel out the knockdown effect from the transgene.

3.4.4 The dilemma for balancing growth and lipid productivity

In the present work, elevated cellular TAG accumulation was achieved by manipulating the two key enzymes, however at the expense of slightly sacrificing the biomass yield and the photosynthetic carbon fixation rate. Such dilemma exists in most of the metabolic engineering attempts for improving biofuel production, since both biomass and lipid synthesis pathways compete for the same photosynthetic assimilates (Tan & Lee, 2016b). In the CIS knockdown line, the central carbon metabolites acetyl-CoA is more efficiently diverted into the *de novo* FA biosynthesis pathway instead of TCA cycle, while in the heterologous S.cG3PDH expression lines, dihydroxyacetone phosphate (DHAP) is shunted away from glycolysis, and utilized to form glycerol 3 phosphate (G3P), the backbone for TAG assembly. Furthermore, the compromised growth is not only caused by the limitation of carbon precursors for biomass production, but also due to the availability of reducing power in the form of NADPH for CO_2 fixation by the Calvin Cycle. In the oil mutants, more reducing power are recruited for lipid biosynthesis, leading to the decreased rate of CO_2 fixation as revealed by the CO_2 dependent fluorescence technique. Therefore, to achieve enhanced lipid productivity without compromising the photosynthetic growth capacity, it is critical to improve photosynthesis for generating abundant carbon assimilates as well as reducing power.

Chapter 4. Random mutagenesis of the heterokont *Nannochloropsis oceanica* CCMP1779 for screening of acidophilic microalgae

Summary

Aquatic microbial oxygenic photoautotrophs (AMOPs) are by far the most productive photosynthetic organisms at solar energy conversion. The marine heterokont *Nannochloropsis oceanica* CCMP1779 (*N.o1779* hereafter) is drawing considerable interests as a resource for biodiesel production due to its robust growth in open cultures and naturally high lipid content. Currently, the only practical means for delivering CO_2 at large scale is to site algal production facilities near fossil power plants and utilize flue gas for algal cultivation. Therefore, it is necessary to identify robust algal strains that can tolerate the resulting acidic environment resulted from excessive dissolved CO_2 in the culture, while performing efficient carbon sequestration and utilization at the presence of high abundance of dissolved inorganic carbon (DIC). In the present study, the strategy of insertional mutagenesis was employed to create a *N.o1779* random mutant library consisting of 1,200 strains, which were subjected to high-throughput screening for identifying promising candidates with desired phenotypes, namely robust growth at acidic pHs (pH = 5.5 and 6.4). LpH23, the winning strain outcompeting WT in the screening process, was further evaluated for its growth potential and photosynthetic capacity using a number of biophysical approaches. Showing advantages in photoautotrophic growth and intrinsic photosynthetic efficiency in terms of water oxidation and CO_2 fixation rates in both the standard laboratory growth condition and acidic environment, LpH23 has great potential to be utilized in the flue gas supplied

cultivation system. Going forward, the mutation site in LpH23 will be genetically localized to identify the mutated gene(s) responsible for the observed phenotype.

4.1 Introduction

Climate change and depletion of the finite fossil fuel resources are not only threatening the global energy security but also significantly contribute to the anthropogenic greenhouse gas (GHG) emissions, causing the most pressing environmental problem, climate change (Ahmad et al., 2011; Ottmar et al., 2011). Renewable energy offers the opportunity to secure energy supply, mitigate global warming, and reduce the negative effect of GHG on environment and human health (Ottmar et al., 2011). Among the various renewable sources, microalgae appear to be an important feedstock of biodiesel that has great potential to displace a substantial amount of fossil fuels over the next few decades (Chisti, 2007b; Fulton, 2004; Rajagopal et al., 2009).

Despite its potential as a promising alternate renewable source, some key improvements including culture cost minimization and oil-rich strain development must occur for microalgae before their successful commercialization for biofuel production (Zhu et al., 2014a). Since adequate supply of carbon source required by the mass cultivation of microalgae represents up to 60% of the costs along with nutrients, utilization of the flue gas from industrial plants could serve as an effective strategy to reduce costs (Zhu et al., 2014a). Flue gas released from the power plants is composed mainly of 10-15% (v/v) CO_2, after the traces of harmful acid gases such as sulfur oxides and nitrogen oxides being removed by the post-combustion gas capture processes (Martelli et al., 2011; Wall, 2007; Zeiler et al., 1995). Though successful attempts in flue gas cultivation have been achieved in a handful of photoautotrophs, the overwhelming majority of microalgae will risk deleterious effects on growth and photosynthesis when

sparged with CO_2 enriched flue gas (Cheng et al., 2016a; Koberg et al., 2011; Solovchenko & Khozin-Goldberg, 2013). While the underlying mechanism responsible for tolerance to elevated CO_2 levels are still poorly understood (Solovchenko & Khozin-Goldberg, 2013), it is generally believed that maintaining the cellular pH homeostasis is critical for the microalgae's tolerance to the flue gas supplied environment, which is not only enriched with dissolved inorganic carbon (DIC), but also substantially acidified (Solovchenko & Khozin-Goldberg, 2013). Therefore, oleaginous microalgal strains that can tolerate acidic environment have great potential to actively grow and efficiently produce lipids in the flue gas supplied open culture.

The oleaginous heterokont, *Nannochloropsis oceanica* CCMP1779 (hereafter *N.o1779*), has drawn considerable attention from the researchers for its robust growth, natural capability of accumulating triacylglycerol (TAG) in high abundance and tolerance to broad environmental and culture conditions (Wang et al., 2012). With the well-established transformation method in this species, insertional mutagenesis approach utilizing a drug resistant DNA cassette can be easily applied to *N.o1779* to rapidly develop new strains with novel phenotypes. In the present study, *N.o1779* is selected as the parental strain for generation of a random mutant library via insertional mutagenesis. With a newly developed high-throughput screening strategy utilizing agar solidified growth medium buffered at gradient pHs (5.5, 6.1, 6.4, 7.2 and 8.2), we have successfully isolated an insertional mutant strain, LpH23, showing enhanced tolerance to low pH compared to WT. Demonstrating advantages in photoautotrophic growth and intrinsic photosynthetic efficiency in acidic environments, LpH23 has great potential to be utilized in the flue gas supplied cultivation system. Going forward, genetic characterization will

be employed to pinpoint the mutation site, allowing a deeper understanding of the regulatory mechanism responsible for the low pH tolerating phenotype in *N.o1779*.

4.2 Material and Methods

4.2.1 Microalgal strain and cultivation condition

Nannochloropsis oceanica CCMP1779 (*N.o1779*) was used in this study as a parental strain to generate the insertional mutant library. It was obtained from the Bigelow National Center for Marine Algae and Microbiota (NCMA, https://ncma.bigelow.org/). *N.o1779* and the mutant library derived from it were maintained on agar plates containing A+ medium supplemented w/o 50 μg/mL of hygromycin B and arrayed in a 96-colony format.

4.2.2 Generation of a random mutant library of *N.o1779*

A library of insertional mutants was generated via transformation of *N.o1779* WT strain with a DNA cassette carrying the *Streptomyces hygroscopicus aph7* gene, which confers resistance to hygromycin B. The DNA cassette was randomly inserted into the nuclear genome of *N.o1779* via electroporation as previously described (Vieler et al., 2012). After electroporation, the cells were allowed to recover for 48 hours in f/2 medium on shaker under continuous illumination before they were spread on selection agar-solidified f/2 medium containing 50 μg/mL of hygromycin B. Resistant colonies were observed about two weeks after electroporation and were transferred into liquid f/2 medium in 96-well plates after another 2 weeks. After growing up in the liquid media for another month, all the independent transformants were further transferred onto agar-solidified A+ medium containing 50 μg/mL of hygromycin B and arrayed in a 96-colony format for maintenance.

4.2.3 High-throughput screening of the random mutant library

4.2.3.1 OD_{750nm} and Chlorophyll fluorescence-based screening

1,200 random mutants were inoculated into liquid A+ medium in 96-well plates and grown at 22 ^{o}C under 40 $\mu E/m^2/s$ illumination in a 16:8 light/dark regime under 2% CO_2 atmosphere. Growth curve of each individual strain was obtained by measuring OD_{750nm} and Chlorophyll content during a growth period of 8 days. About 5.5% (66) of the mutants with the fastest growth rates, and consequently shortest doubling times, were selected for the next round of screening.

4.2.3.2 Low pH tolerance base screening

The 70 mutants selected from the primary screening were inoculated on agar-solidified A+ medium buffered at 5 different pHs (5.5, 6.1, 6.4, 7.2 and 8.2). After 10 days of cultivation under the same growth environment as the primary screening, two mutants that survived and developed denser colonies than WT on the pH 6.1 plate were selected for final confirmation in the 24 well plate with A+ liquid medium buffered at 5 different pHs. The standard A+ medium at pH 8.2 contains Tris (1 g/L, pH 8.2), KH_2PO_4 (0.05 g/L), NaEDTA-$2H_2O$ (0.03 g/L), $FeCl_3$-$6H_2O$ (3.89 x 10^{-3} g/L, 0.1N HCl), NaCl (18 g/L), KCl (0.6 g/L), $NaNO_3$ (1 g/L), $MgSO_4$-$7H_2O$ (5 g/L), $CaCl_2$-$2H_2O$ (0.27 g/L), H_3BO_3 (0.034 g/L), $MnCl_2$-$4H_2O$ (0.004 g/L), $ZnCl_2$ (0.315 x 10^{-3} g/L), Na_2MoO_4-$2H_2O$ (0.043 x 10^{-3} g/L), $CuSO_4$-$5H_20$ (0.003 x 10^{-3} g/L) and CoCl2-6H2O (0.012 x 10^{-3} g/L). To prepare A+ medium at pH 7.2, MOPS (2.09 g/L, pH 7.2) was used to replace Tris (1 g/L, pH 8.2) in the standard A+. To prepare A+ medium at pH 5.5, 6.1 and 6.4, MES

(2.13 g/L) buffered at pH 5.5, 6.1 and 6.4 was used respectively to replace Tris (1 g/L, pH 8.2) in the standard A+ medium.

4.2.4 Chlorophyll extraction and quantification

The chlorophyll pigments were extracted through a 90% methanol extraction procedure. Algal culture was spin down into cell pellets and resuspended in equal volume of 90% methanol. After 30 min dark incubation to ensure efficient disruption of the cell wall and complete extraction of Chl into the solvent, the solution was centrifuged at the maximum speed for 5 min and the supernatant was used to determine the absorbance at 665 nm via the spectrophotometer.

4.2.5 *In vivo* variable Chl-a fluorescence measurement by Fast-Repetition Rate Fluorometry (FRRF)

In vivo variable Chl-a fluorescence measurements were carried out using a home-built laser fast repetition rate (FRR) fluorometer as described previously (Ananyev & Dismukes, 2005). Fifty microliter algal liquid culture sampled from the mid-log phase was dark-adapted for 5 min and then subjected to 50 single turnover flashes (STFs) applied at 100-1000 Hz. The variable Chl emission yield (Fv/Fm=(Fm-Fo)/Fm) was measured on each flash of 20 μs duration and a laser intensity of 80,000 $\mu E/m^2/s$.

4.2.6 *In vivo* flash O_2 measurement by Clark-type electrode

To measure O_2 yield per flash in algal cells, a home-built Clark-type Pt-Ir electrode equipped with a 5 W red LED was used as described previously (Ananyev et

al., 2017). 10 µl algal liquid culture sampled from the mid-log phase was loaded into an aerobic "wet" chamber, dark adapted for 3 min and then subjected to 50 single turnover flashes (STFs) applied at 0.5 Hz. The oxygen yield was measured on each flash of 50 µs duration and a laser intensity of 32,000 $\mu E/m^2/s$. By coupling to a high gain preamplifier with active signal filter, the electrode enable an overall sensitivity of about 1 x 10 − 15 mol O_2/s and time resolution of about 100 ms. The flash induced oscillations of O_2 yield were analyzed by 1) model-independent analysis via Fourier transformation and 2) model-dependent analysis by VZAD, an advanced WOC cycle model as described in prior work.(Ananyev et al., 2016; Vinyard et al., 2013d)

4.2.7 CO_2-dependent *in vivo* variable Chl-a fluorescence measurement

The CO_2 dependent Chl-a fluorescence technique is an extension of the aforementioned "FRRF", which allows the probing of *in vivo* kinetics of the whole electron transport chain. Fifty microliter algal liquid culture sampled from the mid-log phase was dark-adapted for 5 min, and then subjected to 220 flash trains of 50 sequential single turnover flashes (11,000 flashes in total) applied at 100 Hz. The variable Chl emission yield (Fv/Fm=(Fm-Fo)/Fm) was measured on each flash of 20 µs duration and a laser intensity of 80,000 $\mu E/m^2/s$.

4.2.8 Time-resolved O_2 evolution

Time-resolved O_2 evolution of the low pH growing cultures were measured using a home-built bare platinum electrode controlled by Labview software as described previously (Krishnan et al., 2015). Ten microliter culture sampled from its growth

condition was immediately loaded onto the electrode, dark-incubated for 5 min, and illuminated with red light (800 μE m^{-2} sec^{-1}). The full kinetics of O_2 evolution were recorded over 2 min.

4.3 Results and discussion

4.3.1 Generation of a random insertional mutant library for *N.o1779*

Various methods have been reported to generate random mutants of *Nannochloropsis* spp., including UV, chemical mutagenesis or insertional mutagenesis (Beacham et al., 2015; Perin et al., 2015a). Since chemical mutagenesis usually creates multiple point mutations that makes identification of the gene(s) responsible for the observed phenotype complicated and time consuming, we generated the random mutant library by insertion of a DNA cassette conferring resistance to Hygromycin B (Perin et al., 2015a). Two kinds of insertional DNA cassette were prepared from the pNOC401 plasmid, which harbors an *apha7* gene (from *Streptomyces hygroscopicus*) conferring resistance to Hygromycin B. The linearized full plasmid was obtained by digesting pNOC401 with *AhdI*, while the Hygromycin B resistant cassette with the *MmeI* cutting sites containing only the selection marker driven by the Elongation Factor (EF) promoter and terminated by the LDSP termination was PCR amplified from pNOC401. Using the electroporation method as previously described, 800 individual transformants were obtained from the linearized full plasmid, while 400 mutants were obtained from the PCR fragment with *MmeI* cutting sites. The survived antibiotic resistant colonies contained at least one copy of the transgene randomly integrated into their genome. Considering the high gene density in *N.o1779* nuclear genome (11,973 annotated protein-coding genes in 28.7 Mbp, approximately 417 genes/Mbp), the resulting mutants should have a higher chance of gene disruption (Perin et al., 2015a).

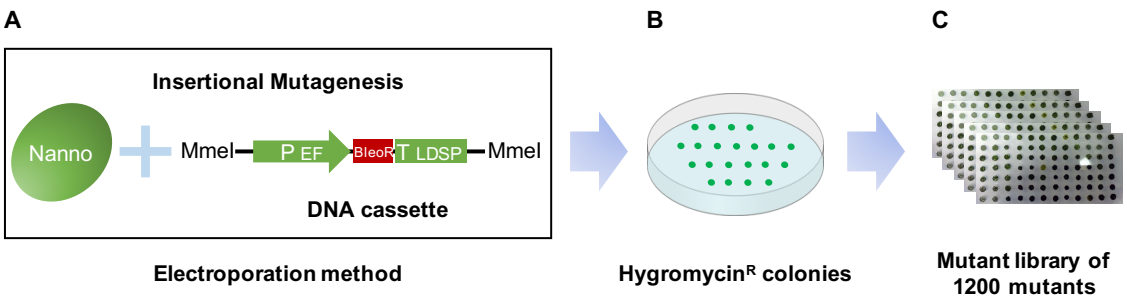

Figure 4.1 Generation of *N.o1779* mutant library by insertional mutagenesis. A) Transformation of *N.o1779* is performed via electroporation with an insertional DNA cassette conferring Hygromycin B resistance. **B)** Electroporated cells were screened on agar-solidified f/2 medium supplemented with 50µg/ml hygromycin. **C)** 1,200 independent antibiotic resistant transformants were picked into a collection of arrays of 96 colonies on agar plates for maintenance and further analysis.

4.3.2 High throughput pH screening of the mutant library

To identify robust growers that are resilient to the acidic environment with low pH, the random mutant library was subjected to a three-step screening procedure: 1) primary screening for robust growth under standard growth conditions; 2) secondary screening for enhanced tolerance to acidic environments; 3) confirmation step of the low pH tolerance. In the primary screening, 1,200 independent random mutants were grown in the 96 well microplates with the standard A+ medium (pH 8.2) under 2% CO_2 atmosphere. During a growth period of 8 days, 66 mutants (5.5%) with the highest intrinsic growth rates, and consequently the shortest doubling times, were identified via the time course measurements of OD_{750nm} and Chl fluorescence intensity using a microplate reader. In the secondary screening, agar-solidified A+ medium buffered at low pHs were prepared to mimic the acidified environment induced by flue gas delivery, and used to examine the tolerance of the selected robust growers to low pH. The A+ medium pHs at 6.4, 6.1 and 5.5 were selected based on the actual equilibrium pHs when the growth medium was purged with 5%, 10% and 15% CO_2 gas. Serving as controls in the low pH screening procedure, pH 8.2 was selected to mimic the sea water environment as the natural habitat of *N.o1779*, and pH 7.2 was also chosen to simulate the environment aerated with 2% CO_2, the concentration reported to achieve the maximal biomass productivity in a lot of microalgal species including *Nannochloropsis oculata* (Chiu et al., 2009). After cultivating the selected mutants on the pH buffered medium for 10 days, a pH dependent growth pattern was clearly observed for most strains including WT, with decreasing pH leading to increasing inhibitory effect on their photoautotrophic growth. As shown in Figure 4.2, on the two control plates, all the strains grew into high density

on the pH 8.2 plate, while a few of them were less healthy with less cell proliferation on the pH7.2 plate. On the three experimental plates, 21% of the selected mutants didn't survive the pH 6.4 treatment, and only 4 strains remained viable on the pH 6.1 plate, while no strain survived on the pH 5.5 plate. By the end of the secondary screening, the two strains showing stronger tolerance and better growth on the pH 6.1 plate than WT were picked for the final confirmation step of their low pH tolerance. Together with WT, they were inoculated into the 24 well plate with A+ medium buffered at the 5 different pHs. After 8 days' cultivation, while all three strains showed healthy growth and comparable cell density at the two control pHs (7.2 and 8.2), only the strain LpH23 survived well at the three low pHs (5.5, 6.1 and 6.4) (**Fig. 4.2 C**).

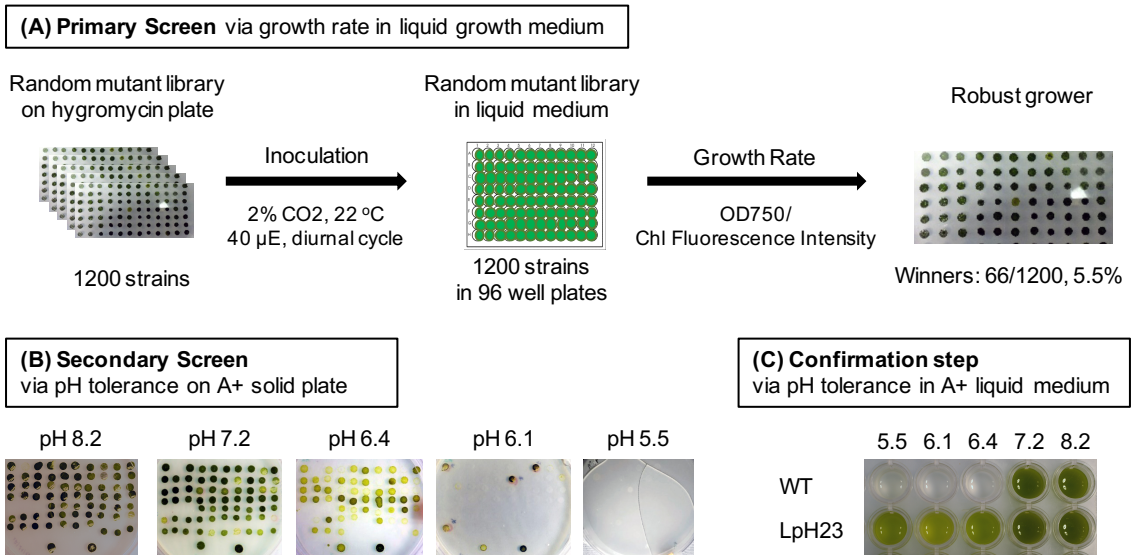

Figure 4.2 High throughput screening of random mutant library for robust growth and enhanced tolerance to low pH. A) Primary screening of the random mutant library for robust growth. 1,200 random mutants were inoculated into A+ liquid medium in 96-well plates and grown at 22 °C under 40 µE/m^2/s light in a 16:8 light/dark regime under 2% CO_2 atmosphere. Growth curves were obtained by measuring OD_{750nm} and Chlorophyll content on a daily basis during a growth period of 7 days. Sixty-six (5.5%) mutants with the fastest growth rates were selected for the secondary screening. **B)** Secondary Screening of the robust growers for enhanced tolerance to low pH. The 66 mutants selected from the primary screening were inoculated on agar-solidified A+ medium buffered at 5 different pHs (5.5, 6.1, 6.4, 7.2 and 8.2) and cultivated under the same growth environment as the primary screening. **C)** Confirmation step of the low pH tolerance. The low pH tolerance of the mutant LpH23 was confirmed in 24 well plate

with liquid growth medium under the same growth environment as the two rounds of screening.

4.3.3. Growth analysis under standard laboratory cultivation condition

The growth potential and photosynthetic efficiency of LpH23 was further evaluated under standard laboratory cultivation condition. WT and LpH23 were grown in a batch culture (17 mL working volume in the standard A+ medium) at 22 ^{o}C under 70 $\mu E/m^2/s$ illumination in a 16:8 light/dark regime. The algal culture was supplied with a continuous delivery of humidified air. During the growth period of 7 days, LpH23 achieved an marginally increased growth rate compared to WT based on the time course measurements of OD_{750nm} and Chlorophyll content (**Fig. 4.3**).

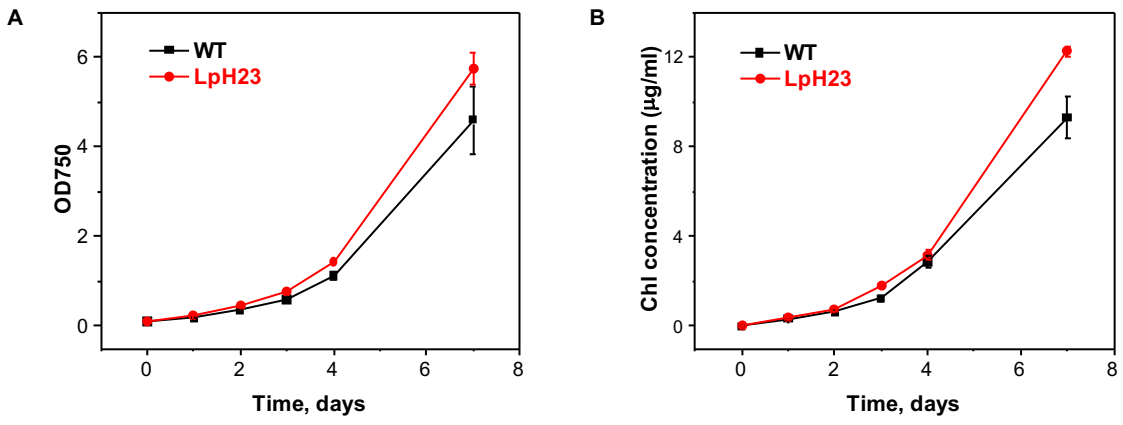

Figure 4.3 Growth curve under optimal growth conditions. Growth kinetics determined by A) optical density at 750 nm and by **B)** chlorophyll content (µg/ml).

4.3.4. Photosynthetic efficiency determined under standard laboratory cultivation condition

To further investigate the photosynthetic characteristics of LpH23 using WT as control, culture of both strains grown under the standard laboratory cultivation condition for 6 days were subjected to the *in vivo* flash O_2 measurement. With the home built Clark-type Pt-Ir electrode, the efficiency of photosynthetic turnover can be directly measured by the oxygen production on a per-flash basis, since oxygen release occurs when 4 successful charge separations are completed by 4 successful adsorptions and use of quanta for photochemistry. A period 4-type oscillatory pattern was observed as the water oxidizing complex (WOC) cycles through each progressive oxidation states due to the sequential flashing of light (Ananyev et al., 2016; Dasgupta et al., 2008; Gates et al., 2016). As shown in Figure 4.4 A, the amplitude, the number of oscillations, and the relative oxygen quantum yield at the steady state are very similar in LpH23 and WT on a per 10^6 cells basis. The Fourier transform of these flash oxygen oscillatory kinetics revealed that the WOC cycle period for oxygen production at 0.5 Hz (P_{FT}) is 4.3 in both LpH23 and WT, indicating little difference between the functional efficiency of WOC in the two strains (**Fig. 4.4 B**). Fitting the same data to VZAD model (Vinyard et al., 2013d) provided the best-fit WOC cycle efficiency parameters in Table 1, showing normal misses (alpha), small double-hits (beta), backward transition (delta), and photoinactivations (epsilon) in both WT and LpH23. The so-called quality factor of the two strains were also calculated as the inverse of the sum of all inefficiencies [$Q=1/(\alpha+\beta+\delta+\varepsilon)$) (Ananyev et al., 2017). Compared to WT with Q = 5.06, LpH23 with Q = 5.25

suggested a slightly more efficient synchronization of S states through the WOC cycle, possibly due to less backward transitions.

An equally powerful tool to assess the functionality of the primary photosynthetic machinery photosystem II (PSII) is the *in vivo* variable Chl-a fluorescence technique. The home built Fast-Repetition Rate Fluorometry (FRRF) allows the PSII charge separation quantum yield to be determined via Fv/Fm, the ratio of variable to total yield of chlorophyll fluorescence (Ananyev & Dismukes, 2005; Ananyev et al., 2016; Dasgupta et al., 2008). FRRF data obtained for the 6-day old WT and LpH23 cultures sampled from the standard laboratory cultivation condition revealed that, in general, LpH23 was able to perform charge separation more efficiently than WT at all the tested flash frequencies (100 Hz, 500 Hz and 1000 Hz). As shown in Figure 4.5, the higher level of steady state Fv/Fm in LpH23 compared to WT is most significant at 100 Hz, while become less and less prominent as the flash frequency increased to 1000 Hz. The same trend was also observed for the period-four oscillations of Fv/Fm, which retained much longer in LpH23 than in WT at the 100 Hz flash frequency, however damping very fast in the higher flash frequencies 500 Hz and 1000 Hz in both strains.

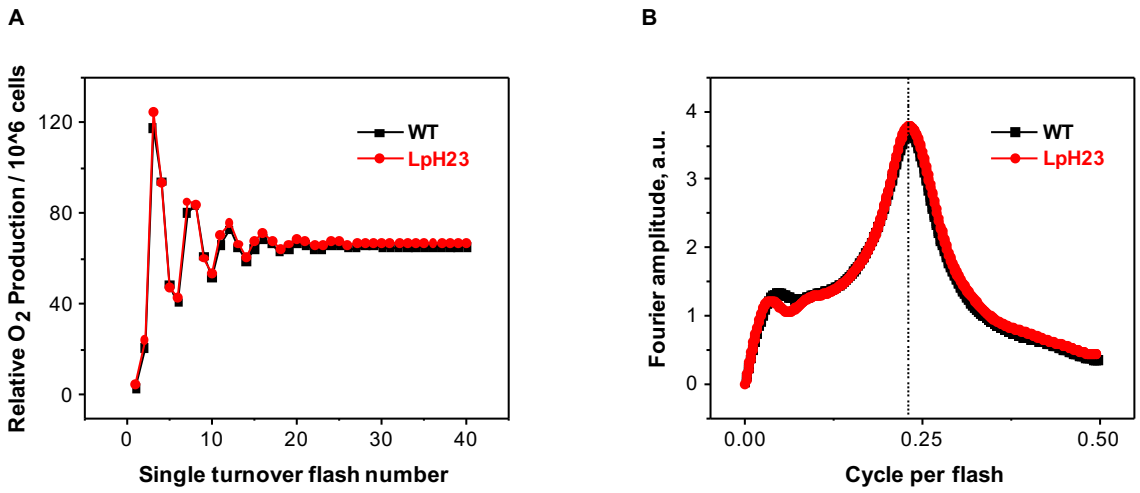

Figure 4.4 Relative flash oxygen yield of *N.o1779* WT and Lph23 cultures grown at standard laboratory cultivation condition for 6 days. A) The relative oxygen production on a per 10^6 cells basis over 40 single turnover flashes. **B)** Fourier transform of the oscillatory flash oxygen kinetics.

Table 4.1 WOC cycle parameters and dark S-state populations. Flash rate 0.5 Hz; dark pre-incubation time 180 s.

Strain	α	β	δ	ε	S0	S1	S2	S3	$P_{calc.}$	Q factor
WT	0.104	0.026	0.062	0.005	0.354	0.597	0.049	0	4.304	5.06
LpH23	0.106	0.035	0.045	0.004	0.331	0.631	0.038	0	4.305	5.25

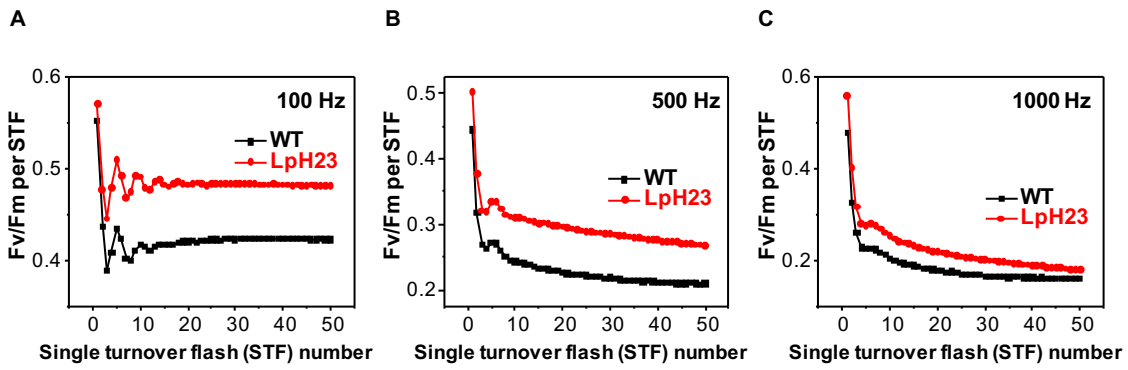

Figure 4.5 Single turnover flashes (STF) induced oscillations in Fv/Fm at A) 100 Hz, **B)** 500 Hz and **C)** 1000 Hz in WT (black) and LpH23 (red) cultures sampled from optimal growth conditions.

4.3.5 Growth and photosynthetic characteristics of LpH23 under acidic environment

In order to investigate the growth and photosynthetic characteristics, especially the carbon fixation efficiency of LpH23 under acidic environment, batch culture of LpH23 was grown in A+ liquid medium buffered at pH 5.5 and 6.4 under 2% CO_2 atmosphere with WT as control. During a growth period of 4 days, LpH23 showed photoautotrophic growth advantage over WT in the tested low pH medium as determined by the time course measurements of OD_{750nm} (**Fig. 4.6 A**). It was also observed that both strains entered the stationary phase at pH 5.5 on day 4 while still actively proliferated at pH 6.4 by the same time. By the end of the growth period, both strains were analyzed by various home-developed Fluorometry and Oximetry techniques with WT as control. The *in vivo* variable Chl-a fluorescence of the two strains from both conditions were measured by the aforementioned "FRRF" technique. As shown in Figure 4.6 B, a higher charge separation quantum yield of LpH23 is suggested by the elevated steady state Fv/Fm, while a more efficient WOC cycling is indicated by the slower damping of Fv/Fm oscillation compared to WT.

The CO_2 dependent FRRF technique, an extension of the regular FRRF, allows the probing of *in vivo* kinetics of the whole electron transport chain using the home built FRR fluorometer. After a 5 min dark incubation to quench all the reaction centers, 50 μl algal sample was subjected to 220 flash trains of 50 sequential single turnover flashes (11,000 flashes in total) at a fixed frequency of 100 Hz. A typical variable chlorophyll fluorescence response after dark adaptation displays 4 distinct time-resolved features: a sharp decline from reduction of the PQ pool, followed by a small broad peak arising from

reduction of NADP+, and then a continuous slope arising from CO_2 fixation by the Calvin-Benson cycle, and finally the plateau representing the steady state CO_2 fixation. For the examined *N.o1779* WT and LpH23 cultures, only 3 features were observed: a sharp decline resulting from the PQ pool turnover, followed by a continuous slope arising from the NADP+ reduction and the initiation of CO_2 fixation, and lastly the steady state Fv/Fm indicating that the CO_2 fixation rate is maximized and stabilized when the equilibrium of the whole electron transport chain is reached. As shown in Figure 4.6 C, the overall variable chlorophyll fluorescence kinetics, denoted as Fv/Fm, is higher in LpH23 than WT at both pHs, while also higher for both strains at pH 6.4 than at pH 5.5 in all 3 phases. The faster rise of Fv/Fm in the second phase followed by the higher steady state level in the plateau, indicate that the faster CO_2 fixation rate and a more efficiency turnover of Calvin cycle are achieved in LpH23 compared to WT.

The higher efficiency of carbon fixation in LpH23 at low pHs was also confirmed by the Oximetry analysis on the time-resolved oxygen evolution. A home built bare platinum electrode allows the kinetic resolution of the transit time to electron acceptor pools downstream of PSII (PQ, NADP+ and CO_2) (Krishnan et al., 2015). After a 5 min dark incubation, 10 μl algal sample was subjected to a 90 sec illumination with a red LED light (800 $\mu E\ m^{-2}\ sec^{-1}$) followed by a 30 sec darkness, during which the full kinetics of oxygen evolution were monitored. As shown in Figure 4.6 D, two distinct phases were observed in both strains, a small spike representing the PQ pool reduction, followed by a continuous slope indicating the carbon fixation. The overall relative oxygen yields over the illumination period was higher for both strains in pH 6.4 than in pH 5.5. Consistent with the results from CO_2 dependent FRRF measurements, it was also

observed that at both pHs, LpH23 achieved steeper slope and thus bigger area under the curve, which is directly proportional to the CO_2 dependent water oxidation rate.

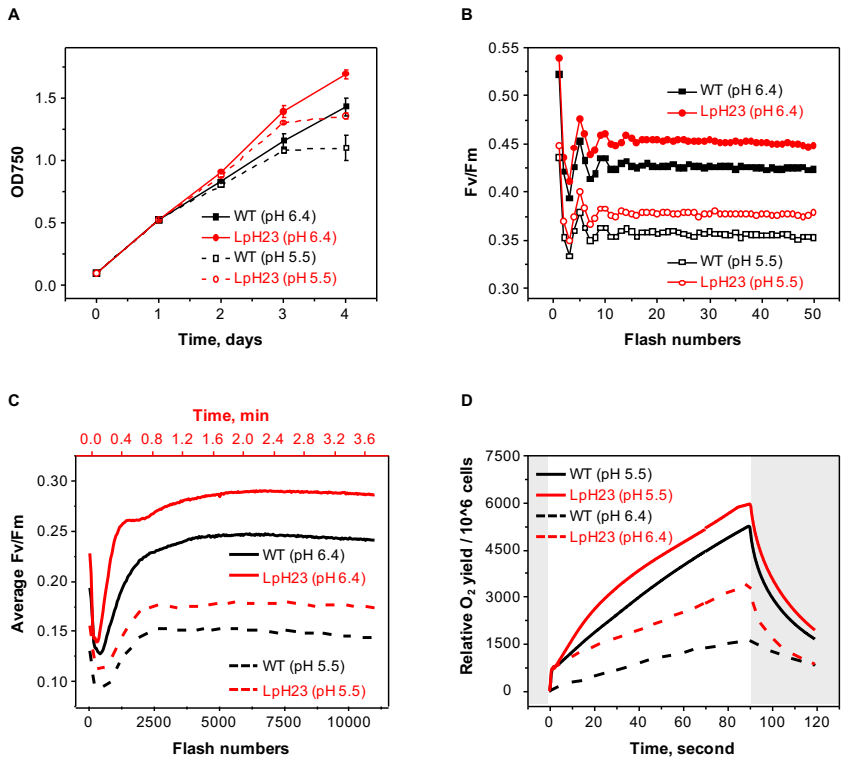

Figure 4.6 Growth and photosynthetic characterization of LpH23 under acidified environments. A) Growth curves of *N.o1779* WT (Black) and LpH23 (Red) cultivated in A+ medium at pH 6.6 (Solid symbols) and pH 5.5 (Empty symbols). *N.o1779* WT (Black) and LpH23 (Red) were sampled at the end of growth period (day 4) and analyzed for their **B)** Single turnover flashes (STF) induced oscillations in Fv/Fm determined by FRRF, as well as their photosynthetic carbon fixation rate determined by **C)** CO_2 dependent chlorophyll fluorescence showing Fv/Fm kinetics over 220 flash trains after carbon fixation inhibited baseline normalization and **D)** transient oxygen evolution during 90 s illumination (white window), followed by 30 s dark incubation (gray window).

4.4 Conclusion

By combining the insertional mutagenesis with acidic pH screening, we isolated an acidic pH tolerant mutant, LpH23, demonstrating photoautotrophic growth advantage in the standard laboratory growth condition as well as the acidic environment. It is highly promising to outperform WT in the cultivation system with the flue gas delivery. The insertional site of antibiotic resistant cassette will be localized, allowing a deeper understanding of the regulatory mechanism responsible for the low pH tolerating phenotype in *N.o1779*.

References

A. Cramer, W., Kallas, T. 2016. *Cytochrome Complexes: Evolution, Structures, Energy Transduction, and Signaling*.

Ahmad, A.L., Yasin, N.H.M., Derek, C.J.C., Lim, J.K. 2011. Microalgae as a sustainable energy source for biodiesel production: A review. *Renewable and Sustainable Energy Reviews*, **15**(1), 584-593.

Ananyev, G., Dismukes, G.C. 2005. How fast can photosystem II split water? Kinetic performance at high and low frequencies. *Photosynth Res*, **84**(1-3), 355-65.

Ananyev, G., Gates, C., Dismukes, G.C. 2016. The Oxygen quantum yield in diverse algae and cyanobacteria is controlled by partitioning of flux between linear and cyclic electron flow within photosystem II. *Biochim Biophys Acta*, **1857**(9), 1380-1391.

Ananyev, G., Gates, C., Kaplan, A., Dismukes, G.C. 2017. Photosystem II-cyclic electron flow powers exceptional photoprotection and record growth in the microalga Chlorella ohadii. *Biochimica et Biophysica Acta (BBA) - Bioenergetics*, **1858**(11), 873-883.

Armbrust, E.V., Berges, J.A., Bowler, C., Green, B.R., Martinez, D., Putnam, N.H., Zhou, S., Allen, A.E., Apt, K.E., Bechner, M., Brzezinski, M.A., Chaal, B.K., Chiovitti, A., Davis, A.K., Demarest, M.S., Detter, J.C., Glavina, T., Goodstein, D., Hadi, M.Z., Hellsten, U., Hildebrand, M., Jenkins, B.D., Jurka, J., Kapitonov, V.V., Kröger, N., Lau, W.W.Y., Lane, T.W., Larimer, F.W., Lippmeier, J.C., Lucas, S., Medina, M., Montsant, A., Obornik, M., Parker, M.S., Palenik, B., Pazour, G.J., Richardson, P.M., Rynearson, T.A., Saito, M.A., Schwartz, D.C., Thamatrakoln, K., Valentin, K., Vardi, A., Wilkerson, F.P., Rokhsar, D.S. 2004. The Genome of the Diatom Thalassiosira Pseudonana: Ecology, Evolution, and Metabolism. *Science*, **306**(5693), 79.

Avenson, T.J., Cruz, J.A., Kramer, D.M. 2004. Modulation of energy-dependent quenching of excitons in antennae of higher plants. *Proc Natl Acad Sci U S A*, **101**(15), 5530-5.

Beacham, T.A., Macia, V.M., Rooks, P., White, D.A., Ali, S.T. 2015. Altered lipid accumulation in Nannochloropsis salina CCAP849/3 following EMS and UV induced mutagenesis. *Biotechnol Rep (Amst)*, **7**, 87-94.

Bligh, E.G., Dyer, W.J. 1959. A rapid method of total lipid extraction and purification. *Can J Biochem Physiol*, **37**(8), 911-7.

Bowler, C., Allen, A.E., Badger, J.H., Grimwood, J., Jabbari, K., Kuo, A., Maheswari, U., Martens, C., Maumus, F., Otillar, R.P., Rayko, E., Salamov, A., Vandepoele, K., Beszteri, B., Gruber, A., Heijde, M., Katinka, M., Mock, T., Valentin, K., Verret, F., Berges, J.A., Brownlee, C., Cadoret, J.-P., Chiovitti, A., Choi, C.J., Coesel, S., De Martino, A., Detter, J.C., Durkin, C., Falciatore, A., Fournet, J., Haruta, M., Huysman, M.J.J., Jenkins, B.D., Jiroutova, K., Jorgensen, R.E., Joubert, Y., Kaplan, A., Kröger, N., Kroth, P.G., La Roche, J., Lindquist, E., Lommer, M., Martin–Jézéquel, V., Lopez, P.J., Lucas, S., Mangogna, M., McGinnis, K., Medlin, L.K., Montsant, A., Secq, M.-P.O.L., Napoli, C., Obornik, M., Parker, M.S., Petit, J.-L., Porcel, B.M., Poulsen, N., Robison, M., Rychlewski, L., Rynearson, T.A., Schmutz, J., Shapiro, H., Siaut, M., Stanley, M.,

Sussman, M.R., Taylor, A.R., Vardi, A., von Dassow, P., Vyverman, W., Willis, A., Wyrwicz, L.S., Rokhsar, D.S., Weissenbach, J., Armbrust, E.V., Green, B.R., Van de Peer, Y., Grigoriev, I.V. 2008. The Phaeodactylum genome reveals the evolutionary history of diatom genomes. *Nature*, **456**, 239.

Campbell, D., Bruce, D., Carpenter, C., Gustafsson, P., Oquist, G. 1996. Two forms of the Photosystem II D1 protein alter energy dissipation and state transitions in the cyanobacterium Synechococcus sp. PCC 7942. *Photosynth Res*, **47**(2), 131-44.

Cheng, J., Huang, Y., Feng, J., Sun, J., Zhou, J., Cen, K. 2013. Mutate Chlorella sp. by nuclear irradiation to fix high concentrations of CO2. *Bioresour Technol*, **136**, 496-501.

Cheng, J., Lu, H., He, X., Yang, W., Zhou, J., Cen, K. 2017. Mutation of Spirulina sp. by nuclear irradiation to improve growth rate under 15% carbon dioxide in flue gas. *Bioresour Technol*, **238**, 650-656.

Cheng, J., Lu, H., Huang, Y., Li, K., Huang, R., Zhou, J., Cen, K. 2016a. Enhancing growth rate and lipid yield of Chlorella with nuclear irradiation under high salt and CO2 stress. *Bioresour Technol*, **203**, 220-7.

Cheng, J., Lu, H., Huang, Y., Li, K., Huang, R., Zhou, J., Cen, K. 2016b. Enhancing growth rate and lipid yield of Chlorella with nuclear irradiation under high salt and CO2 stress. *Bioresource Technology*, **203**, 220-227.

Chisti, Y. 2007a. Biodiesel from microalgae. *Biotechnology Advances*, **25**(3), 294-306.

Chisti, Y. 2007b. *Biodiesel From Microalgae*.

Chisti, Y. 2013a. Constraints to commercialization of algal fuels. *J Biotechnol*, **167**(3), 201-14.

Chisti, Y. 2013b. *Raceways-based Production of Algal Crude Oil*.

Chiu, S.-Y., Kao, C.-Y., Tsai, M.-T., Ong, S.-C., Chen, C.-H., Lin, C.-S. 2009. Lipid accumulation and CO2 utilization of Nannochloropsis oculata in response to CO2 aeration. *Bioresource Technology*, **100**(2), 833-838.

Cirulis, J.T., Strasser, B.C., Scott, J.A., Ross, G.M. 2012. Optimization of staining conditions for microalgae with three lipophilic dyes to reduce precipitation and fluorescence variability. *Cytometry A*, **81**(7), 618-26.

Clarke, A.K., Hurry, V.M., Gustafsson, P., Oquist, G. 1993a. Two functionally distinct forms of the photosystem II reaction-center protein D1 in the cyanobacterium Synechococcus sp. PCC 7942. *Proc Natl Acad Sci U S A*, **90**(24), 11985-9.

Clarke, A.K., Soitamo, A., Gustafsson, P., Oquist, G. 1993b. Rapid interchange between two distinct forms of cyanobacterial photosystem II reaction-center protein D1 in response to photoinhibition. *Proc Natl Acad Sci U S A*, **90**(21), 9973-7.

Colin Gates, G.A., G. Charles Dismukes. 2017. Photoassembly of the CaMn5O5 Catalytic Core and Its Inorganic Mutants in Photosystem II. in: *Encyclopedia of Inorganic and Bioinorganic Chemistry*.

Dasgupta, J., Ananyev, G.M., Dismukes, G.C. 2008. Photoassembly of the Water-Oxidizing Complex in Photosystem II. *Coordination chemistry reviews*, **252**(3-4), 347-360.

Deng, X., Cai, J., Fei, X. 2013a. Effect of the expression and knockdown of citrate synthase gene on carbon flux during triacylglycerol biosynthesis by green algae Chlamydomonas reinhardtii. *BMC Biochem*, **14**, 38.

Deng, X., Cai, J., Fei, X. 2013b. Effect of the expression and knockdown of citrate synthase gene on carbon flux during triacylglycerol biosynthesis by green algae Chlamydomonas reinhardtii. *BMC Biochemistry*, **14**, 38-38.

Dismukes, G.C., Carrieri, D., Bennette, N., Ananyev, G.M., Posewitz, M.C. 2008a. Aquatic phototrophs: efficient alternatives to land-based crops for biofuels. *Current Opinion in Biotechnology*, **19**(3), 235-240.

Dismukes, G.C., Carrieri, D., Bennette, N., Ananyev, G.M., Posewitz, M.C. 2008b. Aquatic phototrophs: efficient alternatives to land-based crops for biofuels. *Curr Opin Biotechnol*, **19**(3), 235-40.

Dorlet, P., Xiong, L., Sayre, R.T., Un, S. 2001. High field EPR study of the pheophytin anion radical in wild type and D1-E130 mutants of photosystem II in Chlamydomonas reinhardtii. *J Biol Chem*, **276**(25), 22313-6.

Du, Z.Y., Benning, C. 2016. Triacylglycerol Accumulation in Photosynthetic Cells in Plants and Algae. *Subcell Biochem*, **86**, 179-205.

Dunahay, T.G., Jarvis, E.E., Dais, S.S., Roessler, P.G. 1996. Manipulation of microalgal lipid production using genetic engineering. *Applied Biochemistry and Biotechnology*, **57**(1), 223.

Dunahay, T.G., Jarvis, E.E., Roessler, P.G. 1995. GENETIC TRANSFORMATION OF THE DIATOMS CYCLOTELLA CRYPTICA AND NAVICULA SAPROPHILA. *Journal of Phycology*, **31**(6), 1004-1012.

Erickson, E., Wakao, S., Niyogi, K.K. 2015. Light stress and photoprotection in Chlamydomonas reinhardtii. *Plant J*, **82**(3), 449-65.

Ferreira, K.N., Iverson, T.M., Maghlaoui, K., Barber, J., Iwata, S. 2004. Architecture of the Photosynthetic Oxygen-Evolving Center. *Science*, **303**(5665), 1831.

Fulton, L. 2004. *Biofuels for transport : an international perspective / International Energy Agency*. OECD, International Energy Agency, Paris.

G. Dunahay, T., E. Jarvis, E., G. Roessler, P. 2008. *Genetic Transformation of the Diatoms Cyclotella Cryptica and Navicula Saprophila*.

Garczarek, L., Dufresne, A., Blot, N., Cockshutt, A.M., Peyrat, A., Campbell, D.A., Joubin, L., Six, C. 2008. Function and evolution of the psbA gene family in marine Synechococcus: Synechococcus sp. WH7803 as a case study. *Isme j*, **2**(9), 937-53.

Gates, C., Ananyev, G., Dismukes, G.C. 2016. The strontium inorganic mutant of the water oxidizing center (CaMn4O5) of PSII improves WOC efficiency but slows electron flux through the terminal acceptors. *Biochim Biophys Acta*, **1857**(9), 1550-1560.

Golden, S.S., Brusslan, J., Haselkorn, R. 1986. Expression of a family of psbA genes encoding a photosystem II polypeptide in the cyanobacterium Anacystis nidulans R2. *EMBO J*, **5**(11), 2789-98.

Govindjee, J.F.K., Johannes Messinger, John Whitmarsh. 2010. Photosystem II. *Encyclopedia of Inorganic and Bioinorganic Chemistry*.

Griffiths, M.J., Harrison, S.T.L. 2009. Lipid productivity as a key characteristic for choosing algal species for biodiesel production. *Journal of Applied Phycology*, **21**(5), 493-507.

Guarnieri, M.T., Levering, J., Henard, C.A., Boore, J.L., Betenbaugh, M.J., Zengler, K., Knoshaug, E.P. 2018. Genome Sequence of the Oleaginous Green Alga, Chlorella vulgaris UTEX 395. *Frontiers in Bioengineering and Biotechnology*, **6**, 37.

Guskov, A., Kern, J., Gabdulkhakov, A., Broser, M., Zouni, A., Saenger, W. 2009. Cyanobacterial photosystem II at 2.9-A resolution and the role of quinones, lipids, channels and chloride. *Nat Struct Mol Biol*, **16**(3), 334-42.

Herrera-Valencia, V.A., Macario-Gonzalez, L.A., Casais-Molina, M.L., Beltran-Aguilar, A.G., Peraza-Echeverria, S. 2012. In silico cloning and characterization of the glycerol-3-phosphate dehydrogenase (GPDH) gene family in the green microalga Chlamydomonas reinhardtii. *Curr Microbiol*, **64**(5), 477-85.

Hieber, A.D., Bugos, R.C., Yamamoto, H.Y. 2000. Plant lipocalins: violaxanthin de-epoxidase and zeaxanthin epoxidase. *Biochim Biophys Acta*, **1482**(1-2), 84-91.

Hlavova, M., Turoczy, Z., Bisova, K. 2015. Improving microalgae for biotechnology--From genetics to synthetic biology. *Biotechnol Adv*, **33**(6 Pt 2), 1194-203.

Holtman, C.K., Chen, Y., Sandoval, P., Gonzales, A., Nalty, M.S., Thomas, T.L., Youderian, P., Golden, S.S. 2005. High-throughput functional analysis of the *Synechococcus elongatus* PCC 7942 genome. *DNA Res*, **12**(2), 103-15.

Hou, D.J., Shi, D.J., Cai, Z.F., Song, D.H., Wang, X.K. 2008. *Regulation of lipids synthesis in transgenic Escherichia coli by inserting cyanobacterial sense and antisense pepcA Gene*.

Jr Metting, F.B. 1996. *Biodiversity and application of microalgae*.

Jungnick, N., Ma, Y., Mukherjee, B., Cronan, J.C., Speed, D.J., Laborde, S.M., Longstreth, D.J., Moroney, J.V. 2014. The carbon concentrating mechanism in Chlamydomonas reinhardtii: finding the missing pieces. *Photosynth Res*, **121**(2-3), 159-73.

Kaminskaya, O.P., Shuvalov, V.A. 2016. Towards an understanding of redox heterogeneity of the photosystem II cytochrome b559 in the native membrane. *Eur Biophys J*, **45**(2), 129-38.

Kindle, K.L. 1990. High-frequency nuclear transformation of Chlamydomonas reinhardtii. *Proc Natl Acad Sci U S A*, **87**(3), 1228-32.

Kittiwongwattana, C., Lutz, K., Clark, M., Maliga, P. 2007. Plastid marker gene excision by the phiC31 phage site-specific recombinase. *Plant Mol Biol*, **64**(1-2), 137-43.

Kliphuis, A.M., de Winter, L., Vejrazka, C., Martens, D.E., Janssen, M., Wijffels, R.H. 2010. Photosynthetic efficiency of Chlorella sorokiniana in a turbulently mixed short light-path photobioreactor. *Biotechnol Prog*, **26**(3), 687-96.

Koberg, M., Cohen, M., Ben-Amotz, A., Gedanken, A. 2011. Bio-diesel production directly from the microalgae biomass of Nannochloropsis by microwave and ultrasound radiation. *Bioresour Technol*, **102**(5), 4265-9.

Kolling, D.R., Brown, T.S., Ananyev, G., Dismukes, G.C. 2009. Photosynthetic oxygen evolution is not reversed at high oxygen pressures: mechanistic consequences for the water-oxidizing complex. *Biochemistry*, **48**(6), 1381-9.

Kos, P.B., Deak, Z., Cheregi, O., Vass, I. 2008. Differential regulation of psbA and psbD gene expression, and the role of the different D1 protein copies in the cyanobacterium Thermosynechococcus elongatus BP-1. *Biochim Biophys Acta*, **1777**(1), 74-83.

Krause, G.H. 1988. Photoinhibition of photosynthesis. An evaluation of damaging and protective mechanisms. *Physiologia Plantarum*, **74**(3), 566-574.

Kreslavski, V.D., Carpentier, R., Klimov, V.V., Murata, N., Allakhverdiev, S.I. 2007. Molecular mechanisms of stress resistance of the photosynthetic apparatus. *Biochemistry (Moscow) Supplement Series A: Membrane and Cell Biology*, **1**(3), 185-205.

Krishnan, A., Kumaraswamy, G.K., Vinyard, D.J., Gu, H., Ananyev, G., Posewitz, M.C., Dismukes, G.C. 2015. Metabolic and photosynthetic consequences of blocking starch biosynthesis in the green alga Chlamydomonas reinhardtii sta6 mutant. *Plant J*, **81**(6), 947-60.

Kromdijk, J., Glowacka, K., Leonelli, L., Gabilly, S.T., Iwai, M., Niyogi, K.K., Long, S.P. 2016. Improving photosynthesis and crop productivity by accelerating recovery from photoprotection. *Science*, **354**(6314), 857-861.

La Russa, M., Bogen, C., Uhmeyer, A., Doebbe, A., Filippone, E., Kruse, O., Mussgnug, J.H. 2012. Functional analysis of three type-2 DGAT homologue genes for triacylglycerol production in the green microalga Chlamydomonas reinhardtii. *J Biotechnol*, **162**(1), 13-20.

Lee, J.Y., Yoo, C., Jun, S.Y., Ahn, C.Y., Oh, H.M. 2010. Comparison of several methods for effective lipid extraction from microalgae. *Bioresource Technology*, **101**, S75-S77.

Lei, A., Chen, H., Shen, G., Hu, Z., Chen, L., Wang, J. 2012. *Expression of fatty acid synthesis genes and fatty acid accumulation in Haematococcus pluvialis under different stressors*.

Li, D.W., Cen, S.Y., Liu, Y.H., Balamurugan, S., Zheng, X.Y., Alimujiang, A., Yang, W.D., Liu, J.S., Li, H.Y. 2016a. A type 2 diacylglycerol acyltransferase accelerates the triacylglycerol biosynthesis in heterokont oleaginous microalga Nannochloropsis oceanica. *J Biotechnol*, **229**, 65-71.

Li, X., Zhang, R., Patena, W., Gang, S.S., Blum, S.R., Ivanova, N., Yue, R., Robertson, J.M., Lefebvre, P.A., Fitz-Gibbon, S.T., Grossman, A.R., Jonikas, M.C. 2016b. An Indexed, Mapped Mutant Library Enables Reverse Genetics Studies of Biological Processes in Chlamydomonas reinhardtii. *Plant Cell*, **28**(2), 367-87.

Li, X.P., Gilmore, A.M., Caffarri, S., Bassi, R., Golan, T., Kramer, D., Niyogi, K.K. 2004. Regulation of photosynthetic light harvesting involves intrathylakoid lumen pH sensing by the PsbS protein. *J Biol Chem*, **279**(22), 22866-74.

Li, X.P., Muller-Moule, P., Gilmore, A.M., Niyogi, K.K. 2002. PsbS-dependent enhancement of feedback de-excitation protects photosystem II from photoinhibition. *Proc Natl Acad Sci U S A*, **99**(23), 15222-7.

Li, Y., Han, D., Hu, G., Dauvillée, D., Sommerfeld, M., Ball, S., Hu, Q. 2010. *Chlamydomonas starchless mutant defective in ADP-glucose pyrophosphorylase hyper-accumulates triacylglycerol*.

Liang, M.H., Jiang, J.G. 2013. Advancing oleaginous microorganisms to produce lipid via metabolic engineering technology. *Prog Lipid Res*, **52**(4), 395-408.

Liu, B., Benning, C. 2013. Lipid metabolism in microalgae distinguishes itself. *Curr Opin Biotechnol*, **24**(2), 300-9.

Liu, Z., Zhang, F., Chen, F. 2013. High throughput screening of CO2-tolerating microalgae using GasPak bags. *Aquat Biosyst*, **9**(1), 23.

Loll, B., Kern, J., Saenger, W., Zouni, A., Biesiadka, J. 2005. Towards complete cofactor arrangement in the 3.0 Å resolution structure of photosystem II. *Nature*, **438**, 1040.

Lutz, K.A., Corneille, S., Azhagiri, A.K., Svab, Z., Maliga, P. 2004. A novel approach to plastid transformation utilizes the phiC31 phage integrase. *Plant J*, **37**(6), 906-13.

Lutz, K.A., Svab, Z., Maliga, P. 2006. Construction of marker-free transplastomic tobacco using the Cre-loxP site-specific recombination system. *Nat Protoc*, **1**(2), 900-10.

Lv, H., Qu, G., Qi, X., Lu, L., Tian, C., Ma, Y. 2013. Transcriptome analysis of Chlamydomonas reinhardtii during the process of lipid accumulation. *Genomics*, **101**(4), 229-237.

Ma, X., Yao, L., Yang, B., Lee, Y.K., Chen, F., Liu, J. 2017. RNAi-mediated silencing of a pyruvate dehydrogenase kinase enhances triacylglycerol biosynthesis in the oleaginous marine alga Nannochloropsis salina. *Scientific Reports*, **7**(1), 11485.

Martelli, E., Kreutz, T., Carbo, M., Consonni, S., Jansen, D. 2011. Shell coal IGCCS with carbon capture: Conventional gas quench vs. innovative configurations. *Applied Energy*, **88**(11), 3978-3989.

McConnell, I., Li, G., Brudvig, G.W. 2010. Energy Conversion in Natural and Artificial Photosynthesis. *Chemistry & Biology*, **17**(5), 434-447.

Merry, S.A., Nixon, P.J., Barter, L.M., Schilstra, M., Porter, G., Barber, J., Durrant, J.R., Klug, D.R. 1998. Modulation of quantum yield of primary radical pair formation in photosystem II by site-directed mutagenesis affecting radical cations and anions. *Biochemistry*, **37**(50), 17439-47.

Mitra, M., Shah, F., Bharadwaj, S.V., Patidar, S.K., Mishra, S. 2016. Cultivation of Nannochloropsis oceanica biomass rich in eicosapentaenoic acid utilizing wastewater as nutrient resource. *Bioresour Technol*, **218**, 1178-86.

Muller, P., Li, X.P., Niyogi, K.K. 2001. Non-photochemical quenching. A response to excess light energy. *Plant Physiol*, **125**(4), 1558-66.

Mulo, P., Sakurai, I., Aro, E.-M. 2012. Strategies for psbA gene expression in cyanobacteria, green algae and higher plants: From transcription to PSII repair. *Biochimica et Biophysica Acta (BBA) - Bioenergetics*, **1817**(1), 247-257.

Mulo, P., Sicora, C., Aro, E.M. 2009. Cyanobacterial psbA gene family: optimization of oxygenic photosynthesis. *Cell Mol Life Sci*, **66**(23), 3697-710.

Munekage, Y., Hojo, M., Meurer, J., Endo, T., Tasaka, M., Shikanai, T. 2002. PGR5 is involved in cyclic electron flow around photosystem I and is essential for photoprotection in Arabidopsis. *Cell*, **110**(3), 361-71.

Murchie, E.H., Niyogi, K.K. 2011. Manipulation of photoprotection to improve plant photosynthesis. *Plant Physiol*, **155**(1), 86-92.

Nilkens, M., Kress, E., Lambrev, P., Miloslavina, Y., Muller, M., Holzwarth, A.R., Jahns, P. 2010. Identification of a slowly inducible zeaxanthin-dependent component of non-photochemical quenching of chlorophyll fluorescence generated under steady-state conditions in Arabidopsis. *Biochim Biophys Acta*, **1797**(4), 466-75.

Nishiyama, Y., Murata, N. 2014. Revised scheme for the mechanism of photoinhibition and its application to enhance the abiotic stress tolerance of the photosynthetic machinery. *Appl Microbiol Biotechnol*, **98**(21), 8777-96.

Nixon, P.J., Michoux, F., Yu, J., Boehm, M., Komenda, J. 2010. Recent advances in understanding the assembly and repair of photosystem II. *Ann Bot*, **106**(1), 1-16.

Niyogi, K.K., Grossman, A.R., Bjorkman, O. 1998. Arabidopsis mutants define a central role for the xanthophyll cycle in the regulation of photosynthetic energy conversion. *Plant Cell*, **10**(7), 1121-34.

Ogami, S., Boussac, A., Sugiura, M. 2012. Deactivation processes in PsbA1-Photosystem II and PsbA3-Photosystem II under photoinhibitory conditions in the cyanobacterium Thermosynechococcus elongatus. *Biochim Biophys Acta*, **1817**(8), 1322-30.

Ottmar, E., Ramon, P.-M., Youba, S., Kristin, S., Dan, A., Thomas, B., John, C., Helena, C., Jean-Michel, D., Andre, F., Manfred, F., Barry, G., Gerrit, H., John, H., Arnulf, J.-W., Susanne, K., Daniel, M.K., Volker, K., Arun, K., Anthony, L., Oswaldo, L., Patrick, M., Lourdes, M., Catherine, M., William, M., José, M., Alain, N., Lars, J.N., John, N., Atiq, R., Jayant, A.S., Janet, S., Roberto, S., Tormod, S., Steffen, S., Ralph, S., Christoph von, S., Aviel, V., Kevin, U., Ryan, H.W., Francis, Y., Timm, Z. 2011. IPCC Special Report on Renewable Energy Sources and Climate Change Mitigation. LBNL.

Passonneau, J.V., Lauderdale, V.R. 1974. A comparison of three methods of glycogen measurement in tissues. *Anal Biochem*, **60**(2), 405-12.

Perin, G., Bellan, A., Segalla, A., Meneghesso, A., Alboresi, A., Morosinotto, T. 2015a. Generation of random mutants to improve light-use efficiency of Nannochloropsis gaditana cultures for biofuel production. *Biotechnol Biofuels*, **8**, 161.

Perin, G., Bellan, A., Segalla, A., Meneghesso, A., Alboresi, A., Morosinotto, T. 2015b. Generation of random mutants to improve light-use efficiency of Nannochloropsis gaditana cultures for biofuel production. *Biotechnology for Biofuels*, **8**(1), 161.

Poliner, E., Pulman, J.A., Zienkiewicz, K., Childs, K., Benning, C., Farre, E.M. 2018. A toolkit for Nannochloropsis oceanica CCMP1779 enables gene stacking and genetic engineering of the eicosapentaenoic acid pathway for enhanced long-chain polyunsaturated fatty acid production. *Plant Biotechnol J*, **16**(1), 298-309.

Radakovits, R., Jinkerson, R.E., Darzins, A., Posewitz, M.C. 2010. Genetic Engineering of Algae for Enhanced Biofuel Production. *Eukaryotic Cell*, **9**(4), 486-501.

Radakovits, R., Jinkerson, R.E., Fuerstenberg, S.I., Tae, H., Settlage, R.E., Boore, J.L., Posewitz, M.C. 2012. Draft genome sequence and genetic transformation of the oleaginous alga Nannochloropis gaditana. *Nat Commun*, **3**, 686.

Rajagopal, D., Sexton, S., Hochman, G., Zilberman, D. 2009. Recent Developments in Renewable Technologies: R&D Investment in Advanced Biofuels. *Annual Review of Resource Economics*, **1**(1), 621-644.

Raven, J.A. 2010. Inorganic carbon acquisition by eukaryotic algae: four current questions. *Photosynth Res*, **106**(1-2), 123-34.

Raven, J.A., Giordano, M., Beardall, J., Maberly, S.C. 2011. Algal and aquatic plant carbon concentrating mechanisms in relation to environmental change. *Photosynthesis Research*, **109**(1), 281-296.

Rawsthorne, S. 2002. Carbon flux and fatty acid synthesis in plants. *Progress in Lipid Research*, **41**(2), 182-196.

Reich, P.B., Hobbie, S.E., Lee, T.D., Pastore, M.A. 2018. Unexpected reversal of C₃ versus C₄ grass response to

elevated CO₂ during a 20-year field experiment. *Science*, **360**(6386), 317.

Robinson, H.H., Yocum, C.F. 1980. Cyclic photophosphorylation reactions catalyzed by ferredoxin, methyl viologen and anthraquinone sulfonate. Use of photochemical reactions to optimize redox poising. *Biochim Biophys Acta*, **590**(1), 97-106.

Roessler, P.G., Bleibaum, J.L., Thompson, G.A., Ohlrogge, J.B. 1994. Characteristics of the Gene That Encodes Acetyl-CoA Carboxylase in the Diatom Cyclotella crypticaa. *Annals of the New York Academy of Sciences*, **721**(1), 250-256.

Roessler, P.G., Ohlrogge, J.B. 1993. Cloning and characterization of the gene that encodes acetyl-coenzyme A carboxylase in the alga Cyclotella cryptica. *J Biol Chem*, **268**(26), 19254-9.

Sander, J., Nowaczyk, M., Buchta, J., Dau, H., Vass, I., Deak, Z., Dorogi, M., Iwai, M., Rogner, M. 2010. Functional characterization and quantification of the alternative PsbA copies in Thermosynechococcus elongatus and their role in photoprotection. *J Biol Chem*, **285**(39), 29851-6.

Sane, P.V., Ivanov, A.G., Sveshnikov, D., Huner, N.P., Oquist, G. 2002. A transient exchange of the photosystem II reaction center protein D1:1 with D1:2 during low temperature stress of Synechococcus sp. PCC 7942 in the light lowers the redox potential of QB. *J Biol Chem*, **277**(36), 32739-45.

Schaefer, M.R., Golden, S.S. 1989. Differential expression of members of a cyanobacterial psbA gene family in response to light. *J Bacteriol*, **171**(7), 3973-81.

Shibamoto, T., Kato, Y., Sugiura, M., Watanabe, T. 2009. Redox potential of the primary plastoquinone electron acceptor Q(A) in photosystem II from Thermosynechococcus elongatus determined by spectroelectrochemistry. *Biochemistry*, **48**(45), 10682-4.

Shibuya, Y., Takahashi, R., Okubo, T., Suzuki, H., Sugiura, M., Noguchi, T. 2010. Hydrogen bond interactions of the pheophytin electron acceptor and its radical anion in photosystem II as revealed by Fourier transform infrared difference spectroscopy. *Biochemistry*, **49**(3), 493-501.

Shikanai, T. 2007. Cyclic electron transport around photosystem I: genetic approaches. *Annu Rev Plant Biol*, **58**, 199-217.

Sicora, C.I., Brown, C.M., Cheregi, O., Vass, I., Campbell, D.A. 2008. The psbA gene family responds differentially to light and UVB stress in Gloeobacter violaceus PCC 7421, a deeply divergent cyanobacterium. *Biochim Biophys Acta*, **1777**(2), 130-9.

Sicora, C.I., Ho, F.M., Salminen, T., Styring, S., Aro, E.M. 2009. Transcription of a "silent" cyanobacterial psbA gene is induced by microaerobic conditions. *Biochim Biophys Acta*, **1787**(2), 105-12.

Silhavy, D., Maliga, P. 1998. Mapping of promoters for the nucleus-encoded plastid RNA polymerase (NEP) in the iojap maize mutant. *Curr Genet*, **33**(5), 340-4.

Sinagawa-Garcia, S.R., Tungsuchat-Huang, T., Paredes-Lopez, O., Maliga, P. 2009. Next generation synthetic vectors for transformation of the plastid genome of higher plants. *Plant Mol Biol*, **70**(5), 487-98.

Solovchenko, A., Khozin-Goldberg, I. 2013. High-CO2 tolerance in microalgae: possible mechanisms and implications for biotechnology and bioremediation. *Biotechnol Lett*, **35**(11), 1745-52.

Spolaore, P., Joannis-Cassan, C., Duran, E., Isambert, A. 2006. *Commercial applications of Microalgae*.

Stephens, E., Ross, I.L., Mussgnug, J.H., Wagner, L.D., Borowitzka, M.A., Posten, C., Kruse, O., Hankamer, B. 2010. Future prospects of microalgal biofuel production systems. *Trends in Plant Science*, **15**(10), 554-564.

Stiekema, W.J., Heidekamp, F., Dirkse, W.G., van Beckum, J., de Haan, P., Bosch, C.T., Louwerse, J.D. 1988. Molecular cloning and analysis of four potato tuber mRNAs. *Plant Mol Biol*, **11**(3), 255-69.

Sugimoto, T., Tanaka, K., Monma, M., Kawamura, Y., Saio, K. 1989. Phosphoenolpyruvate Carboxylase Level in Soybean Seed Highly Correlates to Its Contents of Protein and Lipid. *Agricultural and Biological Chemistry*, **53**(3), 885-887.

Sugiura, M., Iwai, E., Hayashi, H., Boussac, A. 2010a. Differences in the interactions between the subunits of photosystem II dependent on D1 protein variants in the thermophilic cyanobacterium Thermosynechococcus elongatus. *J Biol Chem*, **285**(39), 30008-18.

Sugiura, M., Kato, Y., Takahashi, R., Suzuki, H., Watanabe, T., Noguchi, T., Rappaport, F., Boussac, A. 2010b. Energetics in photosystem II from Thermosynechococcus elongatus with a D1 protein encoded by either the psbA1 or psbA3 gene. *Biochim Biophys Acta*, **1797**(8), 1491-9.

Summerfield, T.C., Toepel, J., Sherman, L.A. 2008. Low-oxygen induction of normally cryptic psbA genes in cyanobacteria. *Biochemistry*, **47**(49), 12939-41.

Sun, A., Davis, R., Starbuck, M., Ben-Amotz, A., Pate, R., Pienkos, P. 2011. *Comparative cost analysis of algal oil production for biofuels*.

Surendhiran, D., Vijay, M. 2014. Effect of Various Pretreatment for Extracting Intracellular Lipid from Nannochloropsis oculata under Nitrogen Replete and Depleted Conditions. *ISRN Chemical Engineering*, **2014**, 9.

Svab, Z., Maliga, P. 1993. High-frequency plastid transformation in tobacco by selection for a chimeric aadA gene. *Proc Natl Acad Sci U S A*, **90**(3), 913-7.

Tai, M., Stephanopoulos, G. 2013. Engineering the push and pull of lipid biosynthesis in oleaginous yeast Yarrowia lipolytica for biofuel production. *Metab Eng*, **15**, 1-9.

Tan, K.W., Lee, Y.K. 2016a. The dilemma for lipid productivity in green microalgae: importance of substrate provision in improving oil yield without sacrificing growth. *Biotechnol Biofuels*, **9**, 255.

Tan, K.W.M., Lee, Y.K. 2016b. The dilemma for lipid productivity in green microalgae: importance of substrate provision in improving oil yield without sacrificing growth. *Biotechnology for Biofuels*, **9**, 255.

Terashima, I., Evans, J.R. 1988. Effects of Light and Nitrogen Nutrition on the Organization of the Photosynthetic Apparatus in Spinach. *Plant and Cell Physiology*, **29**(1), 143-155.

Thawechai, T., Cheirsilp, B., Louhasakul, Y., Boonsawang, P., Prasertsan, P. 2016. Mitigation of carbon dioxide by oleaginous microalgae for lipids and pigments

production: Effect of light illumination and carbon dioxide feeding strategies. *Bioresour Technol*, **219**, 139-49.

Thompson, L.K., Brudvig, G.W. 1988. Cytochrome b-559 may function to protect photosystem II from photoinhibition. *Biochemistry*, **27**(18), 6653-6658.

Tichy, M., Lupinkova, L., Sicora, C., Vass, I., Kuvikova, S., Prasil, O., Komenda, J. 2003. Synechocystis 6803 mutants expressing distinct forms of the Photosystem II D1 protein from Synechococcus 7942: relationship between the psbA coding region and sensitivity to visible and UV-B radiation. *Biochim Biophys Acta*, **1605**(1-3), 55-66.

Tikkanen, M., Mekala, N.R., Aro, E.M. 2014. Photosystem II photoinhibition-repair cycle protects Photosystem I from irreversible damage. *Biochim Biophys Acta*, **1837**(1), 210-5.

Tyystjarvi, E., Aro, E.M. 1996. The rate constant of photoinhibition, measured in lincomycin-treated leaves, is directly proportional to light intensity. *Proc Natl Acad Sci U S A*, **93**(5), 2213-8.

Ünnep, R., Zsiros, O., Solymosi, K., Kovács, L., Lambrev, P.H., Tóth, T., Schweins, R., Posselt, D., Székely, N.K., Rosta, L., Nagy, G., Garab, G. 2014. The ultrastructure and flexibility of thylakoid membranes in leaves and isolated chloroplasts as revealed by small-angle neutron scattering. *Biochimica et Biophysica Acta (BBA) - Bioenergetics*, **1837**(9), 1572-1580.

Vass, I., Cser, K. 2009. Janus-faced charge recombinations in photosystem II photoinhibition. *Trends Plant Sci*, **14**(4), 200-5.

Verhoeven, A.S., Demmig-Adams, B., Adams, I.W. 1997. Enhanced Employment of the Xanthophyll Cycle and Thermal Energy Dissipation in Spinach Exposed to High Light and N Stress. *Plant Physiol*, **113**(3), 817-824.

Vieler, A., Wu, G., Tsai, C.H., Bullard, B., Cornish, A.J., Harvey, C., Reca, I.B., Thornburg, C., Achawanantakun, R., Buehl, C.J., Campbell, M.S., Cavalier, D., Childs, K.L., Clark, T.J., Deshpande, R., Erickson, E., Armenia Ferguson, A., Handee, W., Kong, Q., Li, X., Liu, B., Lundback, S., Peng, C., Roston, R.L., Sanjaya, Simpson, J.P., Terbush, A., Warakanont, J., Zauner, S., Farre, E.M., Hegg, E.L., Jiang, N., Kuo, M.H., Lu, Y., Niyogi, K.K., Ohlrogge, J., Osteryoung, K.W., Shachar-Hill, Y., Sears, B.B., Sun, Y., Takahashi, H., Yandell, M., Shiu, S.H., Benning, C. 2012. Genome, functional gene annotation, and nuclear transformation of the heterokont oleaginous alga Nannochloropsis oceanica CCMP1779. *PLoS Genet*, **8**(11), e1003064.

Vigeolas, H., Geigenberger, P. 2004. *Increased levels of glycerol-3-phosphate lead to a stimulation of flux into triacylglycerol synthesis after supplying glycerol to developing seeds of Brassica napus L. in planta*.

Vinyard, D.J., Ananyev, G.M., Dismukes, G.C. 2013a. Photosystem II: the reaction center of oxygenic photosynthesis. *Annu Rev Biochem*, **82**, 577-606.

Vinyard, D.J., Ananyev, G.M., Dismukes, G.C. 2013b. Photosystem II: The Reaction Center of Oxygenic Photosynthesis. *Annual Review of Biochemistry*, **82**, 577-606.

Vinyard, D.J., Gimpel, J., Ananyev, G.M., Cornejo, M.A., Golden, S.S., Mayfield, S.P., Dismukes, G.C. 2013c. Natural variants of photosystem II subunit D1 tune photochemical fitness to solar intensity. *J Biol Chem*, **288**(8), 5451-62.

Vinyard, D.J., Gimpel, J., Ananyev, G.M., Mayfield, S.P., Dismukes, G.C. 2014. Engineered Photosystem II reaction centers optimize photochemistry versus photoprotection at different solar intensities. *J Am Chem Soc*, **136**(10), 4048-55.

Vinyard, D.J., Zachary, C.E., Ananyev, G., Dismukes, G.C. 2013d. Thermodynamically accurate modeling of the catalytic cycle of photosynthetic oxygen evolution: a mathematical solution to asymmetric Markov chains. *Biochim Biophys Acta*, **1827**(7), 861-8.

Walker, T.L., Collet, C., Purton, S. 2005. ALGAL TRANSGENICS IN THE GENOMIC ERA1. *Journal of Phycology*, **41**(6), 1077-1093.

Wall, T.F. 2007. Combustion processes for carbon capture. *Proceedings of the Combustion Institute*, **31**(1), 31-47.

Wang, C., Li, Y., Lu, J., Deng, X., Li, H., Hu, Z. 2018. Effect of overexpression of LPAAT and GPD1 on lipid synthesis and composition in green microalga Chlamydomonas reinhardtii. *Journal of Applied Phycology*, **30**(3), 1711-1719.

Wang, D., Lu, Y., Huang, H., Xu, J. 2012. Establishing oleaginous microalgae research models for consolidated bioprocessing of solar energy. *Adv Biochem Eng Biotechnol*, **128**, 69-84.

Wei, H., Shi, Y., Ma, X., Pan, Y., Hu, H., Li, Y., Luo, M., Gerken, H., Liu, J. 2017a. A type-I diacylglycerol acyltransferase modulates triacylglycerol biosynthesis and fatty acid composition in the oleaginous microalga, Nannochloropsis oceanica. *Biotechnol Biofuels*, **10**, 174.

Wei, H., Shi, Y., Ma, X., Pan, Y., Hu, H., Li, Y., Luo, M., Gerken, H., Liu, J. 2017b. A type-I diacylglycerol acyltransferase modulates triacylglycerol biosynthesis and fatty acid composition in the oleaginous microalga, Nannochloropsis oceanica. *Biotechnology for Biofuels*, **10**(1), 174.

Wei, L., Xin, Y., Wang, Q., Yang, J., Hu, H., Xu, J. 2017c. RNAi-based targeted gene knockdown in the model oleaginous microalgae Nannochloropsis oceanica. *Plant J*, **89**(6), 1236-1250.

Wijffels, R.H., Barbosa, M.J. 2010. An outlook on microalgal biofuels. *Science*, **329**(5993), 796-9.

Yao, Y., Lu, Y., Peng, K.-T., Huang, T., Niu, Y.-F., Xie, W.-H., Yang, W.-D., Liu, J.-S., Li, H.-Y. 2014. Glycerol and neutral lipid production in the oleaginous marine diatom Phaeodactylum tricornutum promoted by overexpression of glycerol-3-phosphate dehydrogenase. *Biotechnology for Biofuels*, **7**(1), 110.

Zeiler, K.G., Heacox, D.A., Toon, S.T., Kadam, K.L., Brown, L.M. 1995. The use of microalgae for assimilation and utilization of carbon dioxide from fossil fuel-fired power plant flue gas. *Energy Conversion and Management*, **36**(6), 707-712.

Zhang, R., Patena, W., Armbruster, U., Gang, S.S., Blum, S.R., Jonikas, M.C. 2014. High-Throughput Genotyping of Green Algal Mutants Reveals Random Distribution of Mutagenic Insertion Sites and Endonucleolytic Cleavage of Transforming DNA. *The Plant Cell Online*.

Zhu, B., Sun, F., Yang, M., Lu, L., Yang, G., Pan, K. 2014a. Large-scale biodiesel production using flue gas from coal-fired power plants with Nannochloropsis microalgal biomass in open raceway ponds. *Bioresource Technology*, **174**, 53-59.

Zhu, B., Sun, F., Yang, M., Lu, L., Yang, G., Pan, K. 2014b. Large-scale biodiesel production using flue gas from coal-fired power plants with Nannochloropsis microalgal biomass in open raceway ponds. *Bioresour Technol*, **174**, 53-9.

Zhu, X.-G., Long, S.P., Ort, D.R. 2008. What is the maximum efficiency with which photosynthesis can convert solar energy into biomass? *Current Opinion in Biotechnology*, **19**(2), 153-159.

Zienkiewicz, K., Du, Z.-Y., Ma, W., Vollheyde, K., Benning, C. 2016a. Stress-induced neutral lipid biosynthesis in microalgae — Molecular, cellular and physiological insights. *Biochimica et Biophysica Acta (BBA) - Molecular and Cell Biology of Lipids*, **1861**(9, Part B), 1269-1281.

Zienkiewicz, K., Du, Z.Y., Ma, W., Vollheyde, K., Benning, C. 2016b. Stress-induced neutral lipid biosynthesis in microalgae - Molecular, cellular and physiological insights. *Biochim Biophys Acta*, **1861**(9 Pt B), 1269-1281.

Zienkiewicz, K., Zienkiewicz, A., Poliner, E., Du, Z.-Y., Vollheyde, K., Herrfurth, C., Marmon, S., Farré, E.M., Feussner, I., Benning, C. 2017a. Nannochloropsis, a rich source of diacylglycerol acyltransferases for engineering of triacylglycerol content in different hosts. *Biotechnology for Biofuels*, **10**(1), 8.

Zienkiewicz, K., Zienkiewicz, A., Poliner, E., Du, Z.Y., Vollheyde, K., Herrfurth, C., Marmon, S., Farre, E.M., Feussner, I., Benning, C. 2017b. Nannochloropsis, a rich source of diacylglycerol acyltransferases for engineering of triacylglycerol content in different hosts. *Biotechnol Biofuels*, **10**, 8.